IAC TECHNOLOGY DIVISION

Version 1.0

USERMANUAL

July 1, 2011

PROJECT / DESTINATION:

OSIRIS

TITLE:

USER MANUAL (SCIENTIFIC USE)

INSTITUTO DE ASTROFISICA DE CANARIAS

38200 La Laguna (Tenerife) - ESPAÑA - Phone (922)605200 - Fax (922)605210

AUTHOR LIST

Name	Function
Jordi Cepa (IAC)	OSIRIS Principal Investigator
Emilio Alfaro (IAA)	Instrument Definition Team (Instrument builders)
Angel Bongiovanni (IAC)	OSIRIS Scientific Team
Antonio Cabrera Lavers (GTC)	GTC Instrument Specialist
Alessandro Ederoclite (IAC)	OSIRIS Scientific Team
Ignacio González (IFCA-UNICAN)	Instrument Definition Team (Instrument builders)
José Carlos López (IAC)	OSIRIS Control Engineer
Ana María Pérez (IAC)	OSIRIS Scientific Team
Miguel Sánchez (ESAC/INSA)	Instrument Definition Team (Instrument builders)

APPROVAL CONTROL

Control	Name	Function
Revised by:	Jordi Cepa (IAC)	OSIRIS PI
	Emilio Alfaro (IAA)	IDT (Instrument builders)
	Angel Bongiovanni (IAC)	OSIRIS Scientific Team
	Antonio Cabrera Lavers (GTC)	GTC Instrument Specialist
	Héctor Castañeda (IPN)	IDT (Instrument builders)
	Alessandro Ederoclite (IAC)	OSIRIS Scientific Team
	Ignacio González (IFCA-UNICAN)	IDT (Instrument builders)
	José Carlos López (IAC)	OSIRIS Control Engineer
	Ana María Pérez García (IAC)	OSIRIS Scientific Team
	Miguel Sánchez (ESAC/INSA)	IDT (Instrument builders)
Approved by:		
Authorised by:		

DOCUMENT CHANGE RECORD

Issue	Date	Change Description
1	24/03/11	Draft
2	01/07/11	Version 1.0

TABLE OF CONTENTS

1. INSTRUMENT CHARACTERISTICS 8

1.1 OVERVIEW 8
1.1.1 Instrument description 8
1.1.2 OSIRIS focal plane masks 10
1.1.3 Observing modes 11
1.1.4 Main Characteristics 12
1.1.5 Field obscuration and vignetting 13
1.1.6 Field orientation and gap 13
1.1.7 Instrument overheads 14
1.1.8 Environmental conditions 14
1.2 DETECTORS 14
1.2.1 Description 14
1.2.2 OSIRIS standard CCD operation modes 16
1.2.3 OSIRIS CCDs linearity / dark current level / cross-talk 16
1.2.4 Quantum Efficiency 17
1.2.6 CCD windowing 18

2. BROAD BAND IMAGING 19

2.1.1 Sloan broad band filters 19
2.1.1.1 Zero points 21
2.1.1.2 Sky background 21
2.1.1.3 Colour corrections 22
2.1.1.4 OSIRIS/GTC Broad Band Imaging efficiency 22
2.2 PHOTOMETRIC UNIFORMITY 23
2.3 SKY FLAT FIELDS 23
2.4 SLOAN PHOTOMETRIC STANDARDS 23

3. TUNABLE FILTER IMAGING 24

3.1 OSIRIS TUNABLE FILTERS DESCRIPTION 24
3.1.1 Introduction to FabryPerot filters (FPFs) 24
3.1.1.1 Performance of an ideal FPF 24
3.1.1.2 Limitations 26
3.1.1.3 Gap-scanning etalons 27
3.1.2 Charge shuffling 29
3.1.3 Order sorters 29
3.1.4 OSIRIS TF Characteristics and Features 29
3.1.4.1 Dimensions 31
3.1.4.2 Coatings 31
3.2 OSIRIS FOV FOR TUNABLE FILTER IMAGING 32
3.3 OSIRIS TUNABLE FILTER AVAILABLE WIDTHS 34
3.4 ORDER SORTER FILTERS 35
3.5 CALIBRATING THE TF AND TUNING ACCURACY 36
3.5.1 Parallelism 36
3.5.1.1 General considerations 36
3.5.1.2 TF parallelization procedure 36
3.5.1.3 Lack of parallelism 37
3.5.2 Wavelength calibration 39

3.5.2.1 General considerations 39
3.5.2.2 Calibration using the ICM 40
3.5.3 Checking the calibration by using night sky emission lines 41
3.5.4 Tuning accuracy 43
3.5.5 Tuning speed 43
3.6 OBSERVING WITH OSIRIS TUNABLE FILTER 43
3.6.1 Tunable Filter vs. Spectroscopy 43
3.6.2 Observing Strategies 44
3.6.2.1 Selecting off-band wavelengths 45
3.6.2.1.1 Continuum subtraction 45
3.6.2.2 Deblending lines 46
3.6.2.3 On-line FWHM selection 47
3.6.2.4 Deciding target position and orientation 48
3.6.2.5 Removing ghosts, cosmic rays and cosmetics 49
3.6.2.5.1 Field masking 51
3.6.2.5.2 Azimuthal dithering pattern 51
3.6.2.5.3 TF tuning dithering pattern 51
3.6.2.6 Tunable tomography 51
3.6.2.6.1 Technique 51
3.6.2.7 Band synthesis technique 52
3.6.2.7.1 Technique 52
3.6.2.8 SUMMARY 53
3.6.2.8.1 Sources of instrumental photometric errors. 53
3.6.2.8.2 Preparing an observation: a checklist 54
3.7 SPECTROPHOTOMETRIC STANDARDS FOR TF FLUX CALIBRATION 55
3.8 OSIRIS RTF GLOBAL EFFICIENCY 55
3.9 POST-PROCESSING TF DATA 56
3.9.1 Calibration images 56
3.9.1.1 Bias 56
3.9.1.2 Flat fields 56
3.9.2 Night-sky emission line rings 57
3.10 MEDIUM BAND IMAGING WITH TF ORDER SORTERS 58
4. LONG SLIT SPECTROSCOPY 60
4.1 ACQUISITION IN LONG-SLIT SPECTROSCOPIC MODE 61
4.2 FLEXURE 62
4.3 FRINGING 62
4.4 SPATIAL DISPLACEMENT 63
4.5 ARC LINE MAPS 64
4.5.1 Arc-line ghosts 71
4.5.2 Spectral solutions 71
4.5.3 Spectral flat fields 72
4.6 VPHS R2000/R2500 GHOSTING 72
4.7 SECOND ORDER CONTAMINATION 73
4.8 SPECTROPHOTOMETRIC STANDARDS 73
4.9 SPECTROSCOPIC PHOTON DETECTION EFFICIENCY 74
5 OBSERVING WITH OSIRIS 75
5.1 EXPOSURE TIME CALCULATOR (ETC) 75
5.2 GTC PHASE 2 TOOL 75
6 OSIRIS DATA PROCESSING 76

6.1 OSIRIS / GTC KEYWORDS 76
6.2 ASTROMETRY WITH OSIRIS 81
6.2.1 INPUT DATA 81
6.2.2 ASTROMETRIC SOLUTION 82
6.2.3 MOSAIC COMPOSITION 84
6.2.4 COMPOSING A FIRST-ORDER MOSAIC FROM RAW DATA 85

7 OSIRIS OS FILTER CHARACTERISTICS 86

8 OSIRIS GRISMS/VPH EFFICIENCIES 91

9 SLOAN PHOTOMETRIC STANDARDS 94

10 OSIRIS SPECTROPHOTOMETRIC STANDARDS 96

A. LIST OF REFERENCE DOCUMENTS 98

B. REFERENCES 98

LIST OF ABBREVIATIONS

AAO	Anglo Australian Observatory
CCD	Charge Coupled Device
ESAC/INSA	European Science Astronomy Centre / Ingeniería y Servicios Aeroespaciales
ESO	European Southern Observatory
EW	Equivalent Width
FITS	Flexible Image Transport System
FOV	Field Of View
FWHM	Full Width at Half Maximum
GTC	Gran Telescopio Canarias
IAA	Instituto de Astrofísica de Andalucía
IA-UNAM	Instituto de Astronomía – Universidad Nacional Autónoma de México
ICM	Instrument Calibration Module
IDT	Instrument Definition Team
IFCA-UNICAN	Instituto de Física de Cantabria – Universidad de Cantabria
MOS	Multiple Object Spectroscopy
NIR	Near InfraRed
OSIRIS	Optical System for Imaging and low Resolution Integrated Spectroscopy
OS	Order Sorter
PI	Principal Investigator
PSF	Point Spread Function
QE	Quantum Efficiency
S/N	Signal to Noise ratio
TBC	To Be Confirmed
TBD	To Be Defined
TF	Tunable Filter
z	Redshift

1. INSTRUMENT CHARACTERISTICS

1.1 Overview

1.1.1 Instrument description

OSIRIS is the first work-horse imaging and spectroscopic instrument for the GTC. The OSIRIS acronym stands for *Optical System for Imaging and low-intermediate Resolution Integrated Spectroscopy*, which encapsulated in a few words the versatile nature of this instrument that we will describe in this manual.

A key scientific driver in the design of OSIRIS has been the study of star formation indicators in nearby galaxies and more distant objects, back to the furthest observable galaxies with GTC. In particular, star formation in galaxies as a function of redshift is a classical topic and one main objectives of several current projects of instruments for large telescopes both, ground based and aboard satellites.

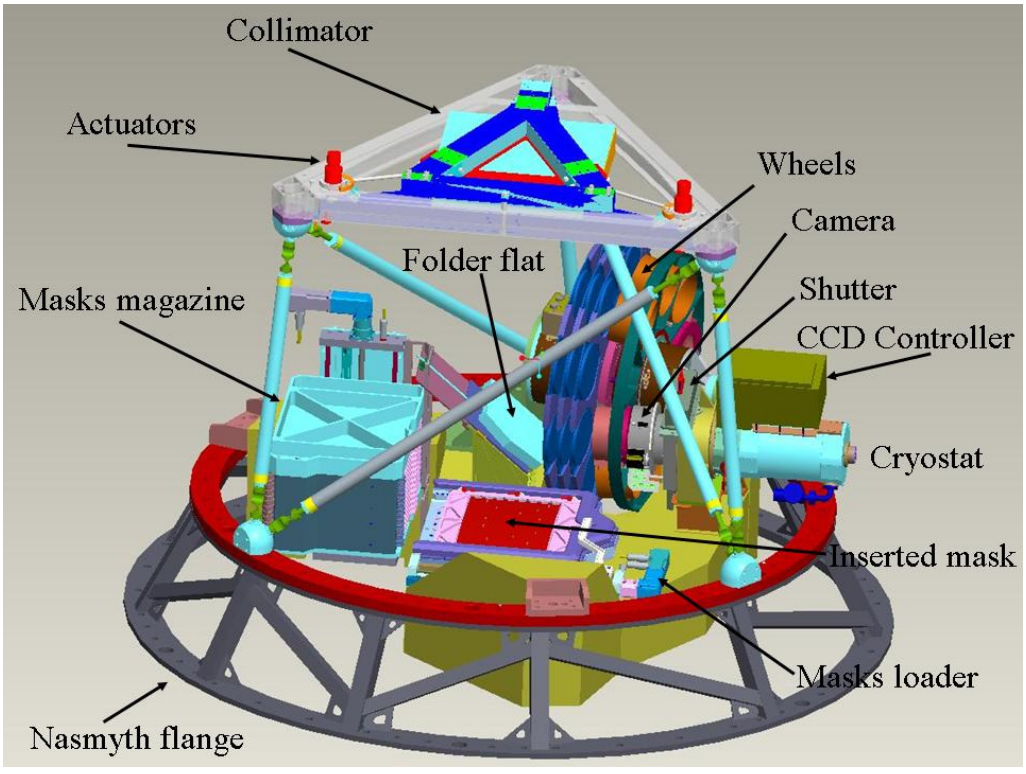

Figure 1.1.- 3D of OSIRIS showing the main subsystems.

OSIRIS is directly attached to the GTC field rotator and guide unit in the GTC Nasmyth-B focal station (Figure 1.1). The instrument optics are designed around the classical concept of collimator plus camera. For reasons of keeping the instrument compact, the optical train is folded and the field is off-axis. Its compact design will allow future migration of the instrument to the Cassegrain focal station. Next we will briefly describe the main components of the instrument, following the light path from the moment the light coming from the telescope enters the instrument through a transparent entrance window.

A masks loader (Figure 1.1) selects and insert/remove masks to/from the telescope focal plane. In addition to user customized masks for multi-object spectroscopy, a number of fixed width long-slit masks are available, as well as a number of special masks to facilitate fast photometry and charge shuffling (see 1.1.2).

Having passed the focal plane, the light reflects of the collimator (Figure 1.1), which is an off-axis quasi-parabolic mirror with elements for support and adjustment. The collimator is open-loop actively controlled to compensate for gravitational flexures of the instrument (Figure 1.1).

The collimated beam next hits a flat fold mirror that directs the light beam towards the filter wheels and the camera optics. Both the collimator and folder are covered with a silver protected coating of high red and blue reflectivity (Figure 1.2).

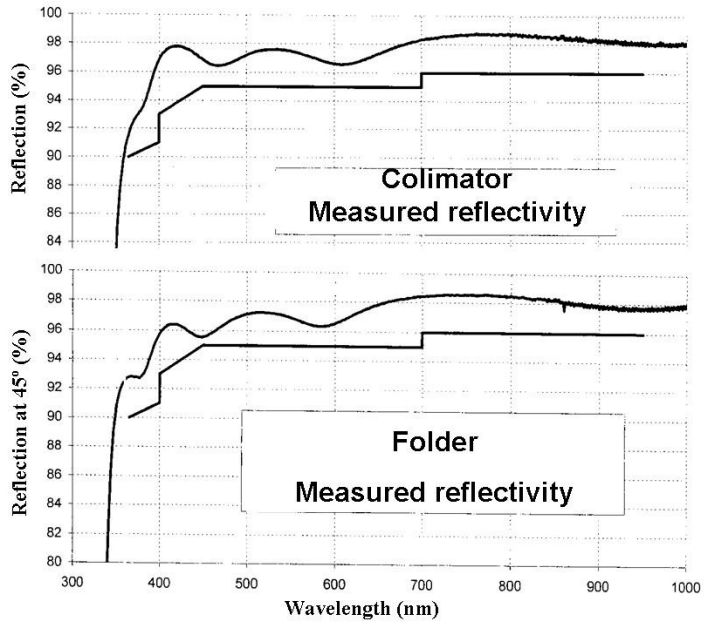

Figure 1.2.- Collimator and folder flat measured reflectivity (curve) with respect to the requirements (straight stepper lines)

Filters, grisms and Tunable Filters (TFs) can be inserted in the collimated beam near the pupil via four filters wheels, three for standard filters and the fourth, at the pupil, for TFs and grisms. Each filter wheel has 9 positions, and the grism wheel holds, apart from the tunable filters, up to 5 dispersive element. Together they allow selecting the adequate combination of these elements for using the different observing modes described in the following subsection. Conventional filters are used for imaging and for order sorting the TFs and grisms. The filters insert into the beam at an angle of 10.5 degrees in order to avoid ghost images.

The all-refractive OSIRIS camera consists of 9 spherical lenses. The last lens is the dewar window. The camera effective focal length of 181 mm provides the required detector scale (0.125 arcsec/pixel) on a flat focal plane that is tilted 1.83 degrees. The shutter is incorporated in between the camera optics.

Light is detected by a mosaic of two detector of 2k×4k red-optimized CCDs in a cryostat

The instrument control subsystem allows mechanisms, tunable filters and the detector to work in a synchronized fashion. Also, it provide users with mechanisms controls and data processing interfaces. This instrument control is be closely integrated with the rest of Telescope Control following the GTC standards. This facilitates a high level of automation of observing sequences.

OSIRIS calibration is performed using spectral lamps provided by the GTC Instrument Calibration Module (ICM), also, external continuum lamps for dome flat fields are available at the telescope.

1.1.2 OSIRIS focal plane masks

The OSIRIS mask holder with 13 positions allows remote changes of focal plane masks such as spectrograph slits, custom-made multi-object masks, or other special-purpose masks. The following masks are available at the instrument:

- Long Slit masks. Available slit widths are: 0.4", 0.6", 0.8", 1.0", 1.2", 1.5", 1.8", 2.0", 2.5", 3.0", 5.0".
- Decentred long slit of 3” width for fast photometry in shuffle mode (Figure 1.3 right).
- Mask of the central 1/3 imaging FOV for TF imaging shuffle (two TF tunings or straddling line, Figure 1.3 middle).
- Frame transfer mask, selecting ½ of the lines in both detectors (Figure 1.3 left).
- Mask shading one detector, for avoiding dithering when obtaining TF imaging of bright crowded or extended fields.
- Pinhole masks (for Long Slit and Multi Object Spectroscopy tests).

Figure 1.3.- From left to right, charge shuffling mask selecting the central 1/3 of the detector lines (the central black circular piece is shown just for reference), frame transfer mask selecting the half of the detector exposed, and the fast photometry mask with the decentred slit of 3 arcseconds width.

1.1.3 Observing modes

The following table provides a summary of the different OSIRIS observing modes, that are described further on in this manual.

Mode	Description
Imaging	
Broad band	SDSS and order sorter sets
Narrow band	With Tunable Filters: Blue (365-686 nm) and Red (646-1000 nm) TF
Single exposure	One wavelength for line and another for continuum
Scan	A set of exposures at several equidistant & contiguous wavelengths
Shuffle	Several wavelengths synchronizing charge shuffling with TF tuning
Spectroscopy	
Long slit	Slit widths defined by available masks
MOS	Using user-customized masks
Standard	Slitlets: sky and object in the same slit
λ-sorting	As above but restricting wavelength range using a filter
Nod & Shuffle	Microslits: alternate sky & object by nodding telescope & shuffling
Standard	Charge is shuffled 1/3 of detector
Microshuffle	As above but shuffling tens of rows instead
λ-sorting	As any of the above but restricting wavelength range using a filter
Fast photometry	
Shuffle	Decentered slit plus charge shuffling
Frame transfer	Defining windows and combining with frame transfer
Fast Spectroscopy	
Shuffle	Customized decentered and rotated 90º short slit
Frame transfer	Off centre slit plus frame transfer on the detector

1.1.4 Main Characteristics

The following table summarises the main instrument characteristics.

Total FOV	8.53 × 8.67 arcminutes with small shadowed area in one side (Figure 1.4)
Unvignetted FOV	7.8 × 7.8 arcminutes
Long slit	8.67 arcminutes
MOS FOV	8.67 × 6.0 arcminutes[1]
Plate scale	0.12718 arcsec/pixel (both imaging and spectroscopy)
Image quality	< 0.15" (80% polychromatic EE)
Distortion	Lower than 2%
Instrument Position Angle	150.540346º
Detector system	Two MAT 4k × 2k (~9.2 arcsec gap[2]) from same Si wafer
Broad band	ugriz filters & medium band TF order sorters (OS)
Tunable Filters	Central λ tunable from 365 through 1000 nm[3] FWHM tunable from ~6 through ~20 Å, depending on λ Lower FWHM is limited by the order-sorting filter, and the higher by the etalon gap range. Tuning time ~10 ms depending on etalon gap. Minimum is ~1 ms Tuning accuracy in λ and FWHM ~1 Å
Spectral resolutions	300, 500, 1.000, 2.000, 2.500 and 5.000[4] Resolution for 0.6" slit width Available spectral ranges R=300 & 500 are limited by second-order light, and higher R by detector[5]
Long slit widths	Masks of fixed widths from 0.4 through 5.0 arcseconds
MOS (masks)	~40 targets per mask (using classical slits of 15" length) or Several hundred (using Nod&Shuffle, μShuffle or λ-sorting)
Flexures	Less than 1 pixel

[1] At R larger than 500, a 5 × 6 arcminute FOV is recommended.

[2] Physical gap is of ~26 pixels (or ~3 arcsec), the gap between photosensitive pixels is of ~72 pixels or 9.2 arcsec. Then, the last quantity is the one to take into account when dithering for covering the gap on the sky.

[3] Current IAC calibration facilities allow calibration from 450 through 950 nm only. In the near future it will be expanded for covering the full OSIRIS wavelength range.

[4] R=5000 VPHs are in manufacturing process.

[5] Dispersive elements (grisms or VPHs) can be rotated 90º for accommodating the spectra along lines or columns. The nominal dispersion direction is along columns (i.e.: along the gap between detectors). Beware of detector gap if rotating the disperser.

1.1.5 Field obscuration and vignetting

As can be appreciated from Figure 1.4, there is an obscuration of the left hand side OSIRIS full FOV of CCD1 due to the edges of the filter wheels and the fold mirror. This was contemplated in the original design and does not affect the specified unvignetted field of view. The obscured area is best avoided, although reliable photometry can be performed on targets located in this region of the detector.

Some vignetting is present in the lower part (lower 500 pixels, unbinned) of the CCDs, due to filter wheel 1. With the filter in position removed, the vignetting is reduced in CCD1 only (Figure 1.4). In all cases the total unvignetted field of view is 7.8×7.8 arcmin.

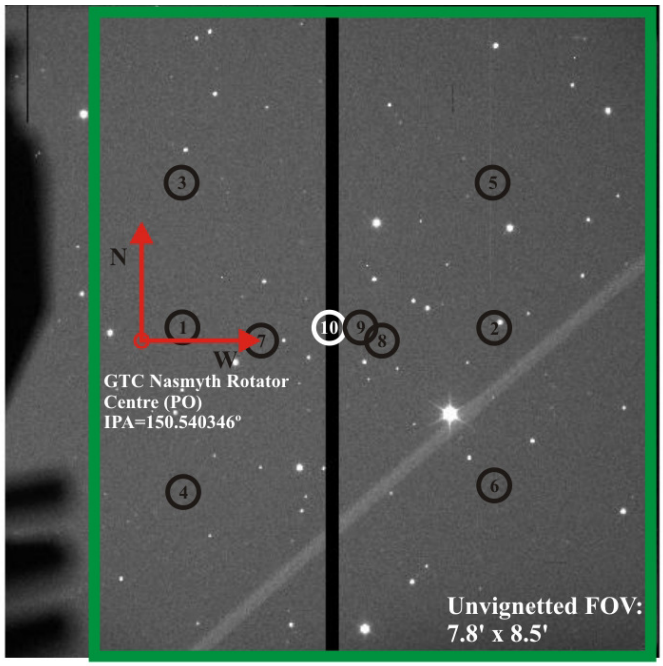

Figure 1.4.- OSIRIS image showing the shadowing produced by the folder flat and filter wheels on one side of CCD1 (left). Since the instrument is off-axis, the centre of the OSIRIS field (10) does not coincide with GTC pointing centre (in red).

1.1.6 Field orientation and gap

The OSIRIS instrument position angle within the GTC reference system is 150.540346º. With this orientation, North is up and East left in the images. This value can be retrieved from KEYWORD IPA at image headers. If a different position angle (P.A.) is requested by the user, the resultant IPA would be 150.540346º - P.A. (with P.A. measured from N to E).

The OSIRIS focal plane is imaged by two CCDs that have a narrow gap between them. This gap is 9.2 arcsecs wide. To cover the full field when defining a dithering pattern, steps of 10 arcsecs (or even 12 arcsecs to be more conservative) perpendicular to the gap are recommended.

1.1.7 Instrument overheads

During instrument design, special efforts have been invested in reducing instrument overheads due to configuration changes (observing modes, masks, and filters or grisms) to the minimum. The following table summarizes the typical time it takes to change a component.

Mask change	Filter Change	Grism Change
40 sec	3 sec	6 sec

These times only reflect the mechanical changes of the components and not the overheads for target acquisition in the different modes, auto-guiding and detector readout.

Changing form one TF to the other takes about 13s. Changing TF wavelength tuning takes at most about 0.1 s, usually 0.02 s, depending on the gap differences between the different tunings.

1.1.8 Environmental conditions

OSIRIS is protected from the environment through its fairly air tight enclosure. Dry air flushes the instrument to avoid dust and moisture entering the instrument and depositing on optical surfaces. This air is provided by GTC instrument services and it is not thermally controlled, but its temperature is quite stable. The aim is to minimize temperature and humidity gradients within the instrument so as to ensure best image stability. Even when inside the dome the humidity raises substantially due to wheather conditions, the humidity inside OSIRIS is kept stable during several hours.

Temperature changes in GTC structure are transmitted quite fast by conduction to OSIRIS structure via the Nasmyth flange to the GTC rotator. Also, although the attached electronic cabinets are thermally isolated, some heat leaks inside the instrument.

1.2 Detectors

1.2.1 Description

The OSIRIS detector system is composed of a mosaic of two buttable 2Kx4K CCDs to give a total 4Kx4K pixels, 15 microns/pixel. The arrays are MAT-44-82 from Marconi (2 channel each, Frame-Transfer type, 20-1000 kHz readout rate). The software allows driving one or both MAT44-82 CCDs, by one or two outputs each. It is also possible to modify the parallel or serial clocks time, so that it is possible to readout the array from 20 kHz per channel up to the CCD readout limit of 1 MHz. It allows frame transfer mode and binning.

The following table summarises the main OSIRIS detector parameters.

Parameter	Value	Comments
Array size	2048×4096	Photosensitive area
Overscan area	[1:24,1:2048]	For bias subtraction
Readout channels[1]	2	Per detector
Shuffle speed	50 μs/line	Used for skipping lines in window mode as well
Readout speeds	100, 200, 500 kHz	20,50kHz & 1 MHz possible (not recommended[2])
RON[3]	3.8 e^- @ 100 kHz 4.5 e^- @ 200 kHz 8 e^- @ 500 kHz	Nominal are 200 kHz for imaging, 100 kHz for spectroscopy & 500 kHz for acquisition
Gain (e^- /ADU)	1.18 @ 100 kHz 0.95 @ 200 kHz	
Linearity	Better than 1%	For 1% to 90% full well
Operating Temp.	154-156 K	
Dark current	2-3 e^- /hour/pixel	
CTE	Vertical >0.999999 Horizontal >0.9999	Measured on grade 5 at laboratory
Binning	2×1, 1×2 & 2×2	Nominal is 2×2
Windows	Up to 5 enabled	Copied on both detectors
Frame transfer	Enabled	For fast photometry & Spectroscopy
Fringing	3% @ 900nm 2% @ 950 nm 4% @ 990 nm	Fringing starts between 850 and 900 nm Measured on grade 5 device at laboratory

[1] Using two channel per detector requires obtaining all images in this configuration and slightly different biases per channel (i.e.: half detector) are obtained

[2] At 950 kHz the RON is so high that the image is not of scientific use, and at speeds lower than 100 kHz the readout time increases at a cost of no significant reduction of RON

[3] RON @ 500 kHz is higher than nominal (~8 e^-), likely due to EMI (as of February 2010)

Readout times can be evaluated in the following way:

Pixels to read / (readout speed x binned pixels x channels used)

For example, reading both $2k \times 4k$ full detectors using two channels per detector with 2×2 binning at 500 kHz takes ~2 s.

Please note that this does not consider the time invested in configuring the SDSU (about 5s), clearing the chip before each exposure (about 4s), and transferring and saving the frame on disk (few more seconds).

Then, since an image is started till is fully acquired, for the two CCDs Output A and no binning, takes 31 seconds at 500 kHz readout speed and about 100 s at 100 kHz.

1.2.2 OSIRIS standard CCD operation modes

As it was described in Section 1.2.1, the CCDs control system offers a wide range of readout modes and gain settings, but for the time being the standard observing modes are shown in the table below. In these modes the detector linearity is guaranteed up to the full 16 bits signal maximum. Read noise is better than 5 electrons in imaging and spectroscopic readout modes.

The acquisition mode is generally used for test images but not for science data. This mode has a significant high noise pattern so it is not suitable for scientific cases. The following table gives an overview of the main characteristics of the standard readout modes.

	Imaging (FAST)	**Spectroscopy (SLOW)**	**Acquisition**
Readout configuration	CCD1+CCD2_A	CCD1+CCD2_A	CCD1+CCD2_A
Readout velocity	200 kHz	100 kHz	500 kHz
Gain (e^-/ADU)[2]	0.95	1.15	1.46
Binning (X x Y)	2 x 2	2 x 2	2 x 2
Readout time	21 sec	42 sec	7.8 sec
Actual readout noise	~4.5 e^-	~3.5 e^-	~8 e^-

A frequent monitorizing of the Gain and Readout noise for the standard operation modes of OSIRIS is done for operational purposes, and the values are updated at the OSIRIS site at GTC web page.

1.2.3 OSIRIS CCDs linearity / dark current level / cross-talk

In the OSIRIS standard operation modes, detector linearity is guaranteed up to the full 16 bits signal maximum (Figure 1.5).

During the first months of operation of the instrument, OSIRIS suffered of a very high dark current resulting from an excessive temperature of the CCD that was not correctly reported by the CCD thermometry system. A redesign of the thermal coupling between the liquid Nitrogen container and the CCD has resulted in a notable improvement of the dark current, which is now at acceptable levels of about 10-12 ADUs/h for a 2 x 2 binned pixel. Hence, since February 2010 no dark images are needed for OSIRIS data analysis.

[2] Those values are for CCD2. Gain for CCD1 is about 5% lower that these.

A slight cross-talk effect between both CCDs in OSIRIS has been measured during instrument commissioning tests. The effect is as small as 2.8 x 10^{-4} respect to the original signal, hence the effect in the scientific images can be neglected.

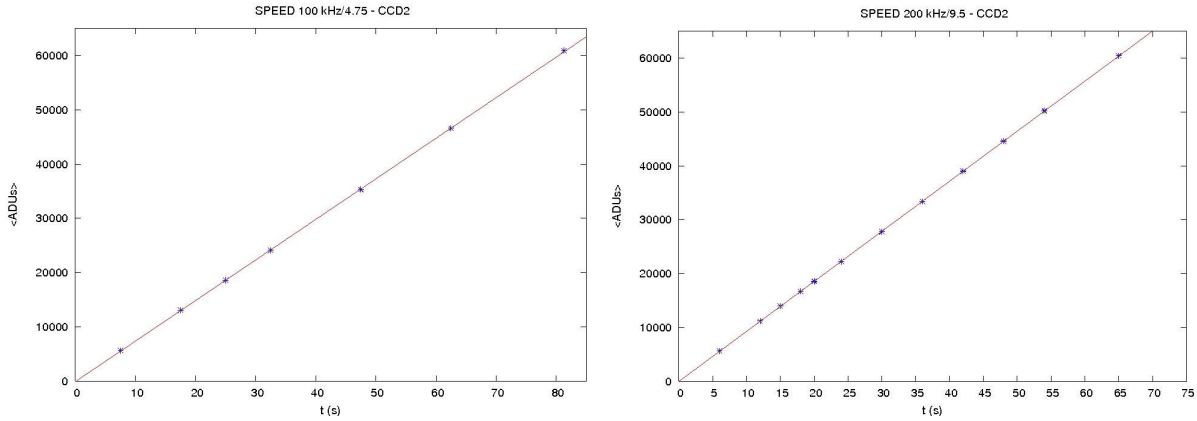

Fig. 1.5.- : Linearity plots for OSIRIS SLOW (left) and FAST (right) operation modes.

Cosmic ray events have been measured in both OSIRIS CCDs, resulting an average of 30 impacts/min, that means around 1800 impacts/h.

1.2.4 Quantum Efficiency

The detectors are optimized for longer wavelengths, but with a low, although reasonable, blue efficiency, of about 20% @ 365nm. Hence observing at these wavelengths is possible, although slow.

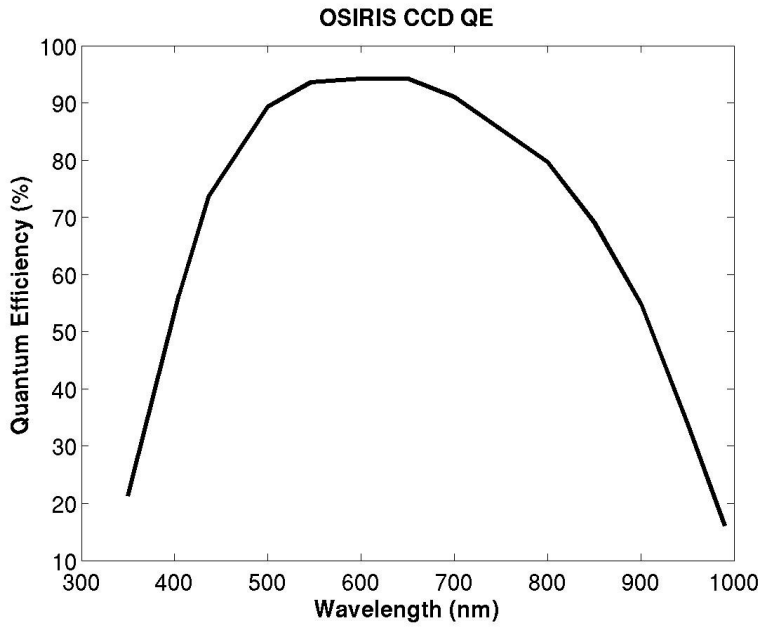

Figure 1.6.-: QE of OSIRIS CCDs.

1.2.6 CCD windowing

OSIRIS CCDs allows to define up to 5 windows at the same time for SIMPLE readout modes, and only a single window for FAST MODES (not available yet).

There are some restrictions that the user has to take into account when defining those windows:

- All the windows must have the same size.
- No overlap is allowed between different windows.
- Windows must be defined in increasing order of their Y coordinate (that coincides with the readout direction). Therefore, Y coordinates for different windows must not overlap (for example, if a window is defined at [1:200,300:499], any other window must begin at Y=500, or conclude at Y=299).
- Windows are replicated in both CCDs. Hence, if N windows are defined in CCD1, the same windows will appear in CCD2, with the same size and position as those of CCD1. Some cross-talk has been noted between windows in both CCDs, for this reason is highly recommended that only use a single CCD when using windowing in OSIRIS.

The readout speed in windowing mode is defined by the combination of the windows size and CCD readout mode. When windows are read out, the CCD section unused is 'split' at the highest readout speed, hence there is no dependence in the total readout time on the windows location in the CCDs.

In any case, if the user is interested in observing with OSIRIS by using windows, please contact well in advance a GTC staff astronomer, in order to choose what is the most convenient setup for the observing program. At the telescope, the GTC staff astronomer will perform the observations, and all the restrictions and particularities in using the windows will be properly considered.

2. BROAD BAND IMAGING

OSIRIS allows broadband imaging over a FOV of 8.53' x 8.67' (7.8' x 7.8' unvignetted) covering the full spectral range from λ=3650 Å to λ=10000 Å , with a high transmission coefficient in particular at longer wavelengths.

All standard OSIRIS filters have been designed to work in a collimated beam with a tilt angle of 10.5º to avoid ghosts due to back reflections into the detector.

The OSIRIS standard pointing in Broad Band imaging mode is at the CCD2 pixel (512,2048)[3] to maximize the available FOV and in order to avoid possible cosmetic effects, which are more abundant in the CCD1. The coordinates introduced by the PI in the Phase-2 tool will be positioned at this central pixel.

2.1.1 Sloan broad band filters

Broad band imaging with OSIRIS covers a spectral range from λ=3650Å to λ=10000 Å using the standard Sloan filters u'(λ3500/600), g'(λ4750/1400), r'(λ6250/1400), i'(λ7700/1500) and z'(λ9100/120).

The following table provides the measured parameters at the IAC optical laboratory at ambient temperature at the centre of the filter and with normal incidence. Due to IAC Laboratory limitations, no measures for u' filter are available aside from those provided by the manufacturer.

Filter	Central wavelength (Å)	FWHM (Å)	Transmission (%)
u'	—	—	—
g'	4815	1530	82.48
r'	6410	1760	94.14
i'	7705	1510	89.00
z'	9695	2610	97.16

The filters are placed in the collimated beam and close to the pupil of the instrument, at an angle of 10.5º with respect to the optical axis of the instrument. Because of the angle the central wavelength [$\lambda_c(10º)$] is shifted with respect to the nominal central wavelength [$\lambda_c(0º)$] and the bandwidth [$\Delta\lambda$] changes slightly, but the transmission curve shape is hardly altered. Furthermore, depending on the location in the focal plane, the light incident on the filter cover a range of angles between -2º y 22º, with the corresponding shift in

[3] Note that those coordinates are unbinned coordinates, whereas the standard operation mode of OSIRIS implies 2 x 2 binning.

wavelength. For the broad-band filters this effect is small as can be seen in the following table.

The maximum spatial variations of the filters with respect to the centre are:

Filter	Central wavelength (Å)	FWHM (Å)	Transmission (%)
u’	—	—	—
g’	30	40	1.05
r’	30	40	1.36
i’	5	10	1.09
z’	0	0	1.39

The absolute spectral responses for each filter (except u’) are provided in Figure 2.1.

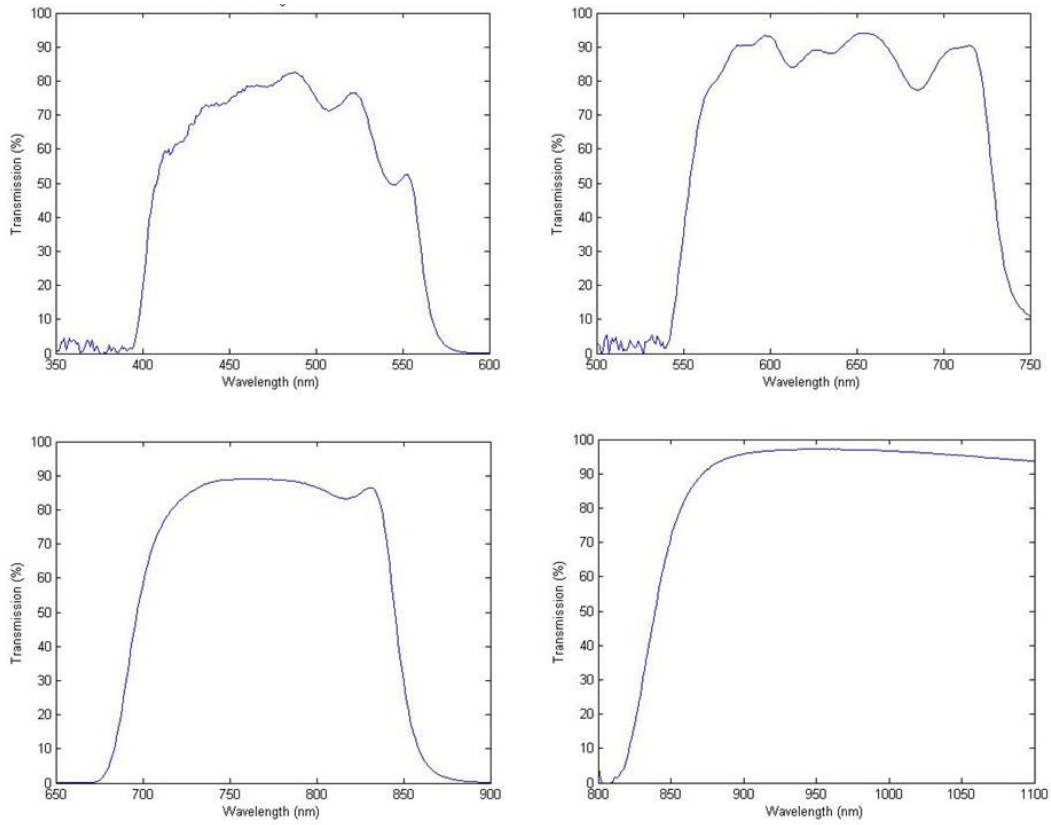

Figure 2.1.- From left to right and top to bottom: measured central spectral response of g’, r, i’, and z’ filters, respectively, with normal incidence.

2.1.1.1 Zero points

From the observation of standard stars during instrument commissioning the following average zero points (1 ADU/s at AM=0) and extinction coefficients have been measured:

Filter	Zero point (mag)	Extinction (mag/airmass)
u'	25.84(±0.08)	0.44(±0.01)
g'	28.85(±0.05)	0.14(±0.03)
r'	29.31(±0.06)	0.07(±0.03)
i'	28.86(±0.05)	0.02(±0.07)
z'	28.27(±0.07)	0.05(±0.02)

With those zeropoints, instrumental magnitudes can be obtained directly using the formula:

$$m = Z - 2.5 \log_{10} [\text{Flux (ADUs/s)}] - k X$$

The zeropoints have been measured at the standard GTC pointing for Broad Band imaging (that is placed at OSIRIS CCD2). Zeropoint values for CCD1 are on average 0.1-0.12 mag smaller in each filter than these.

Standard extinction coefficients for the ORM can be found at:
http://www.ing.iac.es/Astronomy/observing/manuals/ps/tech_notes/tn031.pdf

The limiting magnitudes are measured during photometric sky conditions. Clouds or dust in the atmosphere will reduce the limiting magnitudes. Likewise, changes in the cleanliness and transmission of all optical components will affect the zero points.

An updated version of the daily zeropoint values can be found at:

http://www.gtc.iac.es/en/media/osiris/zeropoints.html

2.1.1.2 Sky background

Estimates of the sky brightness (ADUs /s/ pix) measured at a Elevation 55 deg in the standard OSIRIS Broad Band imaging mode (200 kHz / 9.5 - binning 2 x 2) are:

Filter	Sky Brightness (BRIGHT)	Sky Brigthness (DARK)
u'	15	1
g'	250	25
r'	350	90
i'	290	160
z'	400	325

Although ETC predictions for sky brightness at the ORM are accurate enough, it is recommended to use the values from the table above for a quick estimation of the sky background counts in long exposed images.

2.1.1.3 Colour corrections

Photometric transformations equations (with a arbitrary zero point of 25. magnitudes) are:

$$u' - u'_0 = -0.517(\pm0.053) - 0.071(\pm0.023)\ (u_0 - g_0)$$
$$g' - g'_0 = -3.637(\pm0.040) - 0.078(\pm0.013)\ (g_0 - r_0)$$
$$r' - r'_0 = -4.117(\pm0.017) - 0.114(\pm0.028)\ (r_0 - i_0)$$
$$i' - i'_0 = -3.170(\pm0.015) - 0.079\ (\pm0.041)\ (i_0 - z_0)$$
$$z' - z'_0 = -3.310(\pm0.031) - 0.072\ (\pm0.052)\ (i_0 - z_0)$$

2.1.1.4 OSIRIS/GTC Broad Band Imaging efficiency

The graph below shows the overall photon detection efficiency of GTC and OSIRIS in each of the Sloan filters (the plots include the contribution both of the telescope and instrument optics system).

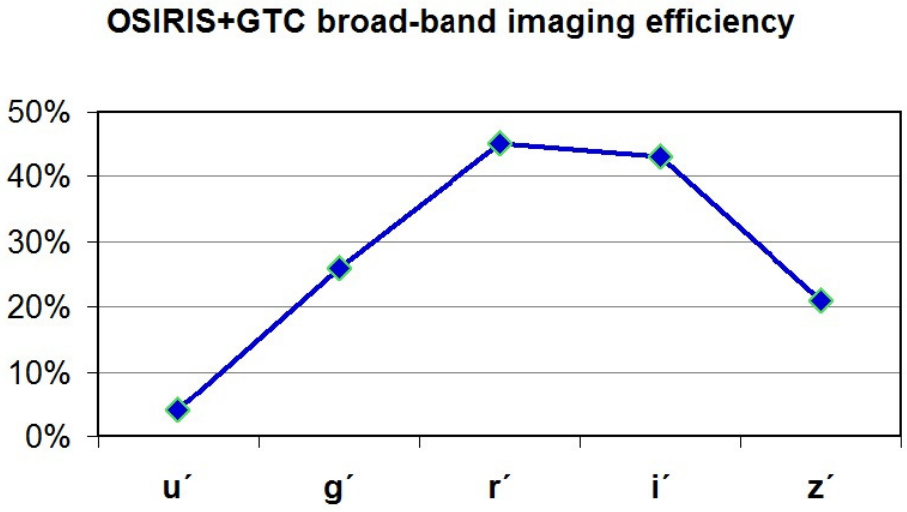

Figure 2.3.- Overall photon detection efficiency of GTC and OSIRIS in each of the Sloan filters.

2.2 Photometric uniformity

Given the structure and speed of OSIRIS shutter (of type moving screen) and that it is near collimated beam, exposures down to 0.1 seconds can be obtained with a uniformity of about 1% over the full field.

2.3 Sky Flat fields

The flat fielding homogeneity in each of the OSIRIS Sloan filters is better than 2.5% over the full unvignetted FOV of the instrument, except in Sloan u', where fluctuations up to 6% with respect to the mean value are found.

Day to day fluctuations in the flat fields are less than 0.05% , and less than 0.1% week to week. Hence, sky flat fields obtained with OSIRIS are well usable up to within a week before or after the observations.

Comparison twilight flat fields with those derived from scientific observations during bright time shows no variations in excess of 0.01%, hence they can be considered practically identical for scientific purposes. These percentage variations are measured globally, while of course locally, due to dust particles that can come and go, the variations may be larger. Moreover, differences between the night sky and the twilight spectrum may result in subtle flat fielding differences.

Comparisons between fky flat fields and dome flats show that the latter suffer from inhomogeneities in the dome illumination. Differences up to 10-15% are found in CCD2 and 2% in CCD1. Therefore dome flats are only recommended for obtaining reliable OSIRIS photometry in CCD1 and as last choice in CCD2.

As a product of the scientific operations with OSIRIS, a series of master flat fields frames can be retrieved from http://www.gtc.iac.es/en/pages/instrumentation/osiris.php. Flat fields were all obtained with exposure times larger than 1 s to minimize possible photometric effects due to OSIRIS shutter and a maximum exposure time of about 20 s (where the detection of stars becomes notable), with an average of 35,000-40,000 ADUs in each individual image. MasterFlats are available separately for each CCD of OSIRIS (as they have a slightly different gain and bias level). The latest master flats are available from the GTC web pages.

2.4 Sloan Photometric Standards

Photometric calibration for OSIRIS Broad Band imaging is done via a Sloan standard set taken from Smith el al. (2002, AJ, 123, 2121). The complete list of standards can be found in Section 9.

3. TUNABLE FILTER IMAGING

3.1 OSIRIS Tunable Filters description

A key aspect of OSIRIS is the use of tunable filters (TFs). OSIRIS TFs are a pair of tunable narrowband interference filters (FabryPerot etalons) covering 370–670 nm (blue 'arm') and 651–935 nm (red 'arm'). They offer monochromatic imaging with an adjustable passband of between 0.6 and 3 nm. In addition, TF frequency switching can be synchronized with movement of charge (charge shuffling or frame transfer) on the OSIRIS CCDs, techniques that have important applications to many astrophysical problems.

3.1.1 Introduction to FabryPerot filters (FPFs)

In its simplest form, a FabryPerot filter (FPF) consists of two plane parallel transparent plates which are coated with films of high reflectivity and low absorption. The coated surfaces are separated by a small distance (typically μm to mm) to form a cavity which is resonant at specific wavelengths. Light entering the cavity undergoes multiple reflections (Figure 3.1) with the amplitude and phase of the resultant beams depending on the wavelength. At the resonant wavelengths, the resultant reflected beam interferes constructively with the light reflected from the first plate cavity boundary and all the incident energy, in the absence of absorption, is transmitted. At other wavelengths, the FPF reflects almost all of the incident energy.

3.1.1.1 Performance of an ideal FPF

The general equation for the intensity transmission coefficient of an ideal FPF (perfectly flat plates used in a parallel beam) as a function of wavelength is

$$\tau_r = \left(\frac{T}{1-R}\right)^2 \left[1 + \frac{4R}{(1-R)^2} sin^2\left(\frac{2\pi\mu d\cos\theta}{\lambda}\right)\right]^{-1}, \quad (3.1)$$

where T is the transmission coefficient of each coating (plate–cavity boundary), R is the reflection coefficient , d is the plate separation, μ is the refractive index of the medium in the cavity (usually air, μ =1) and θ is the angle of incident light. Thus, the FPF transmits a narrow spectral band at a series of wavelengths given by

$$m\lambda = 2\mu d\cos\theta \quad (3.2)$$

where m is an integer known as the order of interference. The peak transmission of each passband is

$$\tau_{r,max} = \left(\frac{T}{1-R}\right)^2 = \left(\frac{T}{T+A}\right)^2, \quad (3.3)$$

where A is the absorption and scattering coefficient of the coatings ($A = 1 - T - R$); and the minimum transmission, halfway between the resonant wavelengths is

Therefore, the contrast between the maximum and minimum transmission intensities is

$$C_r = \frac{\tau_{r,max}}{\tau_{r,min}} = \left(\frac{1+R}{1-R}\right)^2. \tag{3.4}$$

For a FPF contrast greater than 100, the reflection coefficient R of the coatings needs to be greater than or about 0.82.

The wavelenght spacing between passbands, known as the inter–order spacing or free spectral range (FSR), is about

$$\Delta\lambda = \frac{\lambda}{m} \tag{3.5}$$

which is obtained from Equation 3.2 by setting consecutive integral values of m. Each passband has a bandwidth ($\delta\lambda$), full width at halfpeak transmission, given by

$$\delta\lambda_r = \frac{\lambda(1-R)}{m\pi R^{1/2}} \tag{3.6}$$

derived from Equation 3.1. The ratio of inter–order spacing to bandwidth is called the finesse;

$$N = \frac{\Delta\lambda}{\delta\lambda}. \tag{3.7}$$

$$\tau_{r,min} = \left(\frac{T}{1+R}\right)^2. \tag{3.8}$$

For an ideal FPF, it is given by

$$N_r = \frac{\Delta\lambda}{\delta\lambda_r} = \frac{\pi R^{1/2}}{1-R}. \tag{3.9}$$

Thus, we can see that the resolving power of a FPF is equal to the product of the order and the finesse;

$$\frac{\lambda}{\delta\lambda} = mN. \tag{3.10}$$

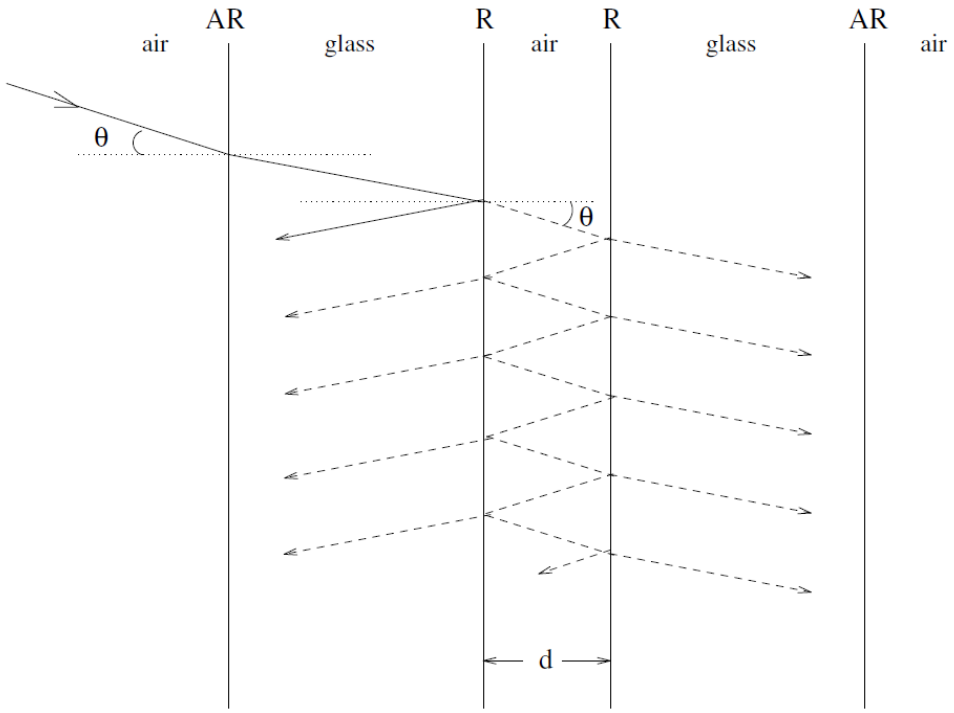

Figure 3.1.- Schematic diagram of interference with a FabryPerot filter. The outside surfaces of the glass are coated with antireflective (AR) coatings, while the inside surfaces are highly reflective (usually $R > 0.8$). The air cavity in the middle is not shown to scale (usually, d is about 10 μm whereas the glass is over 20 mm thick on both sides). At resonant wavelengths, the first reflection (shown with a solid line) interferes destructively with light coming from the cavity in the same direction (dashed lines). The phase difference arises because the first reflection is `internal', while all the other reflections are `external' (with respect to glass). On the other side of the cavity, only constructive interference occurs. At nonresonant wavelengths, destructive interference occurs in the cavity and the first reflection dominates.

3.1.1.2 Limitations

It is apparent from the above equations that to obtain a higher resolution for a given order or to obtain a wider interorder spacing for a given resolution, the finesse needs to be increased. For a finesse greater than 100, a reflection coefficient R of greater than or about 0.97 is necessary (Equation 3.9). However, so far we have considered the ideal situation where the plates are flat and parallel, and the incoming light is parallel. In particular, Equations 3.1, 3.3–3.5, 3.7 and 3.9 refer to this situation using the subscript r to distinguish the results from a real filter. In practice, plate defects and the angular size of the beam limit the maximum finesse obtainable.

The effective finesse (N) is approximately given by:

$$\frac{1}{N^2} = \frac{1}{N_r^2} + \frac{1}{N_d^2} + \frac{1}{N_a^2}, \tag{3.11}$$

where N_r is the reflective finesse from Equation 3.9, N_d is the defect finesse (due to plate defects) and N_a is the aperture finesse (due to the solid angle of the beam).

The defect finesse

$$N_d \sim \frac{2\pi}{2\delta d}, \tag{3.12}$$

where δd is a length scale related to deviations from flat parallel plates. The exact details depend on the type of deviations (Atherton et al. 1981). A FPF manufactured with $N_d \sim 80$ and a reflection coefficient of 0.97 ($N_r \sim 100$) performs with a finesse of about 60.

The aperture finesse

$$N_a \sim \frac{2\pi}{m\Omega}, \tag{3.13}$$

where Ω is the solid angle of the cone of rays passing through the FPF. This equation is related to the λ dependence on θ in Equation 3.2. In terms of astronomical imaging, the effect of aperture finesse is negligible for most objects in the field of view of a telescope. For example, an object which is one degree across (in the collimated beam) imaged with m =50 has N_a ~500 according to Equation 3.13. A more relevant analysis to consider the change in central wavelength of the filter as the ray angle θ is varied in Equation 3.2. For example, a change in ray angle from 1° to 3° produces a change of 0.1% in the central wavelength of the filter at any given order. Therefore, at high resolving powers (~1000), a FPF may not be truly monochromatic across a desired field of view.

3.1.1.3 Gap-scanning etalons

In order to manufacture a tunable FPF, which can change the central wavelength for a given order, it is necessary to be able to adjust either the refractive index of the cavity μ, the plate separation d or the angle θ (as can clearly be seen from Equation 3.2). In a gap-scanning etalon, the plate separation can be controlled to extremely high accuracy.

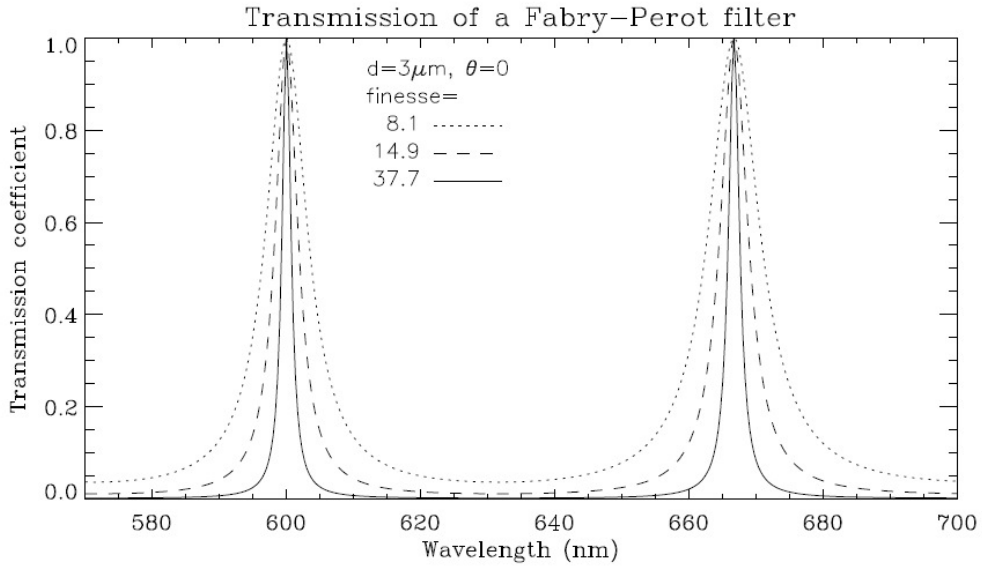

Figure 3.2.-: Variation of the transmission profile of a FPF with finesse. The profiles were determined for an ideal FPF (Equation 2.25) with R = 0.68, 0.81 and 0.92 (A = 0). Orders m = 10 and m = 9 are shown.

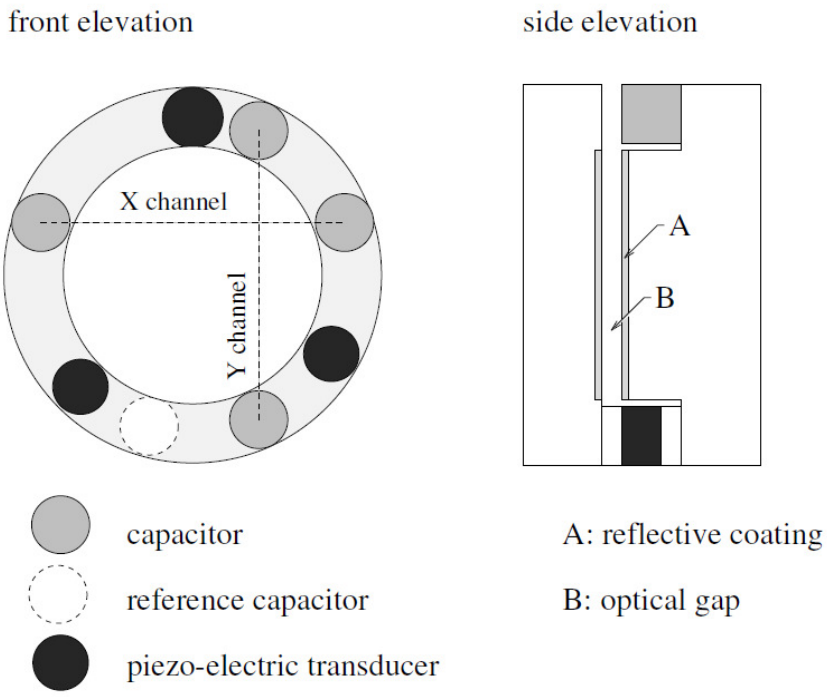

Figure 3.3: Front elevation and side elevation of a *Queensgate Instruments* etalon. Note that the thickness of the optical gap is exaggerated.

In Figure 3.3, we show the structure of a gap-scanning etalon manufactured by *Queensgate Instruments Ltd.* (now *IC Optical Systems*) In recent years, these etalons have undergone considerable improvements. It is now possible to move the plates between any two discrete spacings at very high frequencies (200 Hz or better) with no hysteresis effects while maintaining λ/2000 parallelism (measured at 633 nm). The etalon spacing is maintained by three piezoelectric transducers.

3.1.2 Charge shuffling

Central to almost all modes of OSIRIS use is charge shuffling. Charge shuffling is movement of charge along the CCD between multiple exposures of the same frame, before the image is read out. For shuffled TF imaging an aperture mask ensures that only a section of the CCD frame is exposed at a time. For each exposure, the tunable filter is systematically moved to different gap spacings in a process called frequency switching. This way, a region of sky can be captured at several different wavelengths on a single image. Alternatively, the TF can be kept at fixed frequency and charge shuffling performed to produce timeseries exposures.

The TF plates can be switched anywhere over the physical range at rates in excess of 100 Hz, although in most applications, these rates rarely exceed 0.1 Hz. If a shutter is used, this limits the switching rate to about 1 Hz. Charge on OSIRIS CCDs can be moved over the full area at rates of 30-50 μs/line: it is only when the charge is read out through the amplifiers that this rate is greatly slowed down to the selected readout speed. The high cosmetic quality of OSIRIS CCD allows moving charge up and down many times before significant signal degradation occurs. In this way, it is possible to form discrete images taken at different frequencies where each area of the detector may have been shuffled into view many times to average out temporal effects in the atmosphere.

3.1.3 Order sorters

A FabryPerot Filter clearly gives a periodic series of narrow passbands. To use a FPF with a single passband, it is necessary to suppress the transmission from all the other bands that are potentially detectable. This is done by using conventional filters, called order sorters because they are used to select the required FPF order.

3.1.4 OSIRIS TF Characteristics and Features

The OSIRIS TF, manufactured by *IC Optical Systems*, with plate separations accurately controlled by means of capacitance micrometry, has the appearance of a conventional Fabry-Perot etalon in that it comprises two highly polished glass plates (Figure 3.4). Unlike conventional *ICOS* etalons, it also incorporates very large piezoelectric stacks (which determine the plate separation) and high performance coatings over half the optical wavelength range. The plate separation can be varied between about 3-4μm to 10 μm.

The highly polished plates are coated for optimal performance over 370–960 nm using two separate etalons, one optimized for short wavelengths and one for longer wavelengths. The coating reflectivity determines the shape and degree of order separation of the instrumental profile. This is fully specified by the coating finesse, *N*, which has a quadratic dependence on the coating reflectivity. The OSIRIS TF was coated to a finesse specification of $N = 50$ (red) -100 (blue) which means that the separation between periodic profiles is, respectively, fifty-one hundred times the width of the instrumental profile. At such high values, the profile is Lorentzian to a good approximation. For a given wavelength, changes in plate spacing, *d*, correspond to different orders of interference, *m*. This in turn, dictates the resolving power (*mN*) according to the finesse.

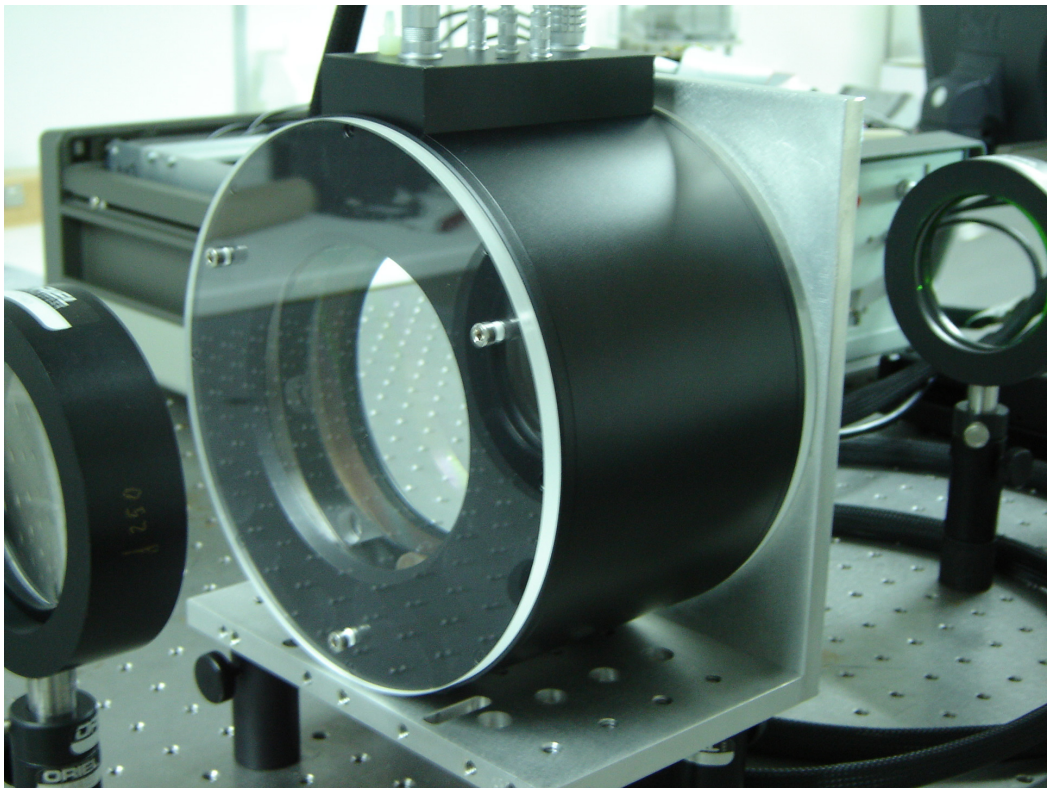

Figure 3.4.- OSIRIS red etalon at the IAC Optical Lab, while undergoing calibration tests.

In general, as can be appreciated in Eq. 3.2, for a given order, small changes in *d* change slightly the wavelength, while for a given wavelength the change of order requires a larger change in *d*. This is important to keep in mind.

With very good approximation, the spectral response of a TF, given by eq. (3.1) can be expressed by,

$$T = \left\{ 1 + \left[\frac{2(\lambda - \lambda_0)}{\delta\lambda} \right]^2 \right\}^{-1}, \tag{3.14}$$

where λ_0 is the wavelength at maximum transmission.

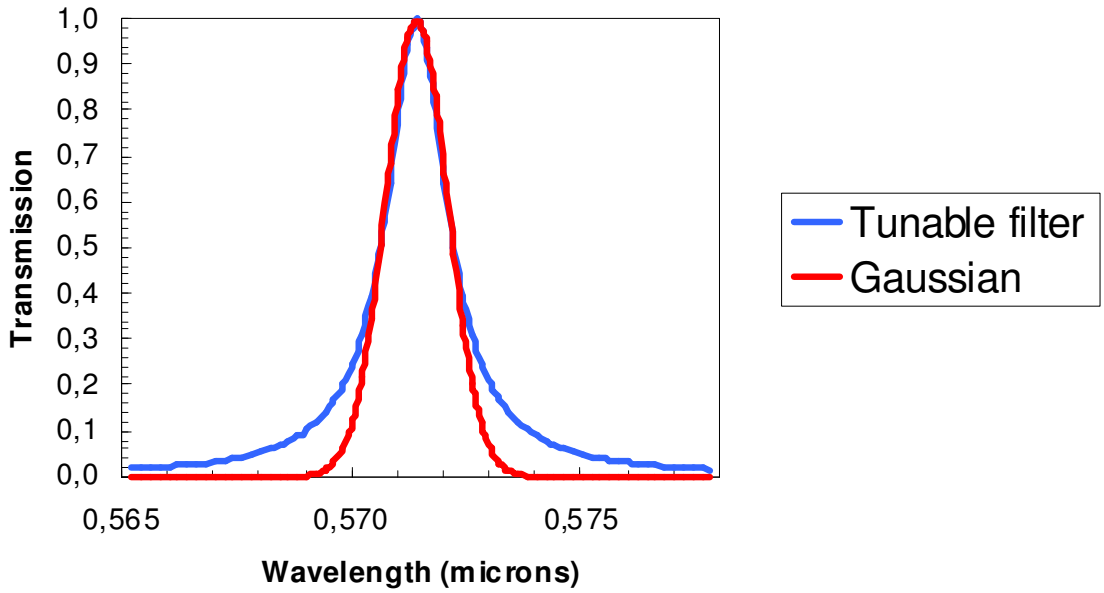

Figure 3.5.- Spectral response of a TF wrt. a Gaussian. The TF response can be considered Gaussian with a good approximation above FHWM, but is more winged below FWHM. This has to be taken into account when selecting the on and off frequencies.

3.1.4.1 Dimensions

The OSIRIS TF are model ET-100. Then the clear aperture is 100 mm diameter. The units are approximately 170 mm diameter by 100 mm of thickness and have a weight of approximately 8 kg.

3.1.4.2 Coatings

This is a critical aspect of TF performance as shown in section 3.1.1. For the OSIRIS TF the main difficulty is achieving a relatively constant reflectivity for a wide spectral range: from 370 to 670nm for the blue TF and from 650 through 1000nm for the red TF. This implies multilayered coatings, i.e.: thick coatings. Then the minimum distance (widest FWHM) between plates is driven by the minimum distances between the coating surfaces, not the plate surfaces.

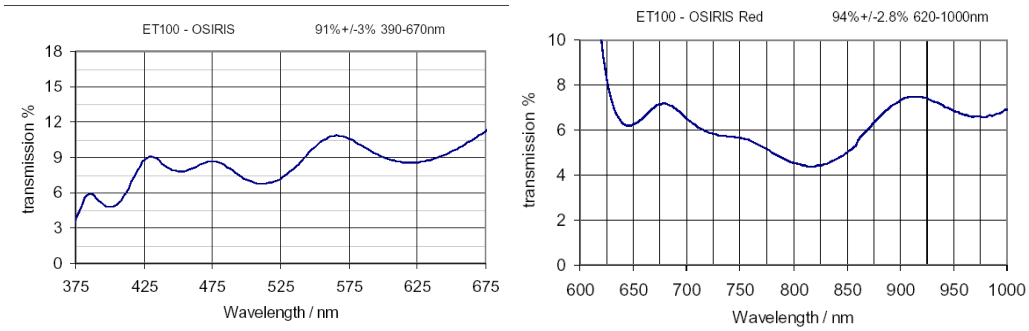

Figure 3.6.- Mean transmissions T for the blue (left) and red (right) OSIRIS TF. The mean reflectivity R = 100 – T % with a very good approximation. This results in a mean R = 91% for the blue TF and 94% for the red TF.

The wavelength dependence of the reflectivity R translates into a wavelength dependence of the FWHM range. Also, please note that the R is well behaved above 425 nm for the blue TF and above 650 nm for the red TF. Hence deviations are expected at lower wavelengths.

3.2 OSIRIS FOV for Tunable Filter Imaging

OSIRIS TF provides a circular FOV of 4 arcmin radius, where is assured that the observations will not have any contamination of other interference orders in the filter. The TF, as any interference filter, changes its response with the incident angle θ according to the formula,

$$\lambda_\theta = \frac{\lambda_0 \sqrt{n^2 - \sin^2 \theta}}{n} \tag{3.15}$$

where λ_0 is the central wavelength for normal incidence, λ_θ for the incident angle θ and n the refraction index.

As a consequence, for filters in a collimated beam (OSIRIS case), beams from different points of the GTC focal plane reach the TF at increasing incident angles, with symmetry with respect to the optical centre. Then there is a progressively increasing shift to the blue of the central wavelength as the distances *r* to the optical centre increase, according to Eq. 3.15. However, since the beams coming from the same point of the FOV are parallel, the FWHM is nearly the same. This is the case of OSIRIS, since OSIRIS TF are located in the pupil of the collimated beam. Since this is a pure geometric effect, the wavelength variation is completely fixed and predictable because it depends only on the incident angle, that is completely determined by the ratio between the telescope and the instrument collimator focal distances:

$$\lambda(r) = \lambda_0 \left[1 - 7.9520 \cdot 10^{-4} \left(\frac{r}{arc\,\min} \right)^2 \right] \tag{3.16a}$$

Where r is obtained from the OSIRIS plate scale of 0.127 arcsec/pixel. This equation allows obtaining an accuracy of ≈1-2Å at the edge of the 8 arcminute diameter TF FOV (that is the worst case), depending on wavelength. This accuracy is enough for most purposes, since the accuracy of the TF tuning is of ≈1-2Å. However, were more accuracy required, the following full expression can be used instead:

$$\lambda(r) = \lambda_0 \left[\sqrt{1 + \left(\frac{f_{GTC}}{f_{Coll}} r \right)^2} \right]^{-1} = \lambda_0 \left[\sqrt{1 + 1.5904 \cdot 10^{-3} \left(\frac{r}{\text{arcmin}} \right)^2} \right]^{-1} \qquad (3.16b)$$

since the measured focal lengths are f_{GTC} = 169888±2mm (Castro et al. 2007) and f_{Coll} = 1240.90±0.05mm (SESO 2006), where wavelength or temperature variations can be neglected.

The TF optical center is located at pixel (2118, 1966) of CCD1, including the 50 pixels of overscan, within the gap of the CCDs, and 20 pixels away from the right edge of the CCD1[4]. The wavelength observed with the TF relative to this point changes following Eq (3.16).

Users should be aware that the wavelength tuning is not uniform over the full field of view of OSIRIS.

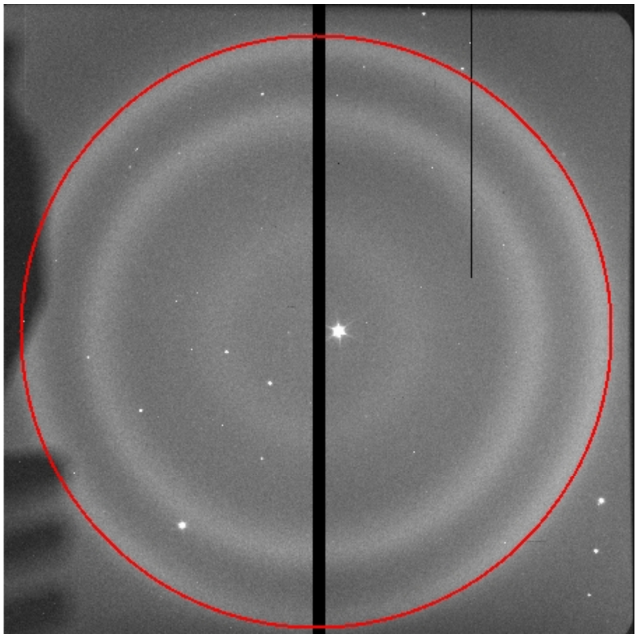

Figure 3.7.- Image with OSIRIS RTF tuned at 732.5 nm, showing the 4 arcmin radius where no contamination from other interference orders is assured. This is the operative FOV of the OSIRIS RTF.

[4] Note that those coordinates are unbinned coordinates, whereas the standard operation mode OSIRIS implies 2 x 2 binning.

The position of the objects in the Tunable Filter observing mode depends on the requirements of the PI since the value of the wavelength changes with the object's position in the FOV. The PI must indicate, in the Phase-2 form, the coordinates to which the telescope will be pointing and the CCD pixel position corresponding to these coordinates. By default, the pointing will be done at 15 arcsecs from the optical center of the system, in the pixel (100, 1966) at the CCD2[5].

3.3 OSIRIS Tunable Filter available widths

When working with the OSIRIS tunable filters the user needs to take into account two parameters: the observing wavelength and the required FWHM.

The range of operation of the OSIRIS Red Tunable Filter (the only available at the telescope) is from 651 nm to 934.5 nm (this range will be increased in future upgrades of the instrument).

It should also be noted that the practical use of the Red Tunable Filter is more restrictive than was originally anticipated. The minimum width achievable is 1.2 nm, that is imposed by the design of the order-sorting filters, in order to avoid contamination by other interference orders within the FOV. There is also a maximum width, depending on the wavelength range, as follows:

- 2.0 nm for $\lambda < 800$ nm
- 1.5 nm for 800 nm $< \lambda < 850$ nm
- 1.2 nm for $\lambda > 850$ nm

In addition to the information of the maximum tunable widths with the TFs as a function of wavelength (see table above) Figure 3.8 shows the available range of widths as a function of wavelength. The minimum width is 1.2 nm for all the wavelength to avoid contamination due to other orders in a circular FOV of 4 arcmin radius (this value is also the maximum usable width for wavelengths longwards of 850 nm).

[5] Note that coordinates are unbinned coordinates, whereas the standard operation mode of OSIRIS implies 2 x 2 binning.

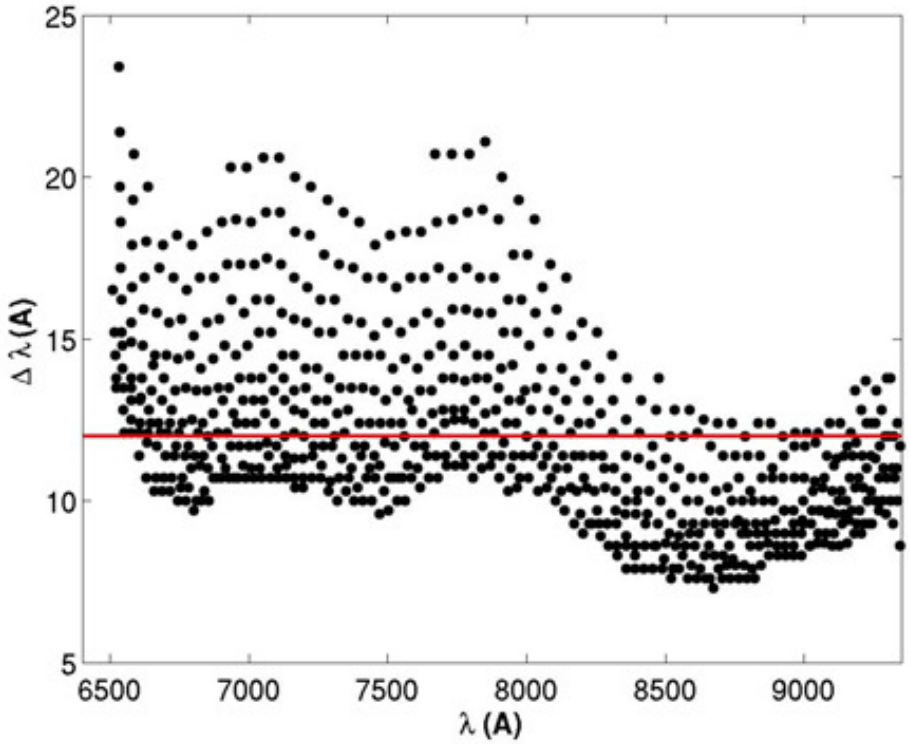

Figure 3.8.- Available TF widths vs wavelength for all the operative range of OSIRIS RTF. The minimun width achievable is shown as a red line, that is also the maximum width for $\lambda > 850$ nm.

When preparing TF observations it is highly recommended to use the TF Setup Tool available at: http://www.gtc.iac.es/en/pages/instrumentation/osiris.php. This tool allows to obtain the available widths for our wavelength of interest, as well as to define the corresponding Order Sorter Filter that has to be used for the observation (see Section 7).

3.4 Order Sorter Filters

The use of the tunable filters implies the utilization of order sorter filters (OS) in order to select the wavelength band that avoids confusion between different orders of interference of the Fabry-Perot. The observing wavelength defines which order shorter filter should be selected.

The available set of order sorter filters provides for a suitable filter for all wavelengths. Order sorter filters overlap in wavelength, but their working range ensures suppression of other orders. The OS are tilted 10.5 degrees with respect to TF and grisms, to avoid ghosts due to backwards reflections from the detector (the TF is not tilted and therefore suffers reflections. The description and characteristics for the complete OS filter set can be found in Section 7.

3.5 Calibrating the TF and Tuning accuracy

3.5.1 Parallelism

3.5.1.1 General considerations

TF parallelization consist in determining the X and Y values that keep plates parallel, and depends on Z and λ. OSIRIS TF Parallelism is very robust, and does not vary with time even when switching off and on again the TF controller. Hence, once the XY values for a certain Z and λ range are determined, they can be used around these Z and λ values from then on. Checking parallelism values from time to time is recommendable.

3.5.1.2 TF parallelization procedure

This parallelisation procedure for the TF is a task to be done during the day. The basis consists of maximizing the intensity of the light in the optical centre of the TF, when tuned to the wavelength of an emission line from a calibration lamp, while varying X and Y. This is the same procedure to be employed for wavelength calibration, but then varying Z. A lack of parallelism (XY) or a poor of wavelength tuning (Z) will reduce the intensity measured. This procedure is achieved by inserting a wide centred long slit, and stepping the charge on the CCD while varying X, Y or Z in a systematic fashion. The TF must be tuned to the wavelength of an emission line (i.e.: the Z must be the one corresponding to the emission line)

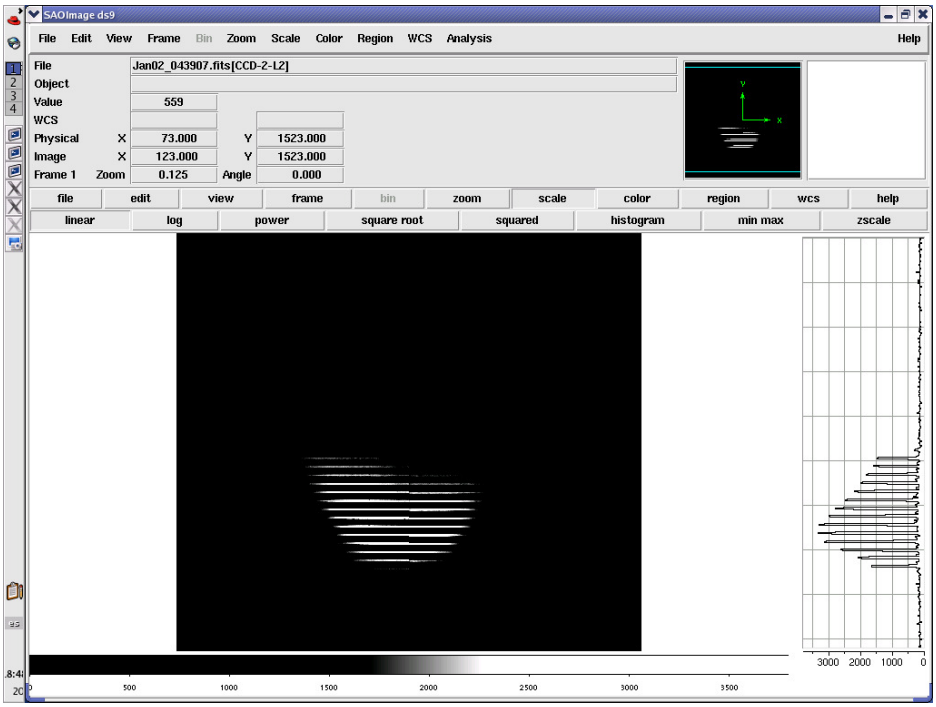

Figure 3.9.- Example of a X calibration image of 14 steps of 50 bits. Seen in the image is a slit illuminated by an arc lamp. The slit is centered on the field. After each exposure the charge is shifted downwards, the X setting of the TF changed, and a new image of the slit is taken. After a sequence of

several steps the CCD is read out, which results in a series of slit images as is shown here. N note that in the X calibration, the slit image intensities are not symmetric.

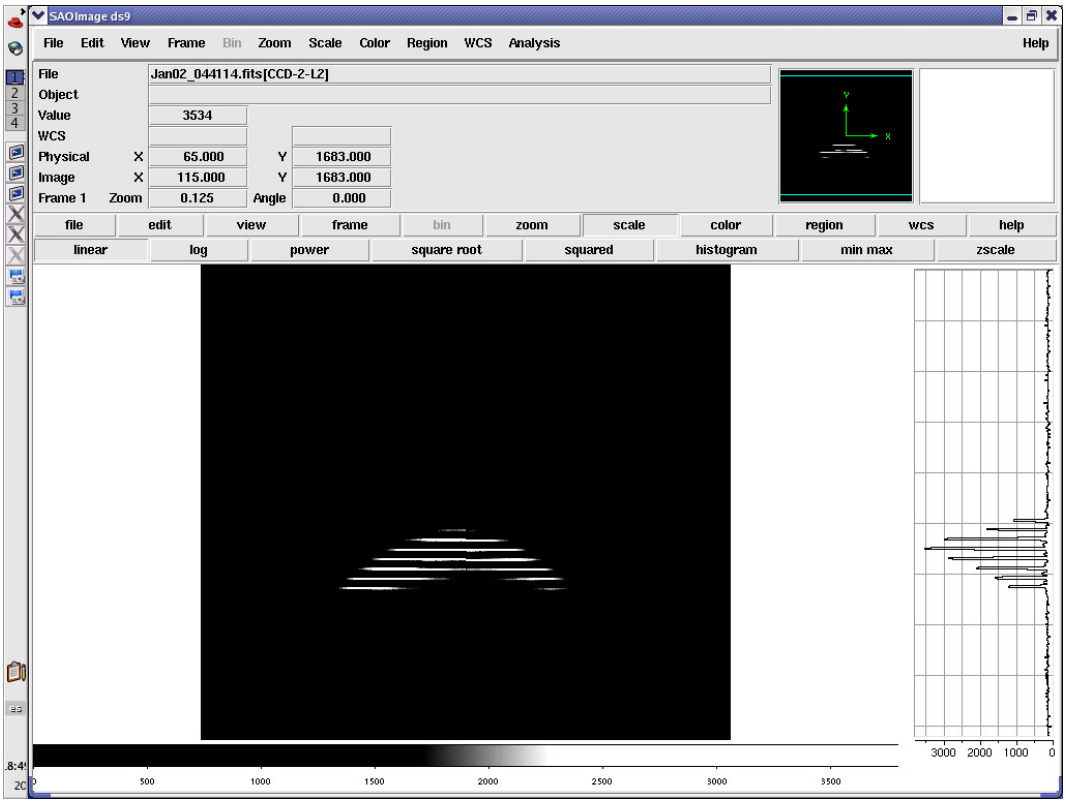

Figure 3.10.- Example of a Y calibration image of 8 steps of 25 bits.. Note that in the Y calibration, the slit image intensities are not symmetric.

3.5.1.3 Lack of parallelism

If the TF plates are not parallel the result will be:

- Distorted rings of the night sky emission lines and of calibration lamp lines.
- Asymmetric wavelength calibration (Z) scans, that are in opposite directions depending whether there is an excess or lack in X or Y values (see figure 3.11)
- Lower intensities of slit images in wavelength calibration (Z) scans
- Wavelength shifts

The main consequences for the data are:

- Transmission losses
- Wider FWHM and distorted spectral response

The XY resolutions used for parallelism calibration, 50 and 25 bits, respectively, have been chosen as the most convenient. Larger steps are not accurate enough and the XY errors affect wavelength and transmission as shown in the following table (approximate values to serve as example only) for the red TF.

± errors Red TF	λ shift (nm)	$\delta T/T$ (%)
ΔX=±50	0.1	4
	0.1	4
ΔY=±25	0.3	3
	0.2	0

It is important to keep a good parallelism better than 50 bits in X and 25 in Y. Again, note that Y is more sensitive.

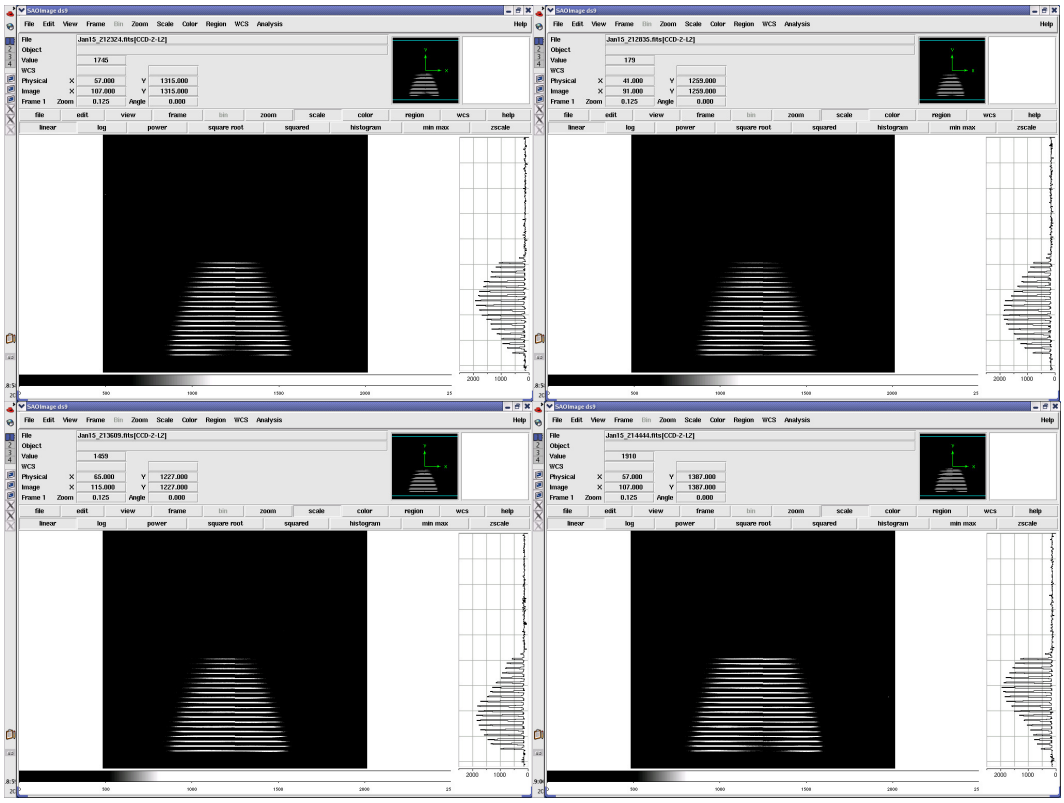

Figure 3.11.- Example of intensity losses and resulting asymmetric slit image intensity profiles obtained for the same Z calibration scan, in the following situations: top-left using Xbest+50 the Z scan is asymmetric and concave **below** the maximum intensity. Top-right using Xbest−50 the Z scan is asymmetric and concave **above** the maximum intensity. Bottom-left using Ybest+25 the Z scan is asymmetric and concave **above** the maximum intensity. Bottom-right using Ybest−25 the Z scan is asymmetric and concave **below** the maximum intensity.

3.5.2 Wavelength calibration

3.5.2.1 General considerations

Parallelization is a day-time procedure, because it is very stable in time and even with temperature changes and instrument rotation. Wavelength calibration, on the other hand, is a nightly procedure, since the Z-λ calibration depends upon many factors, and the calibration must be checked during the night, even for the same wavelength and order.

The wavelength calibration consists of establishing the relation between Z values in bits and the wavelength. This relation is non-linear enough, so that a linear approximation can be deemed valid only locally. Through tests of the TF carried out under controlled environmental conditions the relation between Z and wavelength has been derived for every order and through the full wavelength range that each TF can cover.

Extensive tests show that The λ-Z curve may be offset in Z by a constant factor, depending on the environmental conditions with a precision of 5 bits in Z (i.e.: better than 0.1nm). However, it is necessary to determine the offset for Z mimicking as closely as possible the true observing conditions. So in essence, wavelength calibrating the TF consists of determining this offset. This is done at the telescope by using a calibration lamp of the ICM.

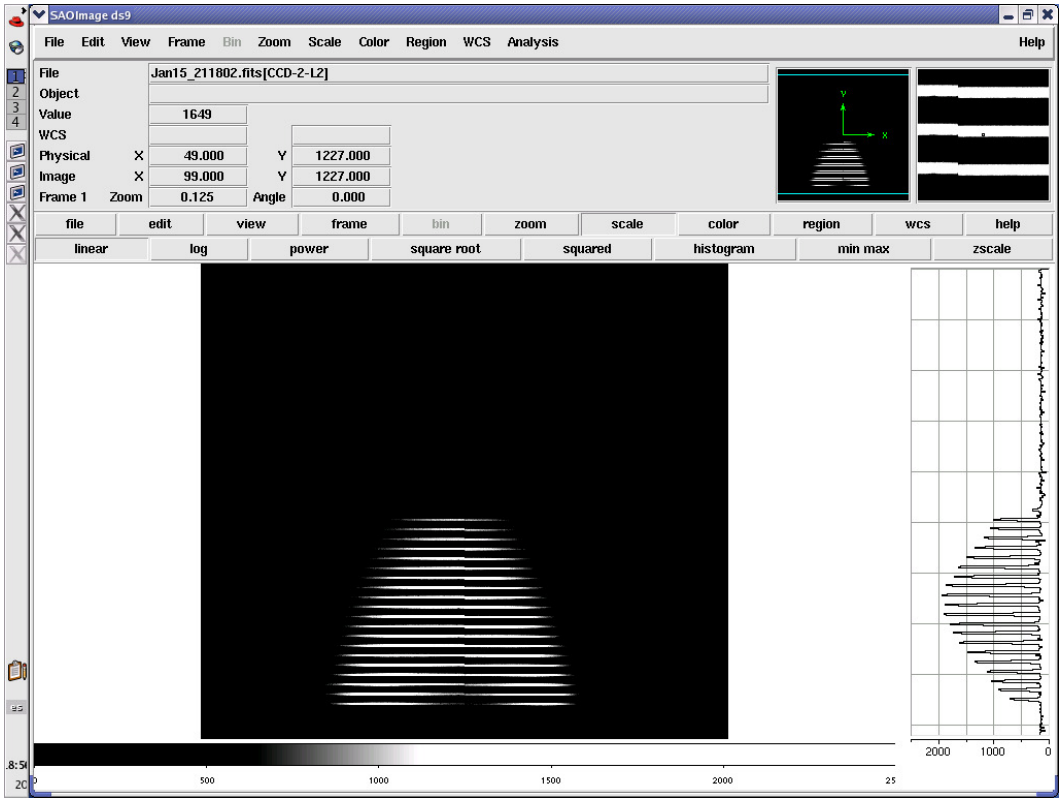

Figure 3.12.- Z calibration scan. 20 slit images can be seen. The first one is the bottom one. The tuning lies between image 11 and 12 as can be appreciated both from the maximum intensity and symmetry. Non symmetric intensities are suspicious of lack of parallelism.

3.5.2.2 Calibration using the ICM

The calibration procedure using the ICM has already been described within the parallelization procedure of the previous section. An accurate wavelength calibration can be obtained only after parallelization, i.e.: determining the best XY values for the given range of Z and wavelength.

Wavelength calibration depends, at least, of the following:

- Humidity. This is potentially an important factor, but since the instrument is flushed with dry air[6] its effect is for practical purposes insignificant.

- Temperature. This produces a highly non-linear effect where the etalon undergoes several phases of different variations. ET100 are quite large and take up to three hours to stabilize versus temperature changes. However this is not as serious as it seems, since implies only calibrating more frequently, depending on the history and the temperature gradient. It has been demonstrated to be safe operating with TF temperature gradients of at least 0.6ºC/hour, produced by temperature differences between TF and telescope of several degrees, as long as calibration is checked every 20 or 30 minutes. When the temperature gradient is of the order of 0.1-0.2 ºC/hour the tuning can be considered stable for at least one hour. Telescope gradients are normally far smaller In the future the instrument control system will take care of this effect at user's request.

- Instrument rotator angle. The calibration of the TF is highly dependent on the angle of the rotator, and hence on the orientation of the TF. We can find differences of up to 40 bits (~8A) between two rotator positions (see fig below). In order to avoid this we define for TF operation the following useful range ($-160° < \theta < -40º$ and $50º < \theta < 160º$). This range ensures a stable calibration accuracy of ±0.1nm and, if the rotator is moving less than 10°, the calibration can be considered virtually unchanged, with the precision given by the self-calibration (± 0.02nm = 1 bit).

  During the normal operation the observer predicts in advance, using the coordinates of the object and its instrument position angle, the position of the rotator to a specific time in order to ensure that the observations are performed in the useful range.

  This variation is independent both of wavelength and distance between plates (Z).

- TF history: if plates collide, the TF calibration might change. This is unlikely to happen since the Z range has been limited to safe values.

[6] However, caution must be taken when opening the instrument for changing filters or masks shortly before observations. See environmental conditions in user manual.

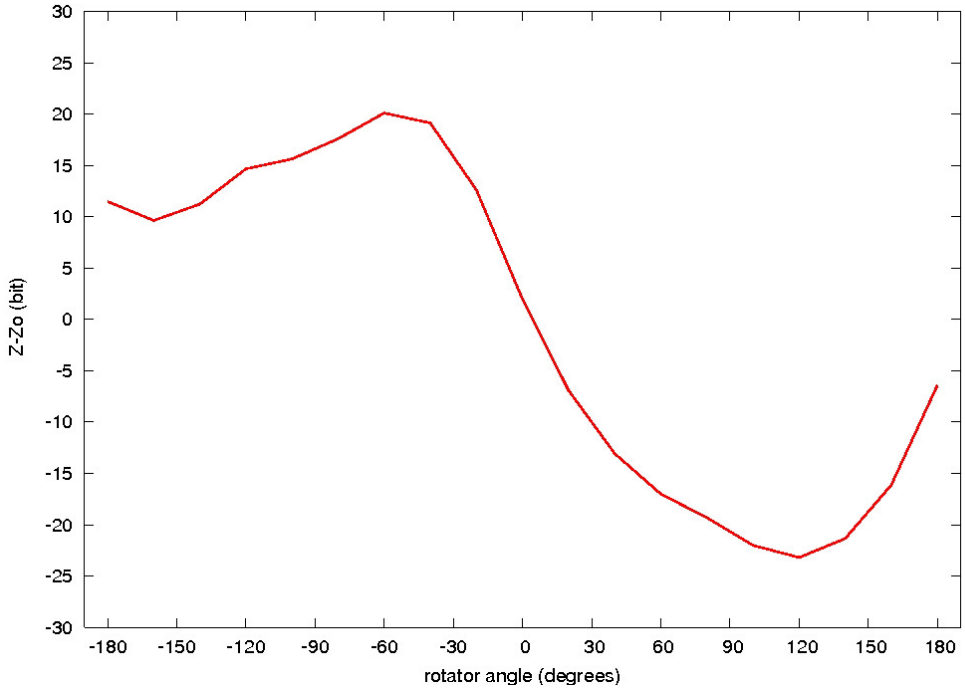

Figure 3.13.- Variation of the TF tuning (Z) with the rotator angle.

All those factors produce day to day variations in the TF calibration. For this reason the TF has to be calibrated before every observing block.

3.5.3 Checking the calibration by using night sky emission lines

The OH group produce relatively strong emission lines, specially redwards of 700nm. These are a nuisance in broad-band and narrow-band imaging as they are for long-slit spectroscopy. However, they happens at precise wavelengths and with definite relative intensities and can be used for calibrating spectra or, as in this case, the tunable filter. Since the FOV is fully illuminated by these emission lines, rings are produced. Knowing the wavelength of the emission line, the radius of the ring, that can be obtained using ds9, the tuned central wavelength can be derived.

As a rule of thumb, for a wavelength drift lower than 0.1nm, the variation Δr of the ring radius r should be, in the worst case:

$$\frac{\Delta r}{r} \leq 0.02 \qquad (3.17)$$

For better accuracy,

$$\frac{\Delta r}{r} \leq \frac{n}{2\Delta\lambda}, \tag{3.18}$$

where n is the number of nm of the allowed drift, and $\Delta\lambda$ is the wavelength variation in nm from the centre of the TF (λ_c) to the ring (Eq. 3.16),

$$\Delta\lambda = -7.9520 \cdot 10^{-4}\, \lambda_c r^2, \tag{3.19}$$

with the radius r in arcminutes.

If the ring radius varies in more than the tolerated value, the Z must be changed. If r increases, the Z must decrease and vice versa. This

The above expressions can be used for and external check of fast recalibration without using the calibration lamps. However, it is advisable to use the calibration lamps to avoid errors from a tired and sleepy user.

For a good sky line map, the reader is referred to Hanuschik (2003), that can be found on-line at http://www.eso.org/observing/dfo/quality/UVES/pipeline/sky_spectrum.html.

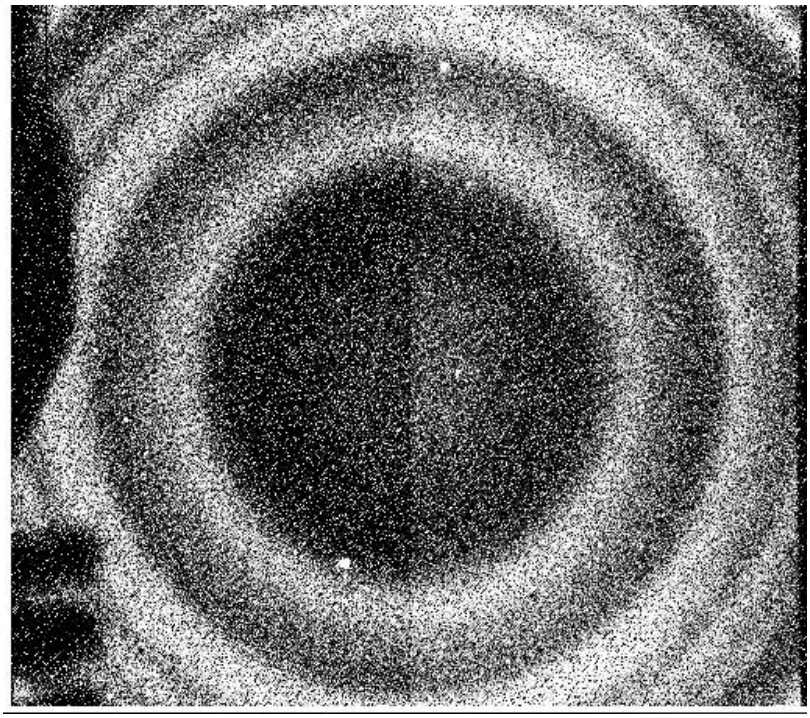

Figure 3.14.- Sky ring at 894.35 nm with the OS 878/59 with FWHM 1.21 nm, tuning the TF at 898.2nm for obtaining a ring radius of ~1100 pixels. The exposure time is of 120 s.

3.5.4 Tuning accuracy

The theoretical tuning accuracy is 0.02 nm in wavelength and FWHM as provided by the CS-100 etalon controller (in most cases this is the typical value of 1 bit in Z). The real accuracy in practical terms is driven by the wavelength calibration accuracy, that can be of the order of 0.1-0.2 nm.

3.5.5 Tuning speed

The tuning can be changed in an interval between 10 to 100 ms, depending on the change in Z. For large Z differences, the TF control system automatically moves the etalon in steps to avoid "out of range" failures. For fast modes it is advisable limiting the range of Z movement to the minimum (hundreds).

3.6 Observing with OSIRIS Tunable Filter

3.6.1 Tunable Filter vs. Spectroscopy

For a complex instrument such as OSIRIS, with a wide variety of observing modes and sub modes, one of the concerns of the user is whether the chosen mode is the most appropriate for the observing program. Since tunable filter imaging is a relatively new, and not widespread mode, most confusions arise between the convenience of the use of this mode versus spectroscopy.

In brief, the main advantages of TF versus spectroscopy is the ability to flux calibrate the emission (a tricky issue in MOS and even in long slit spectroscopy: slit slicing the image, differential refraction, centring errors,…), and of obtaining 2D emission line maps for targets over the FOV, either extended or of small size. The main disadvantage is that only one wavelength can be observed at a time. The following table and the flux diagram below help deciding the most appropriate mode.

Tunable imaging	**Spectroscopy**
1 or few spectral lines	Wide spectral range (at low R)
2D spectral features	1D (long slit) or very small area (IFU)
All targets in FOV (high ρ fields)	Number of spectra per mask limited
Reliable flux calibration	Uncertain (LS, IFU), unreliable (MOS) flux calibration
Low spectral resolution	Velocity fields & line profiles (at high R)
Approximate redshift should be known	Redshift knowledge not required
Position not required (survey) On-the-fly observations enabled. For ex: Galaxy clusters TF pre-imaging avoid IFU mosaic	Position required (pre-imaging. This introduce biases) Drilling masks overheads

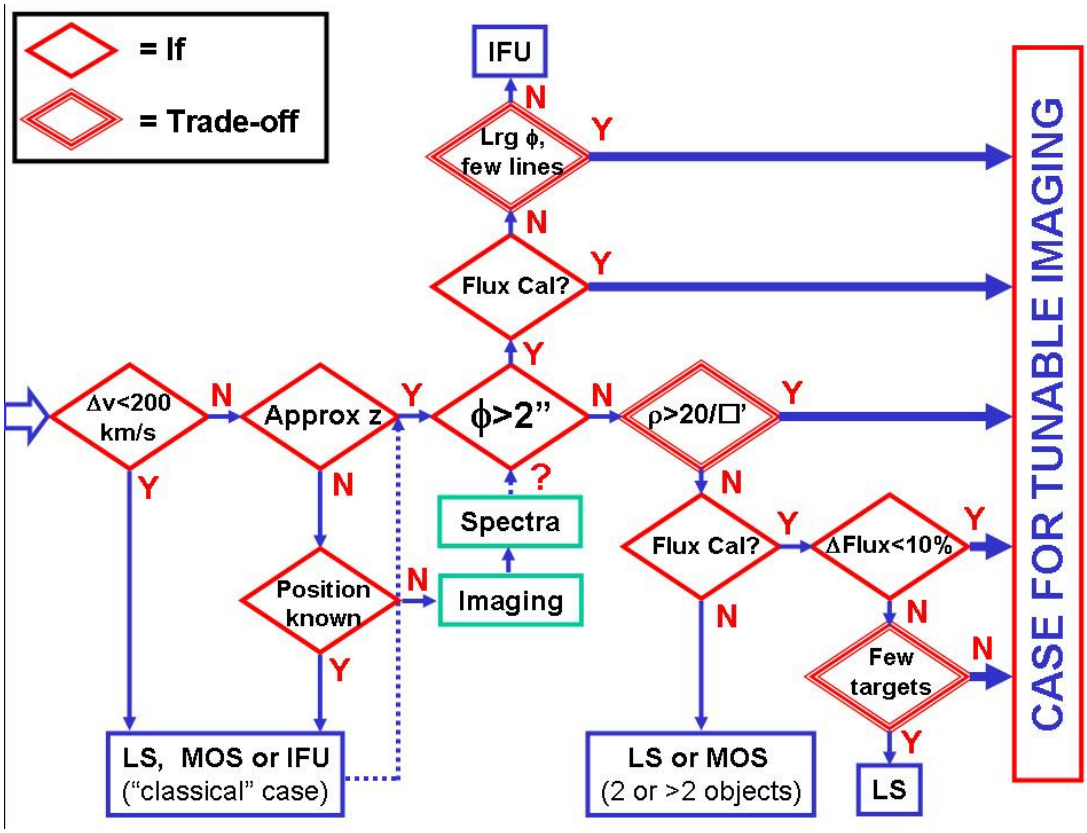

Figure 3.15.- Tree for deciding the most appropriate mode: TF versus spectroscopy. Δv is the line width or velocity dispersion, ϕ the target diameter, ρ the density of targets, and ΔFlux the error flux required.

3.6.2 Observing Strategies

The observing strategies for a TF are driven by the following instrumental effects:

1. The spectral response of the TF: more peaked and with more wings than a Gaussian or a squared 5-layer interference filter (Figure 3.5
2. The diametric ghosts
3. The centre to edge wavelength variation

and affects the way to design an observation depending on the characteristics of the sources:

- Photometric accuracy requested. **Please note that from now on we will refer to photometric accuracy of instrumental origin, not due to readout or photon noise**.
- Possible neighbouring lines to the one studied

- Velocity field or line width of the target
- Size of the target
- Redshift of the target

playing with the possible variables:

- TF central wavelength for your ON and OFF images
- TF FWHM
- Position of the source in the FOV
- Rotator position

These points mark the difference with respect to direct imaging with conventional filters. In other words, in tunable imaging the design of an observation is extremely important, as is the observing procedure is, otherwiseeasily uselass data can be the result.

In the following sections we provide derive recommended observing strategies depending on the type of sources, and the scientific aims, by explaining the impact of the previous parameters.

3.6.2.1 Selecting off-band wavelengths

3.6.2.1.1 Continuum subtraction

In line imaging, two images are usually required: the on-line image and the off-line (or continuum) image. The on-line image has line plus continuum photons and the off-line only continuum photons, to be subtracted from the on-line image to give the emission line (continuum free) image.

This can be done in two ways:

1. Using the TF for line and continuum has the advantage that the spectral response and FWHM are identical, and that you can select the continuum as nearby as desired from your line, thus alleviating possible continuum variations with wavelength. It is even possible, using the technique of shuffled exposures (Section 6.1.1.1) to on-line averaging continuum on both sides (blue and red) of the line and averaging possible seeing and atmospheric variation. In this way it is possible to achieve a very good continuum and sky subtraction with a direct pixel-to-pixel difference between your on-line and your continuum image. However, TF have quite narrow FWHM and hence the exposure times are quite large.

2. Using a medium band (and OS) or broad band filter (Sloan-SDSS). In this case continuum subtraction is not as good, and certainly not as direct, and must be faced with

caution. Since the continuum filter is tens of times wider that TF, the exposure times required are reduced accordingly.

If the TF is to be used for continuum subtraction, the TF tuning of the off-band has to be chosen so that no or few emission enter into the continuum filter. This is driven by the photometric accuracy required via the following expression, derived from Eq. (3.14),

$$\frac{|\lambda - \lambda_0|}{\delta\lambda} = \frac{1}{2}\sqrt{\frac{1-T}{T}} \tag{3.20}$$

This equation can be interpreted, in this case, as providing the transmission T, normalized to unity, of your continuum filter, tuned at λ_0 and of FWHM $\delta\lambda$, at the wavelength λ of the on-line tuning.

For example, let assume that the continuum must be chosen with a contribution from the emission line lower that 5%. Then, for a given FWHM of say 1.8 nm, the tuning of the continuum must be placed 4nm away from the line tuning. Of course wider FWHM require increasing the wavelength difference between on and off-line tunings.

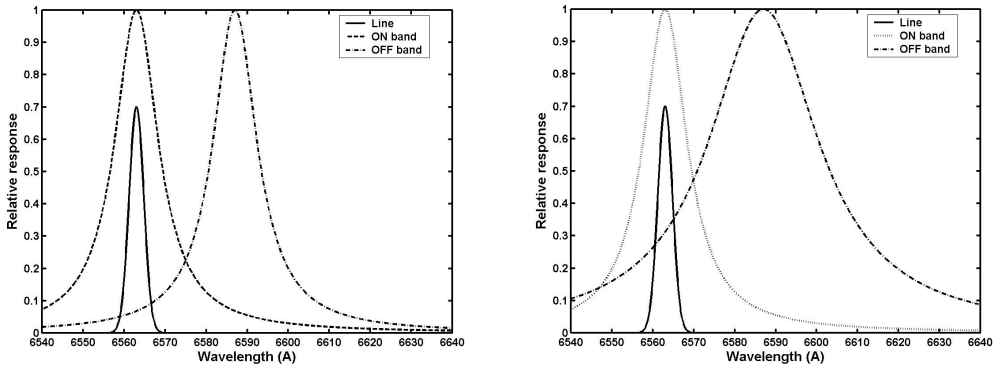

Figure 3.16.- Left: A proper tuning of the off-line wavelength minimizes contribution from your line to the continuum according to Eq. (3.16). Right: Increasing the FWHM of the off-line tuning will require increasing the wavelength difference between on and off-line wavelength tunings. The distances are larger than expected since the TF spectral response has more wings than a standard interference filter.

3.6.2.2 Deblending lines

Equation 3.20 can also be used for deblending lines. Known the redshift, one tuning for each line can be observed. From the line separation and the FWHMs of the tunings, the contribution of the other lines to each tuning can be estimated, and corrected simply via simultaneous equations system.

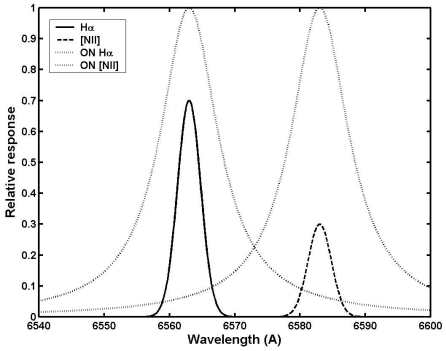

Figure 3.17.- Hα can be deblended from [NII]658.4nm if the redshift or Doppler shift is known, via defining a simultaneous equation system with TF transmissions derived from the TF FWHM and line relative positions.

3.6.2.3 On-line FWHM selection

The TF FWHMs are quite narrow, and nearly Gaussian from peak to half transmission. Then the line width must be quite narrower than the TF FWHM or otherwise some flux will be lost. It can be easily demonstrated that, assuming Gaussian line profiles, the flux error can be approximated by,

$$\text{Flux error}(\%) = \frac{1}{2\ln 2}\left(\frac{\delta l}{\delta \lambda}\right)^2 \tag{3.21}$$

where $\delta\lambda$ is the TF FWHM and δl is the line width. For example, observing a line with the same width than the TF result in loosing ~28% of the flux (a more precise calculation gives 36%).

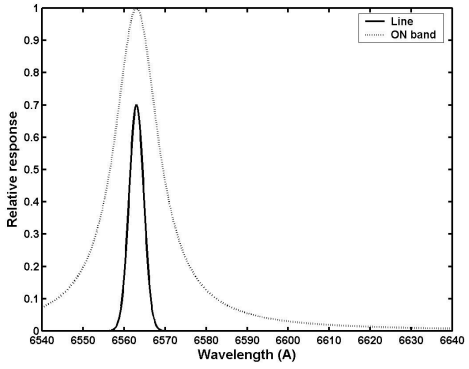

Figure 3.18.- Comparison of TF and line profiles.

The following table can be used for selecting to most suitable FWHM according to the expected line width. Please note that they are approximate values.

$\delta\lambda/\delta$	**Flux error (%)**
1.0	36
1.5	22
2.0	14
2.5	10
3.0	7
3.5	5
4.0	4

Table 3.1.- Approximate error fluxes depending on line width (δ) and TF FWHM ($\delta\lambda$).

For example, the typical velocity field of a spiral galaxy (250 km/s) at zero redshift, would require TF FWHM of at least 1nm at Hα, for an error smaller than 5%[7], and the minimum FWHM recommended for the red TF is of 1.2nm. Hence this is not a problem in this case, but it might be for [OII]372.7nm (blue TF) or when observing objects at significant redshifts where the line widths are expanded[8] by the factor (1+z). Since the range of available FWHM are quite limited, if a certain photometric accuracy is required and the needed FWHM cannot be obtained, it is possible to synthesize a wider FWHM by summing images of a scan (see further on in this document).

3.6.2.4 Deciding target position and orientation

The presence of ghosts and the centre to edge wavelength variation drive target position on the OSIRIS FOV.

To avoid excessive wavelength variation, the target should be as centred as possible, but it cannot be placed right in the centre because, aside of falling into the gap between detectors, a mirrored ghost image of the source will overlap with the real image. This might be acceptable in some cases, for example if the user is interested in radial dependences only. However, in general, the target should be placed near the optical centre of the TF, but fully off it. Near the TF centre but on CCD2 (the rightmost) is a convenient location.

If the object is elongated, the wavelength variation can be minimized by turning the GTC rotator to align the major axis of the target perpendicular to the radial direction for the TF optical centre (Figure 3.19).

However, since the target is not at the centre of the TF, the TF must be tuned to the red of the line, so that the target is observed at the wavelength of the line required. This can be evaluated using Eq. 3.16. For example, a target of a diameter of 2 arcminutes should be placed somewhat more than 1 arcminute from the centre. Then the wavelength corresponding to the zero redshift Hα at this position is not 656.3 nm but 656.8 nm.

---

[7] Please note that 250km/s is the FULL velocity field, not the velocity field at FWHM.

[8] Please do not forget this “detail”.

Even with the above strategy, and unless the target is very small, the wavelength dependence across the FOV will produce that some parts of the target are observed at different wavelengths. The induced photometric error can be evaluated using Eq. 3.16 and 3.20. For example, for the same example above, the wavelength of the edge of the target near the TF centre is 656.8 nm and the wavelength at the edge of the target in opposite direction is 654.7 nm. The photometric errors induced by this line decentring are, respectively, 7% and 45% (from Eq. 3.20) if a FWHM of 3.5 nm is assumed. Then, it is possible to choose a TF tuning wavelength that minimizes this variation: when the wavelength difference at both edges of the target is the same. For example, tuning at 657.3 nm gives a photometric error equal at both edges of the target and of the order of 25%. Of course **the velocity field of the target must be taken into account in this procedure** since it increase the photometric errors (if the velocity field is known, it is possible to adjust the target and rotator position to minimize it).

Were this photometric error too much, it is possible to synthesize a wider FWHM by adding TF scans (see 3.6.2.7).

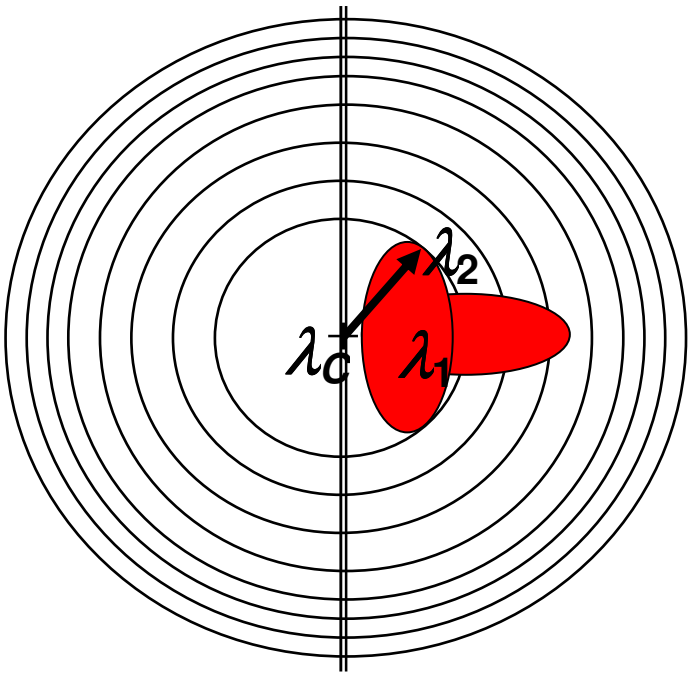

Figure 3.19.- Changing rotator angle is useful for minimizing the wavelength variation across the target.

3.6.2.5 Removing ghosts, cosmic rays and cosmetics

One feature of etalons is that they produce ghosts. In any astronomical instrument, the detector is a source of light: any light that is not detected or absorbed is reflected. This light reflected by the detector follows the same optical path in opposite direction, entering the etalon and reflecting in the most reflective surface, i.e.: that of the reflective coating of the etalon cavity, going back and hitting the detector in a place symmetric with respect to the optical centre of the etalon. This has three important implications for the observer

1. Diametric ghosts are symmetric with respect to the centre of the etalon (Figure 3.20), that in the case of OSIRIS is almost the centre of the OSIRIS field, in the gap between detectors at the line ~1966 (unbinned coordinates).

2. Diametric ghosts can be easily removed by the classical dithering procedure since moving the image in one direction shifts its ghost in the opposite direction with respect to the TF optical centre. When stacking up the images taking as reference the image of the target, all ghosts fall in different pixels and can be removed with average sigma clipping of similar algorithms

3. Only very bright, usually saturated sources, generate ghosts (Figure 3.20). Hence, unless very bright sources are in the FOV and their ghosts could spoil the image of the target, there are no need to worry about it (in OSIRIS, the integrated flux of the ghost images is less than 1.7% of the integrated flux of the main source).

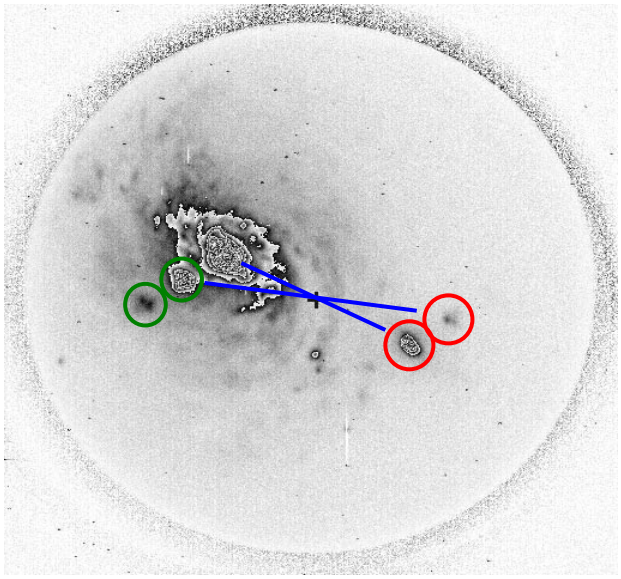

Figure 3.20.- Example of ghosts in a TF. The cross marks the optical centre. The red circles mark the diametric ghosts of the centre of the galaxy and that of an exponential ghost, while the green ones marks the exponential ghosts. The second exponential ghost does not produce a noticeable diametric ghost.

Exponential ghosts cannot be removed by dithering. Luckily OSIRIS TF does not have this kind of ghosts.

Of course ghosts drive the location of the target in the FOV, as is dealt in this document in Section 3.6.2.4. As stated above, ghosts can be removed using the same dithering method that removes for instance detector cosmetics. However dithering move the target in the TF FOV, i.e. it changes the wavelength at which the target is observed. This is specifically severe at the edges of the FOV, where the wavelength dependence with location is larger. There are several ways to alleviate this problem that will be described in the following subsections. But note that in many cases ghosts do not required to be removed since they can be seen only for very bright sources.

3.6.2.5.1 Field masking

Inserting a focal-plane mask that covers half the field and hides detector CCD1 avoids ghosts coming from that part of the field. In this case dithering is not necessary to detect ghosts.But obviously in this case only half the field can be used and therefore normally not an attractive option.

3.6.2.5.2 Azimuthal dithering pattern

When only one relatively small source is of interest, the dithering can be done following the circle of equal wavelength.

3.6.2.5.3 TF tuning dithering pattern

If several relatively small targets spread on the FOV are to be observed, it is possible to do a three point dithering where the TF tuning is changed to minimize wavelength variations at the edge of the TF FOV in **one direction**. Then different sections of different images can be combined. This is valid only when using tunable tomography.

3.6.2.6 Tunable tomography

3.6.2.6.1 Technique

Tunable tomography or TF scanning consists of obtaining a set of images of the same pointing at different consecutive wavelengths (Figure 3.21). The characteristic parameters are:

- Initial and final wavelength (or Z)
- Step in wavelength $\Delta\lambda$ (not equivalent to a constant ΔZ since the λ–Z relation is in general not exactly linear)[9]

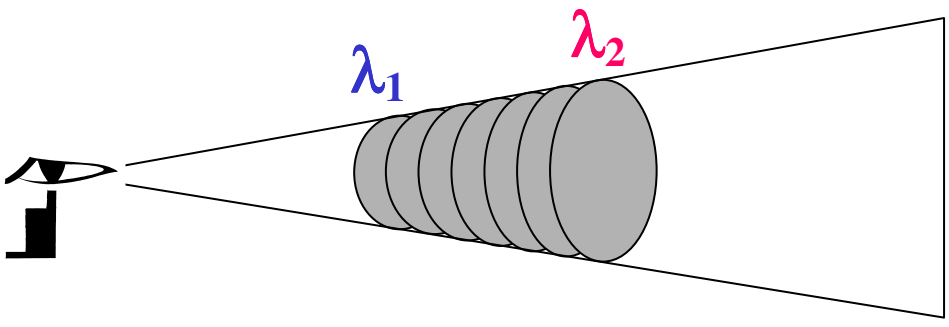

Figure 3.21.- Tunable tomography consists in scanning a wavelength range using the TF. For the same telescope pointing, a set of images at different wavelengths are taken.

[9] Please note that further on this document $\Delta\lambda$ is NOT the FSR of Eq. 3.5 and 3.7, but the scan step or wavelength step between consecutive exposures in tunable tomography.

The step must be carefully chosen since for a given wavelength range to be scanned, a step too fine will increase the observing time and overheads required, but a step too coarse would introduce larger photometric errors, that can be evaluated using Eq. 3.20, but now considering that the maximum error will be half the scan step (i.e.: in the worst situation an emission line would be located in the middle of a step),

$$\frac{\Delta\lambda}{\delta\lambda} = \sqrt{\frac{1-T}{T}} \,. \tag{3.22}$$

In this observing mode, the different images are not combined, but analyzed separately. Usually aperture photometry of the sources of each image provide "pseudo-spectra" that are used for identifying emission lines and determining its fluxes and Doppler shifts or redshifts.

In the case that the TF images are going to be used for continuum subtraction, the images of the same scan (or several of them added together) can be used for this purpose, as long as they are separated enough to achieve the required photometric accuracy based on TF FWHM, scan step and the number of images (Sec. 0). This might require obtaining some additional images at the end and/or the beginning of the scan (at the end and beginning would allow averaging possible continuum variations).

Examples of applications of this method are:

- Scanning a spectral region for de-blending neighbouring lines
- Scanning a target looking for systems of high velocity faint or diffuse ionized gas
- Scanning blank fields searching for serendipitous emission line targets in a certain volume of universe determined by the FOV and the initial and final wavelength for every emission line detected
- Scanning the velocity field of galaxy clusters allows determining emission line objects and even the cluster velocity dispersion
- Scanning a certain emission line of a target of inaccurate redshift

3.6.2.7 Band synthesis technique

3.6.2.7.1 Technique

As before, but in this case the final destination is not analyzing images separately but adding them together providing a "wider" synthetic filter (Figure 3.22).

The main difference is that in this case one additional image must be obtained at the beginning and at the end of the scan (in a conventional filter equivalence this would be similar to the zone where the spectral response is varying and the flat zone has not been reached yet), and that the photometric accuracy refers to the wiggles generated when adding

the images (Figure 3.22). Alternatively instead of obtaining this "extra" images, it is possible to correct them by multiplying by the appropriate factor > 1 that can be easily calculated.

As a guideline, the photometric accuracy that can be achieved as a function of the scan step is summarized in the table below (Figure 3.22).

$\Delta\lambda/\delta\lambda$	$\delta I/I$ (%)
1	20
2/3	5
1/2	2

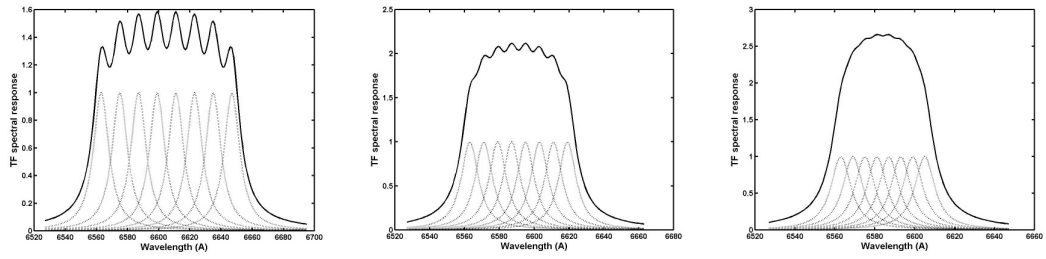

Figure 3.22.- Theoretical examples of the band synthesis technique. Left: a scan step equal to the TF FWHM gives photometric uncertainties of ~20%. Middle: a scan step 2/3 of the TF FWHM gives photometric uncertainties of ~5%. Right: a scan step equal to half the TF FWHM gives photometric uncertainties of ~2%. The first and last images are either not used or corrected via the corresponding multiplicative factor.

Of course the images obtained can be used both for Tunable tomography and band synthesis. For example: in tunable tomography, images can be combined in, for example, pairs or terns to increase S/N in the case of faint targets (depending on line widths and TF FWHM), or all added together to serve as pseudo-broad band image for target detection.

Examples of applications of this method are:

- Scanning the velocity curve of a large spiral galaxy compensating for the centre to edge wavelength variation
- Scanning a wide spectral line (i.e.: that of a high redshift galaxy or a QSO)

3.6.2.8 Summary

3.6.2.8.1 Sources of instrumental photometric errors.

The sources of photometric errors of instrumental origin (again, please note that contributions of readout or photon noises must be considered aside) are:

- The FWHM of the TF, depending on line width (driven by velocity dispersion, velocity field, peculiar velocities, and redshift). This can be evaluated using Eq. 3.21 or Table 3.1, and if appropriate can be corrected using the method of band synthesis (Sec. 3.6.2.7).

- The contribution of the line to the off-band or to other lines to the on-line image. Can be evaluated using Eq. 3.20

- The wavelength variation across the target. Depends on the size and the velocity field. Can be evaluated using Eqs. 3.16 and 3.20. If required can be corrected using the method of band synthesis (Sec. 3.6.2.7).

- Dithering that varies the wavelength of pixels of the source from one image to a dithered one. Can be evaluated using Eqs. 3.16 and 3.20. If required can be corrected using the method of band synthesis (Sec. 3.6.2.7) or choosing a suitable dithering pattern combined with TF tuning (Sec. 3.6.2.5.2 and 3.6.2.5.5).

3.6.2.8.2 Preparing an observation: a checklist.

According to the previous sections, depending on the scientific program, the line to be observed, the type of target, its size, velocity field or velocity dispersion, redshift of Doppler shift, accuracy of this shift, and the number of targets, it is necessary to determine:

- Position of the target(s) in the FOV

- Orientation of the detector on the sky

- Wavelength to be tuned (in the centre of the TF)

- Dithering pattern to be used

- Technique to be used: single exposures, shuffled images, fast photometry, TF tomography or band synthesis

- FWHM to be used. Use calculator for exploring possibilities. This might drive reconsidering the technique to be used if FWHM is too narrow.

- Wavelength range to be scanned (for TF tomography or band synthesis)

- Exposure time

- Use of TF, OS or broad-band filters for continuum subtraction

3.7 Spectrophotometric standards for TF flux calibration

The TF flux calibration is done using standard spectrophotometric stars as usual, using the same settings as for obtaining the science data, that is, an image from the standard star at each of the wavelengths and with the same TF FWHM used for obtaining the science images.

The complete list of spectrophotometric standard stars for TF flux calibration can be found in Section 10. They are the same that are used in Long Slit Spectroscopic observing mode.

3.8 OSIRIS RTF global efficiency

The graph below shows the overall photon detection efficiency of OSIRIS RTF at GTC, including the contribution both of the telescope and instrument optics system (Sánchez-Portal et al. 2010). For comparison, the points show the global results for the Sloan filters r', i', and z'.

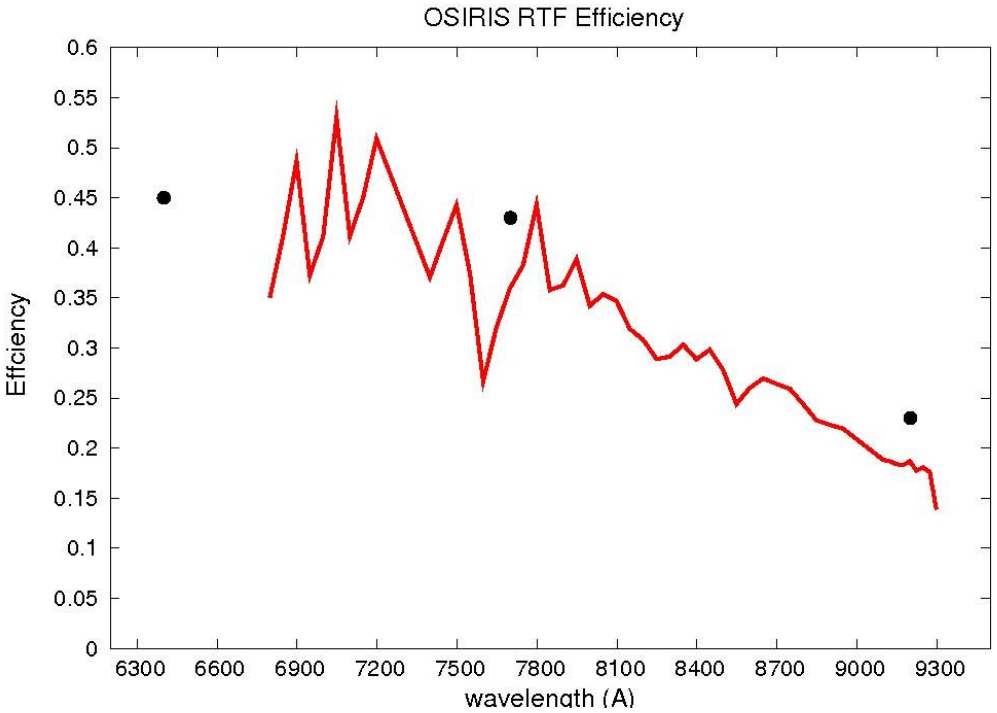

Figure 3.23.- Overall photon detection efficiency of GTC and OSIRIS with the RTF. The peaks in the TF sensitivity function are due to the atmospheric absorption bands, that can be traced using the RTF in small $\Delta\lambda$ steps.

3.9 Post-processing TF data

The TF data reduction procedure is like that of narrow-band direct imaging: requires de-biassing, flat fielding, combining dithered images (if required), flux calibration using aperture or PSF photometry of spectrophotometric standard stars, and continuum subtraction (if required).

The main differences with narrow-band direct imaging are:

- For removing cosmic rays, cosmetics or sky rings, only dithered images at the same tuning (Z) can be combined[10], taking care of the possible wavelength shift of the dithered images, specially at the edges of the TF FOV (see Sec. 3.6.2.5 for some hints on alleviating this problem)

- Depending on the type of sources, subtracting continuum images might be unnecessary if a pseudo-spectra is obtained by aperture photometry of the sources observed at different contiguous wavelengths (Sec. 3.6.2.6)

- Images of the same field at different contiguous wavelengths can be combined in the band synthesis technique (Sec. 3.6.2.7)

- In the red spectral domain sky rings appear (see Sec. 3.9.2).

3.9.1 Calibration images

3.9.1.1 Bias

Images to correct for the electronic bias of the CCDs should be obtained and applied as usual. These same readout speed and binning must be selected.

3.9.1.2 Flat fields

During the normal operation of OSIRIS at GTC, flat fields for the TF observations are obtained using dome flat fields, with the TF tuned to the same wavelengths of the science observations. It is practically impossible to get a series of enough sky flat fields at all the wavelengths requested for a typical program due to time limitations.

Some features that can be observed at some wavelengths in the TF dome flats are also present in sky flat images, hence they are not due to particularities of the dome illumination. We consider that the dome flat fields are adequate for their purpose and little is gained from using TF sky flat fields. The main features in the illumination pattern seen in the dome flats are also noted in the science images.

---

[10] As images obtained using different conventional filters would not be combined for this purpose either.

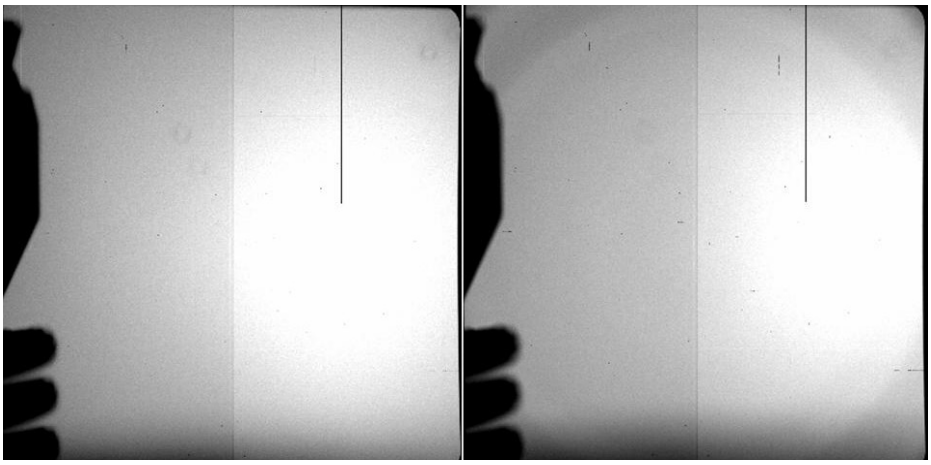

Figure 3.24.- TF dome and sky flat at 715.0 nm, where the same features can be observed.

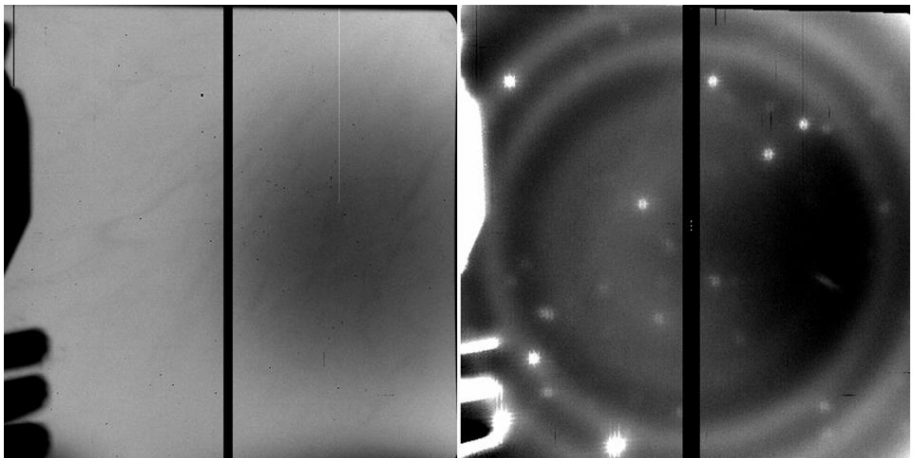

Figure 3.25.- TF dome flat at 660 nm, and a sky image at 660 nm obtained from an artificially dithered raw science image

3.9.2 Night-sky emission line rings

The OH atmospheric emission lines are observed through the TF as rings (Figure 3.14), due to its centre-to-edge wavelength variation. They are equivalent to the fringing observed in direct broad band imaging and, like it, are an **additive** effect. They increase the background photon noise in the zones affected by the ring, thus reducing the S/N in these zones.

Sky rings not necessarily require correcting as long as the ring is not on the target, and the target is not too faint. Nevertheless, if a correction is required, there are several ways to proceed:

- If the targets are not very large, a superflat with the sky ring pattern can be obtained by combination of dithered and smoothed images, even of different pointings: (i) smoothing the dithered images to be corrected using a kernel that wipes small-scale structures (sources) but keeps large-scale structures (the rings), (ii) obtain the media of the combined smoothed **unmatched** dithered images using a rejection algorithm (the sources are not in the same position due to the dithering, but the rings does since their position depend on the wavelength tuned only). Even images of different pointings can be used as long as the wavelength tuned is the same. (iii) Subtracting the resulting superflat from the original images.

- Running, for example, SExtractor to remove sources thus creating again a superflat.

- Using specially devised programs for creating a synthetic ring image by fitting an azimuthal average of the image, and subtracting it

- Fitting a 2D surface to the ring, creating a synthetic ring image, and subtracting it

Synthetic ring images do not introduce photon noise in the final image, as the other methods does.

3.10 Medium Band Imaging with TF Order Sorters

The TF Order Sorter filters can also be used for direct image observations. Measurements made during the commissioning of OSIRIS (January 2010) have provided zeropoint values for some of the most significant OS. These values are given in absolute magnitudes (m_{AB}) at airmass = 1, using these measures of spectrophotometric standard stars.

OS	m_{AB}(standard)	Zeropoint
OS657	15.25 ± 0.05	27.86 ± 0.09
OS666	15.27 ± 0.05	27.72 ± 0.02
OS709	15.35 ± 0.05	27.89 ± 0.05
OS770	15.45 ± 0.10	27.73 ± 0.02
OS858	14.35 ± 0.05	27.58 ± 0.03
OS902	14.48 ± 0.05	27.07 ± 0.09

Please note that the OS are tilted 10.5 degrees to avoid ghosts due to backwards reflections from the detector, therefore, their central wavelength is shifted with respect to the nominal central wavelength with a drift in wavelength along the FOV following the tilting axis, that is approximately the detector gap. This is the same effect that was discussed in Section 2.1.2 for OSIRIS Sloan broad-band filters, but in this case the effect is more noticeable as the filters are narrower.

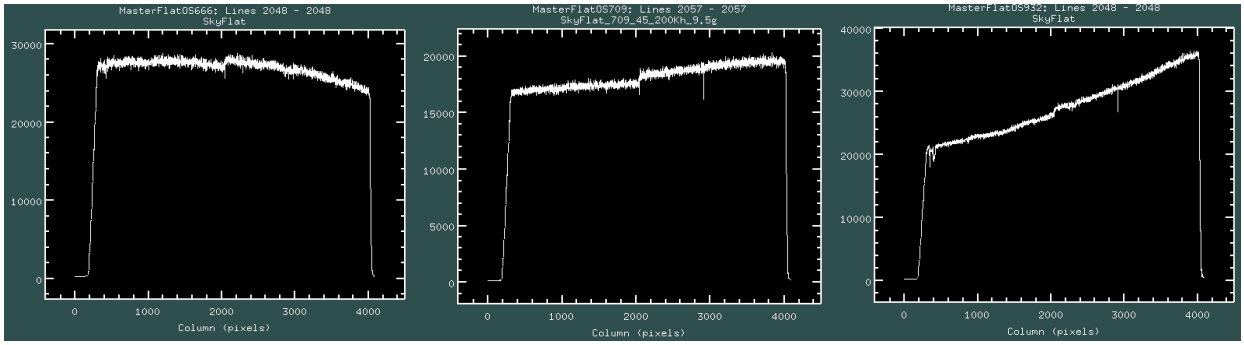

Figure 3.26.- Horizontal cut for three Sky Flat images taken with OS666 (left.), OS709 (center) y OS932 (right.). The intensity gradient observed is due to the combination of a different contribution of the Sky lines and a different sensitivity of the CCDs (from redder to bluer wavelengths)

For calibrating the data obtained with the OS filters when used in imaging mode, the spectrophotometric standards for both tunable filter imaging and long-slit spectroscopy observations can be used (see Table in Section 10). The spectral responses of each of the OS filters are available at: http://www.gtc.iac.es/en/pages/instrumentation/osiris.php#Red_OS

The OS high inclination also makes impossible to use two contiguous OS to produce a single narrower filter. This is due to internal reflections occurring in different layers of the filters that lead to the formation of ghosts. Their intensity and position in the field vary depending on the combination of filters that is, the position of the rotator, etc. This mode of operation is not offered.

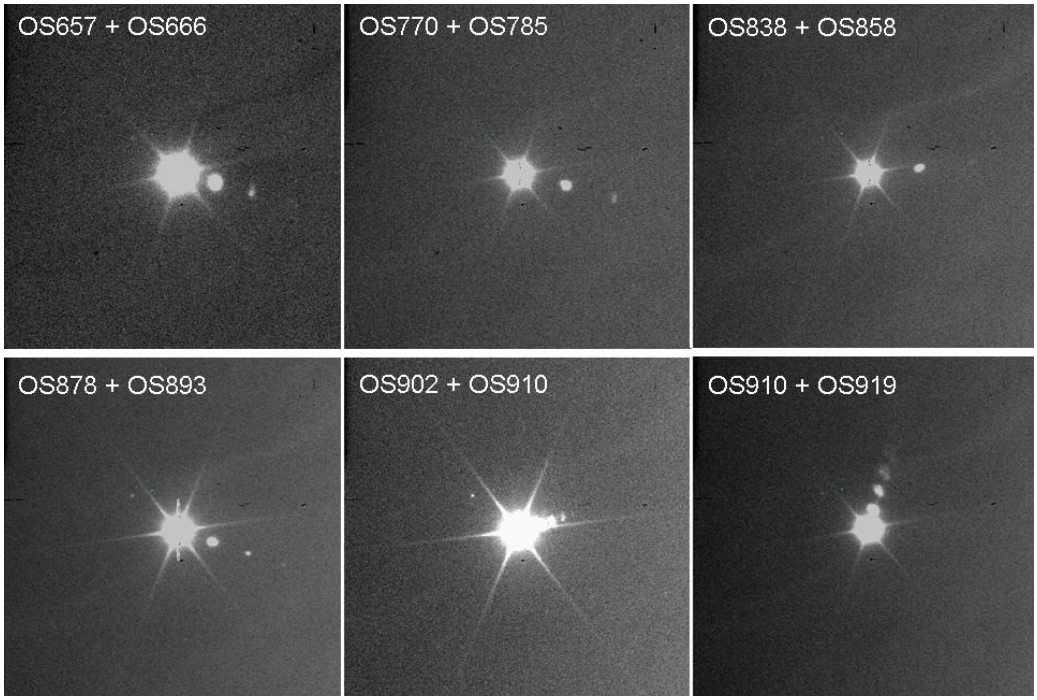

Figure 3.27.- Some examples of ghosts observed when using a combination of two contiguous OS.

4. LONG SLIT SPECTROSCOPY

OSIRIS facilitates long-slit spectroscopic observations. A selection of 8.67' long slits of different widths are available, which, in combination with a selection of dispersive elements in the collimated beam provides for efficient low to medium-resolution spectroscopy. Available slit widths are: 0.4", 0.6", 0.8", 1.0", 1.2", 1.5", 1.8", 2.0", 2.5", 3.0", 5.0".

OSIRIS has a wide variety of grisms and volume-phased holographic gratings (VPHs) covering low to intermediate resolutions, from R=300 up to R=2500. The following table summarises the resolutions and spectral ranges available (for a slit width of 0.6 arcsec). For the end-to-end efficiencies including telescope, instrument and detector, the measured transmissions measured so far are in Section 8.

ID	λ_c(A)	λ Range (A)	D[11] (A/pix)	R[9] (λ/Δλ)	Peak Efficiency	Type
R300B	4560	3000-10000	**2.48**	**360**	70%	Grism
R300R	6865	4800-10000	**3.87**	**348**	70%	Grism
R500B	4830	3440-7600	**1.77**	**537**	68%	Grism
R500R	7310	4800-10000	**2.44**	**587**	67%	Grism
R1000B	5510	3630-7500	**1.06**	**1018**	65%	Grism
R1000R	7510	5100-10000	**1.31**	**1122**	65%	Grism
R2000B	4780	3950-5700	**0.43**	**2165**	87%	VPH
R2500U	4025	3440-4610	**0.31**	**2555**	70%	VPH
R2500V	5210	4500-6000	**0.40**	**2515**	80%	VPH
R2500R	6590	5575-7685	**0.52**	**2475**	80%	VPH
R2500I	8740	7330-10000	**0.68**	**2503**	80%	VPH

For R higher than 1000, the spectral range covered is limited by detector size. Lower resolutions are limited by second order light. Red-optimized dispersers require the use of an order sorter filter (GR, see Figure 4.1) to suppress the second-order light.

[11] Measured at λ_c(A). Dispersion correspond to unbinned coordinates, hence in standard OSIRIS operation mode, the effective dispersion is 2*D.

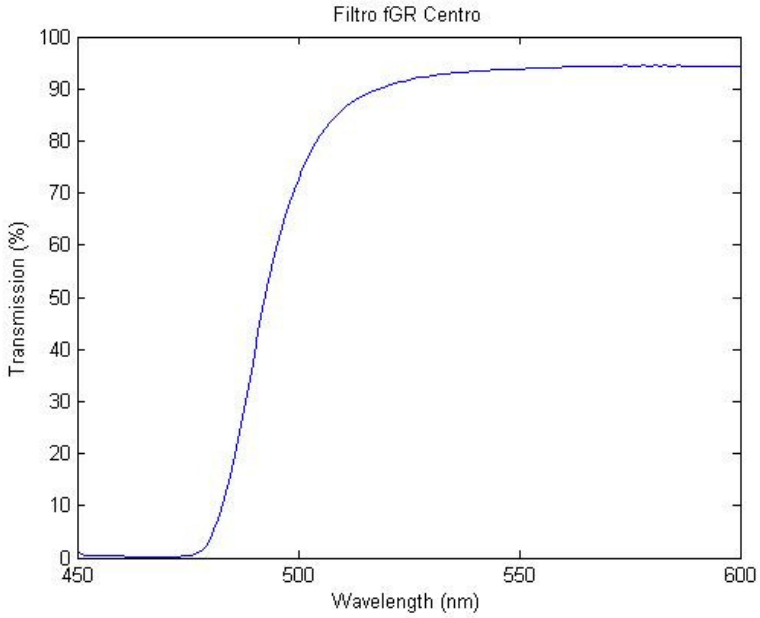

Figure 4.1.- Measured central spectral response of spectroscopic OS.

The spectral direction in OSIRIS coincides with the vertical direction on the detector, hence spectra are not affected by the gap between both CCDs.

4.1 Acquisition in Long-Slit Spectroscopic mode

In long-slit spectroscopy mode, point sources are centered on the slit at the coordinate X = 500 (X = 250 with binning) of the CCD2. This position minimize the amount of cosmetic effects of the CCD2 compared to those on the CCD1. On this area the distortion of the spectra is very low and sufficiently far from the central gap in order to allow a good sky subtraction.

To ensure accurate centering on the slit an acquisition image and a through-slit images are normally taken. During the observation, after the acquisition image is obtained with the target placed at the pixel X=500 in CCD2 an iterative process for slit alignment is employed until the object is well centered. This is verified by taking through-slit images.. For this reason the coordinates for the target in the acquisition and through-slit images can be slightly different.

4.2 Flexure

OSIRIS allows a very stable spectral calibration, with no significant drifts with rotator position (< 1 pix) thanks to its active collimator. Therefore, the calibrations for each observation can be taken at the beginning or at the end of the night regardless of the orientation of the instrument when the science observation is carried out. Figure 4.2 shows an example of the wavelength shift as a function of rotator angle, for two spectral resolutions.

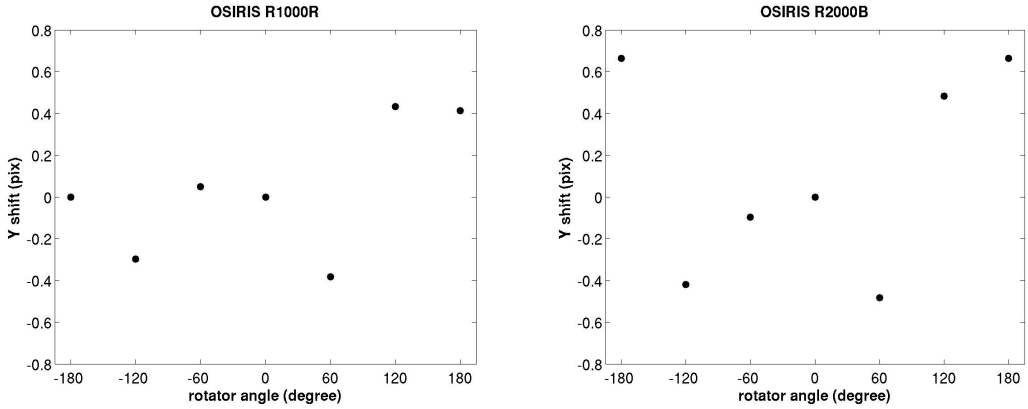

Figure 4.2.- Shift in the spectral direction (Y) for the arcs emission lines with rotator position for OSIRIS R1000R (left) and R2000B (right). The more extreme variations are lower than 1 pix (binned).

4.3 Fringing

The measured value of fringing in the OSIRIS CCD is <1% for λ < 9000 A and 5% for λ > 9300 A (with a slightly increase to 7% at higher resolutions, R=2500), so it is relevant only at higher wavelengths (and in the range z ' in imaging mode). Figure 4.3. shows an example of fringing vs. wavelength obtained with OSIRIS R500R.

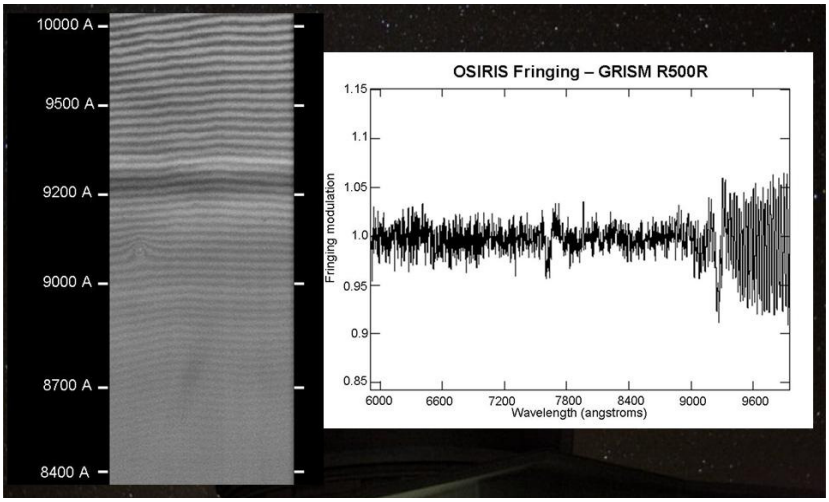

Figure 4.3.- OSIRIS fringing vs wavelength, obtained with the R500R grism.

The effect of possible wavelength drifts due to flexures in OSIRIS has been measured in order to evaluate its influence on the fringe pattern. As a practical example, for VPH R2500I (which is the VPH most affected by fringing), the fringing is doubled when a shift of 6 pixels is produced in the spectra, while no noticeable effects are shown for shifts up to 3 pixels. As instrument flexures causes displacements no larger than 1 pixel in the wavelength calibrations (see section 4.2), the fringing in OSIRIS will not be affected by this. Hence, there is no need to obtain a spectral flat calibration taken with the same orientation as the science images.

In case fringing is of critical importance, to reduce the fringing effect it is recommended to the user to use an offsetting pattern (ABBA, ABAB, AB, etc..) when observing at wavelengths larger than 9000 A, and also for getting a better sky subtraction. This strategy strongly recommended at higher resolutions (VPHs R2500R and R2500I).

4.4 Spatial displacement

Upon inserting a VPH dispersing element into the optical train a small displacement between the target position in the acquisition image and the spectrum position in the spatial direction can be observed. In OSIRIS, only VPH R2500I shows a notable displacement (larger than 1 arcsec) while in the rest of VPHs this effect is negligible (some grisms are also shown for comparison). Please note this when observing extended objects or crowded regions with this VPH, to avoid confusion between different spectra:

Grism / VPH	ΔX (pix)	Grism / VPH	ΔX (pix)
R300B	-0.5	**R2000B**	-2.0
R300R	0.0	**R2500U**	5.0
R1000B	0.5	**R2500V**	1.5
R1000R	0.5	**R2500R**	0.5
---	---	**R2500I**	15.0

4.5 Arc line maps

Instrument Calibration Module (ICM) at GTC has three different calibration lamps: HgAr, Ne and Xe. Below, the arc lines for the OSIRIS grisms/VPH are shown, together with the exposure times used for produce these, for reference. The following table summarises the optimal exposure times for each lamp when powering on two lamps for each type using the standard spectroscopic configuration (100 kHz readout speed, binning 2 × 2, gain = 4.75).

Grism/VPH	Xe	Ne	HgAr
R300B	10 s	1.5 s	6 s
R300R + GR	6 s	1 s	8 s
R500B	---	1.5 s	6 s
R500R + GR	7 s	1.5 s	10 s
R1000B	---	1.7 s	5 s
R1000R + GR	8 s	1.7 s	6 s
R2000B	1200 s (*)	600 s (*)	7 s
R2500U	1200 s (*)	---	20 s
R2500V	1200 s (*)	20 s	5 s
R2500R + GR	---	3 s	30 s
R2500I + GR	5 s	11 s	30 s

(*) For some of the OSIRIS R2000/2500 VPHs long exposed lamp images are required to obtain enough signal which allows a good line identification. For this reason, a master arc collection with the arc lamps images obtained with OSIRIS R2000/2500 VPHs with the 0.6” slit can be retrieved from:

http://www.gtc.iac.es/en/pages/instrumentation/osiris/osiris2.php#Spectroscopy

Note that this master arc collection was obtained using a 0.6” slit. If the scientific program use another slit, a possible small drift in the lines could be observed due to the different position of the slit in the OSIRIS focal plane. To use the master arc it is necessary to correct for a possible drift in the lines by correlating the short exposure lamp frame with the master frame.

OSIRIS R300B: HgAr + Xe + Ne calibration lamps

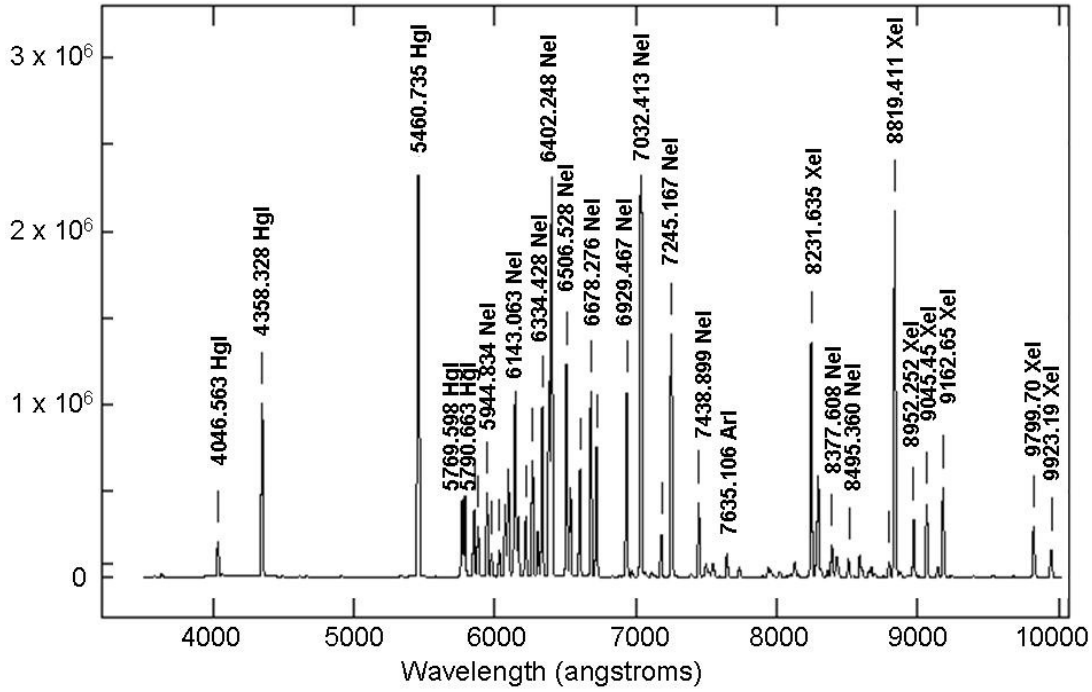

OSIRIS R300R: HgAr + Xe + Ne calibration lamps

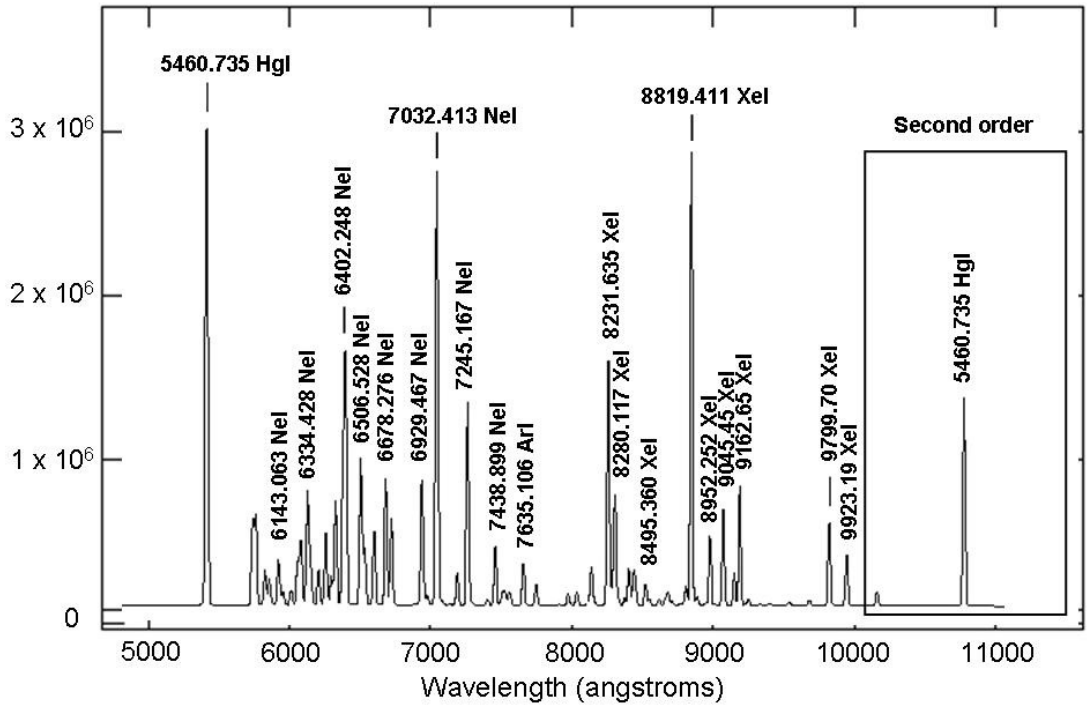

OSIRIS R500B: HgAr + Ne calibration lamps

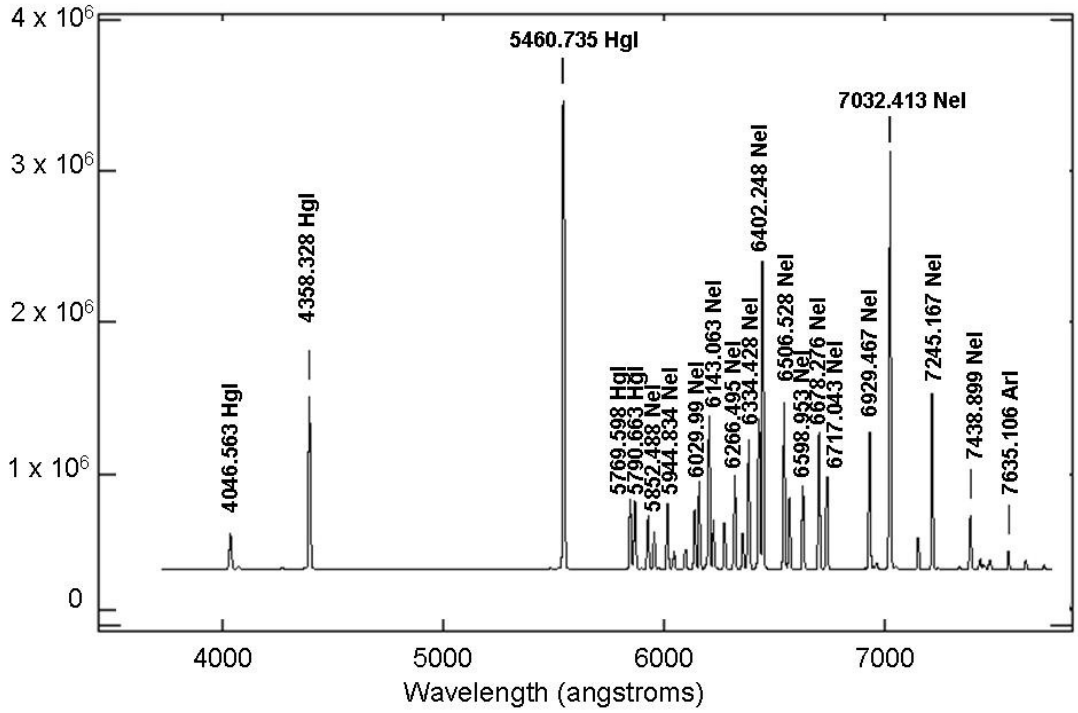

OSIRIS R500R: HgAr + Xe + Ne calibration lamps

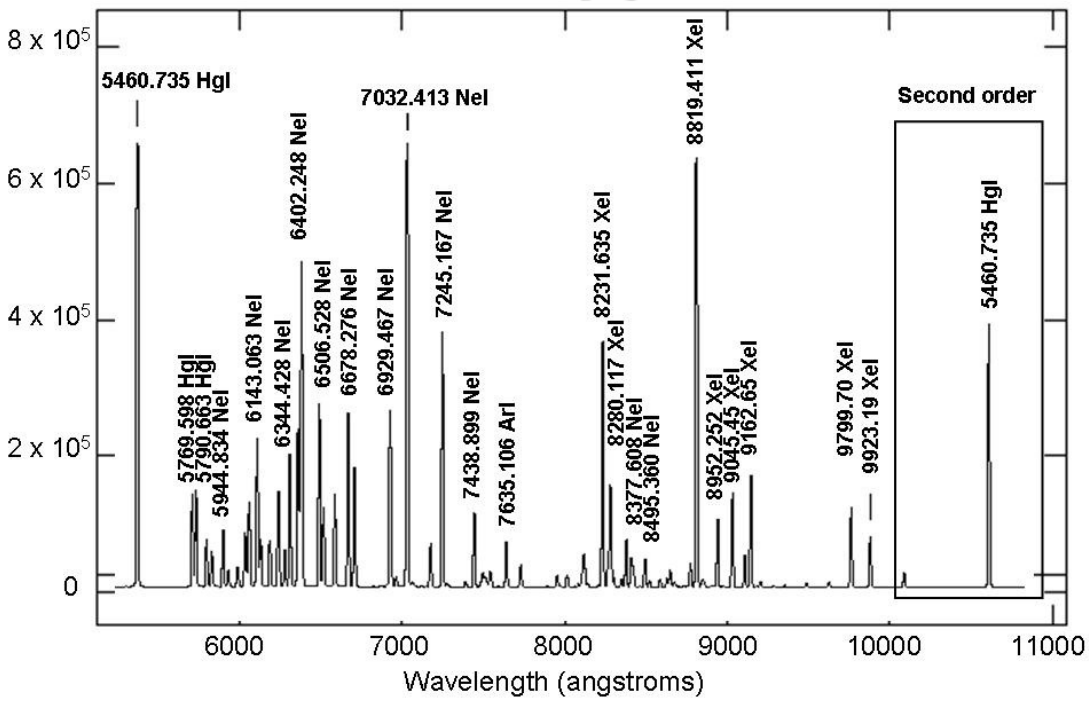

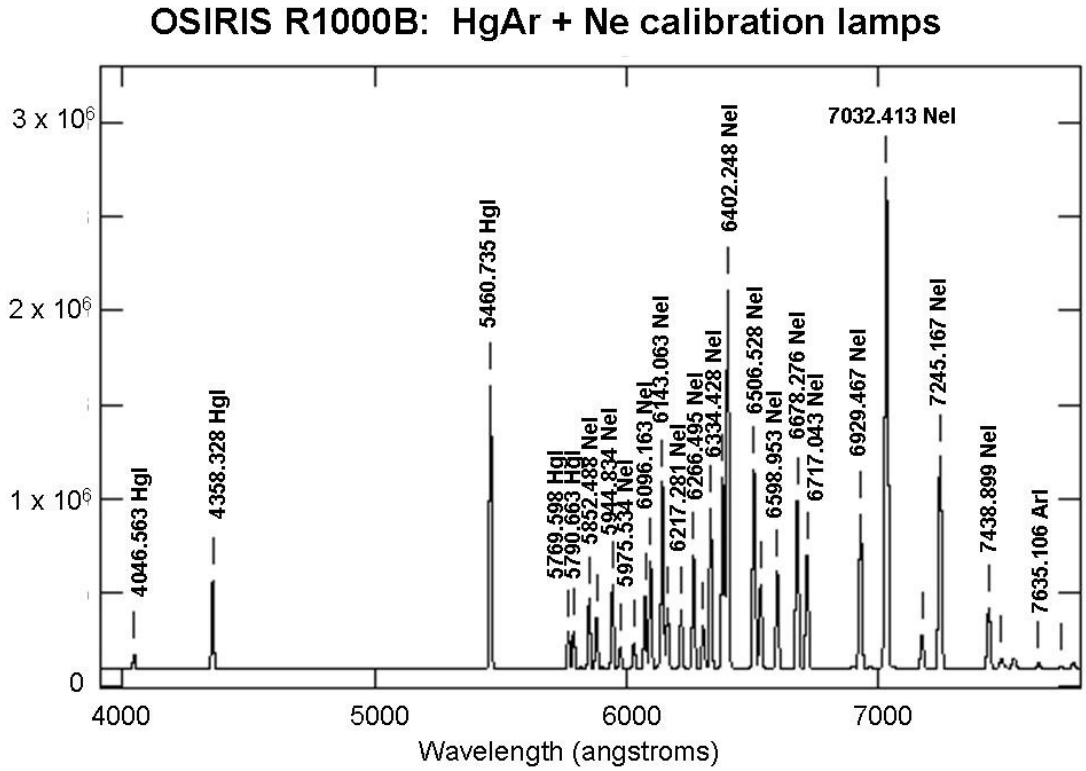
OSIRIS R1000B: HgAr + Ne calibration lamps
3 x 10^6
2 x 10^6
1 x 10^6
0
4000
5000
6000
7000
Wavelength (angstroms)
4046.563 HgI
4358.328 HgI
5460.735 HgI
5769.598 HgI
5790.663 HgI
5852.488 NeI
5944.834 NeI
5975.534 NeI
6096.163 NeI
6143.063 NeI
6217.281 NeI
6266.495 NeI
6334.428 NeI
6402.248 NeI
6506.528 NeI
6598.953 NeI
6678.276 NeI
6717.043 NeI
6929.467 NeI
7032.413 NeI
7245.167 NeI
7438.899 NeI
7635.106 ArI

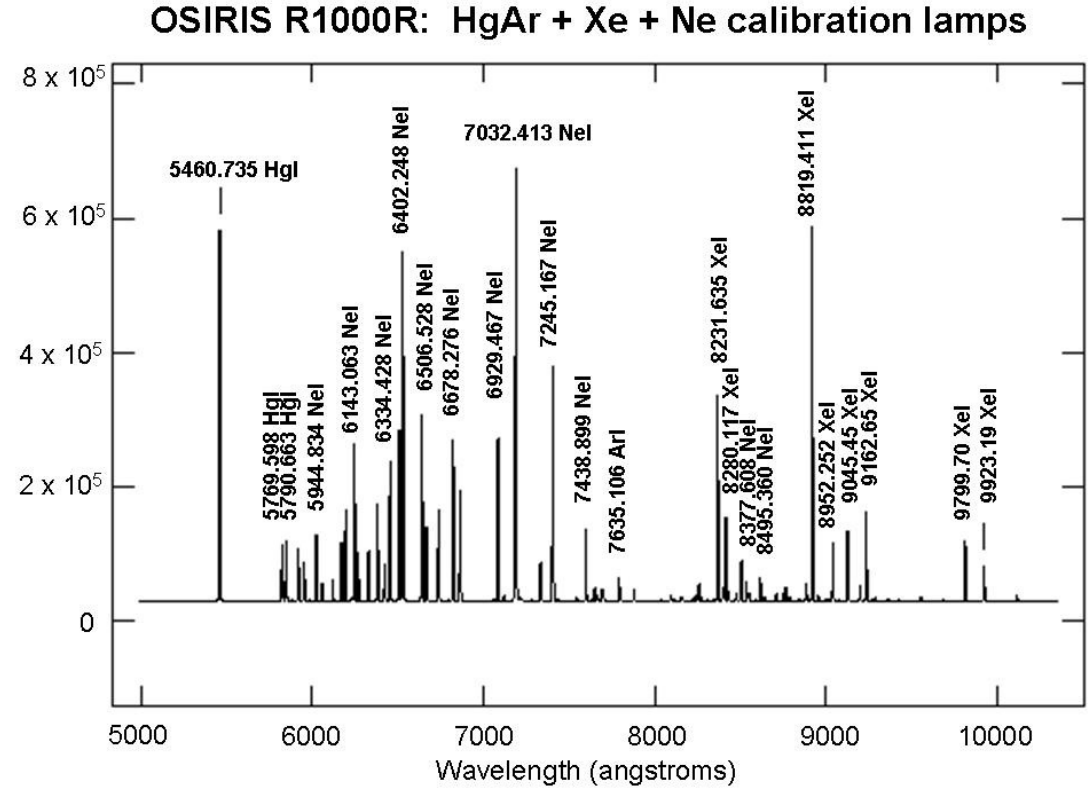
OSIRIS R1000R: HgAr + Xe + Ne calibration lamps
8 x 10^5
6 x 10^5
4 x 10^5
2 x 10^5
0
5000
6000
7000
8000
9000
10000
Wavelength (angstroms)
5460.735 HgI
5769.598 HgI
5790.663 HgI
5944.834 NeI
6143.063 NeI
6334.428 NeI
6402.248 NeI
6506.528 NeI
6678.276 NeI
6929.467 NeI
7032.413 NeI
7245.167 NeI
7438.899 NeI
7635.106 ArI
8231.635 XeI
8280.117 XeI
8377.608 NeI
8495.360 NeI
8819.411 XeI
8952.252 XeI
9045.45 XeI
9162.65 XeI
9799.70 XeI
9923.19 XeI

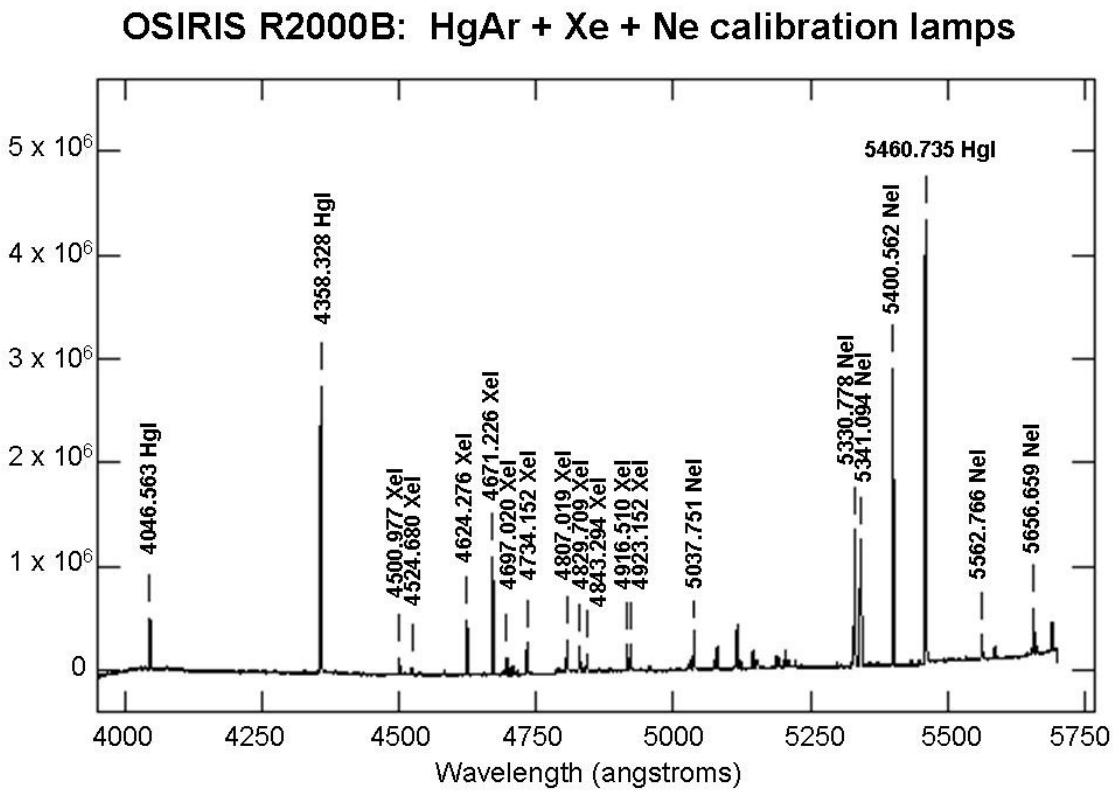
OSIRIS R2000B: HgAr + Xe + Ne calibration lamps
5 x 10^6
4 x 10^6
3 x 10^6
2 x 10^6
1 x 10^6
0
4046.563 HgI
4358.328 HgI
4500.977 XeI
4524.680 XeI
4624.276 XeI
4671.226 XeI
4697.020 XeI
4734.152 XeI
4807.019 XeI
4829.709 XeI
4843.294 XeI
4916.510 XeI
4923.152 XeI
5037.751 NeI
5330.778 NeI
5341.094 NeI
5400.562 NeI
5460.735 HgI
5562.766 NeI
5656.659 NeI
4000
4250
4500
4750
5000
5250
5500
5750
Wavelength (angstroms)

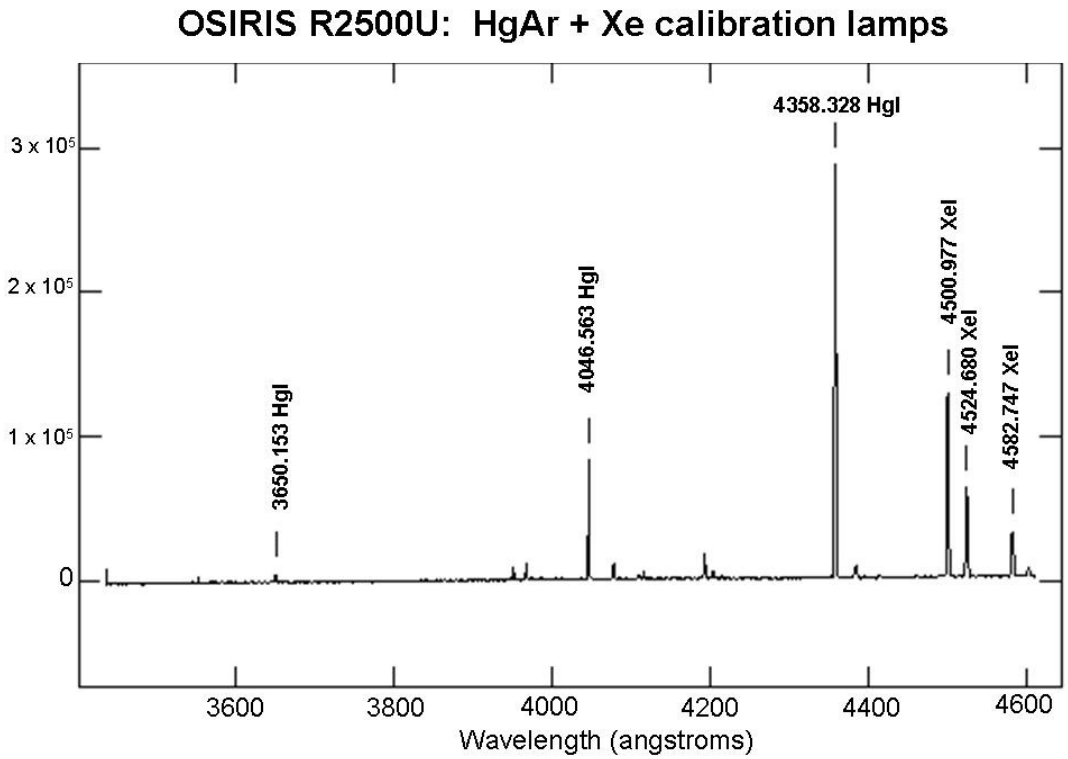
OSIRIS R2500U: HgAr + Xe calibration lamps
4358.328 HgI
4046.563 HgI
3650.153 HgI
4500.977 XeI
4524.680 XeI
4582.747 XeI
3 x 10^5
2 x 10^5
1 x 10^5
0
3600
3800
4000
4200
4400
4600
Wavelength (angstroms)

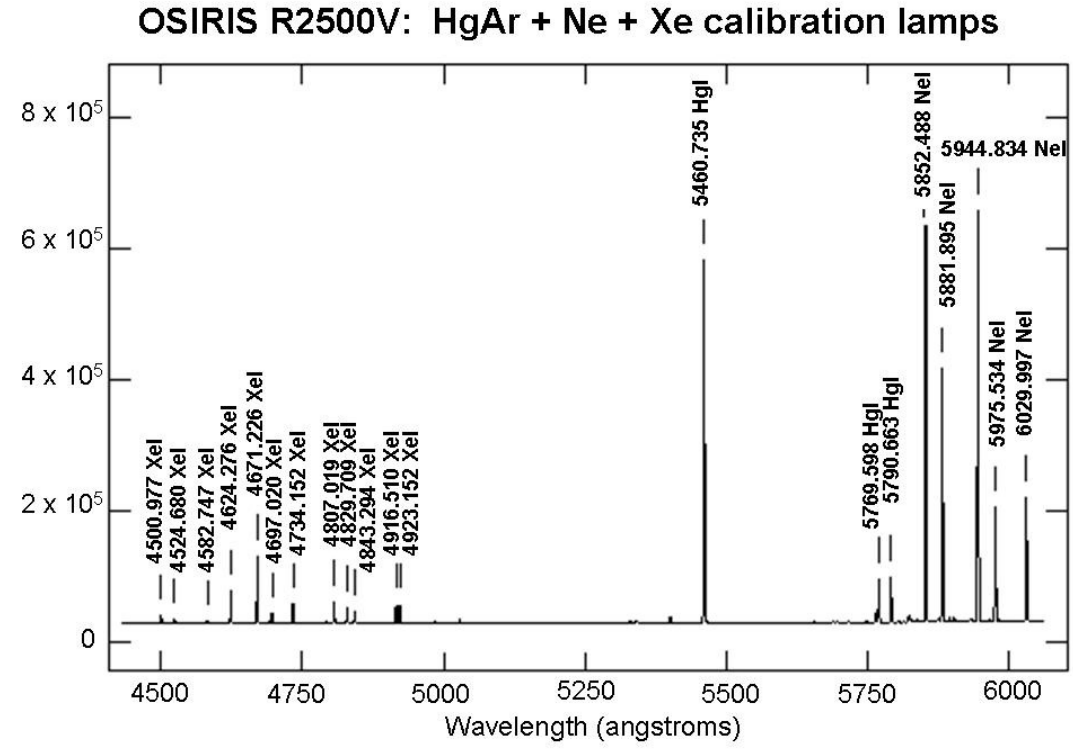
OSIRIS R2500V: HgAr + Ne + Xe calibration lamps
5460.735 HgI
5852.488 NeI
5944.834 NeI
5881.895 NeI
5975.534 NeI
6029.997 NeI
5769.598 HgI
5790.663 HgI
4500.977 XeI
4524.680 XeI
4582.747 XeI
4624.276 XeI
4671.226 XeI
4697.020 XeI
4734.152 XeI
4807.019 XeI
4829.709 XeI
4843.294 XeI
4916.510 XeI
4923.152 XeI
8 x 10^5
6 x 10^5
4 x 10^5
2 x 10^5
0
4500
4750
5000
5250
5500
5750
6000
Wavelength (angstroms)

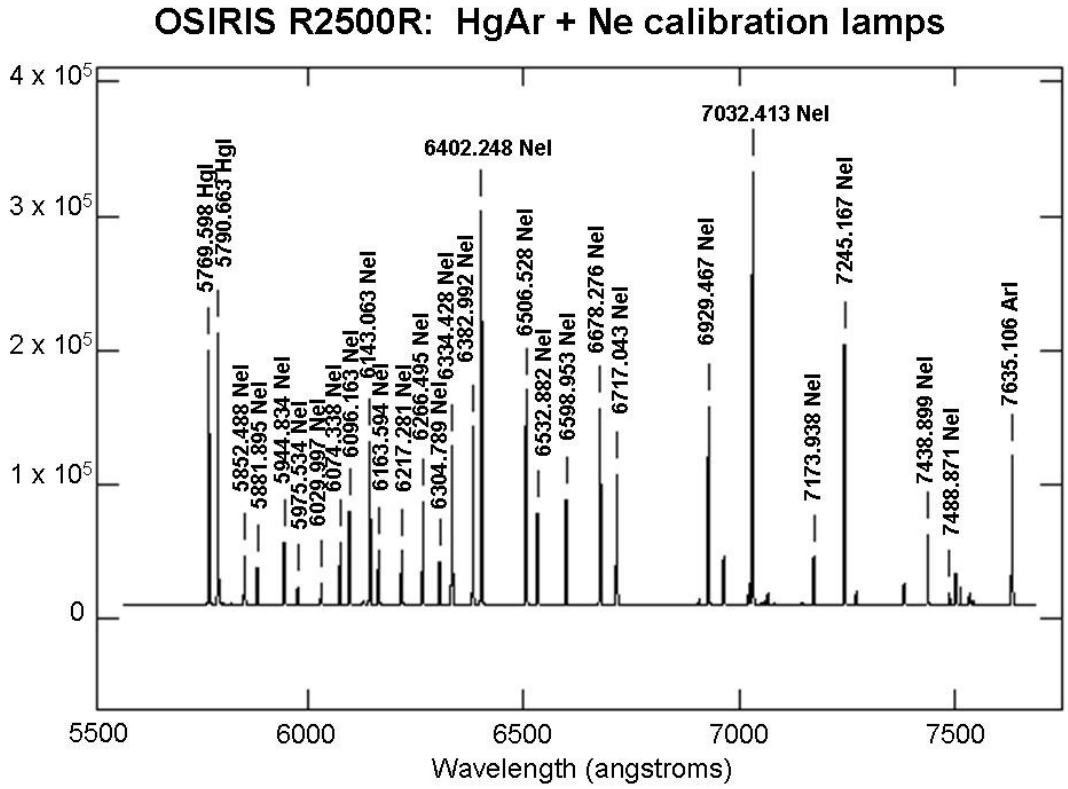
OSIRIS R2500R: HgAr + Ne calibration lamps
4 x 10^5
3 x 10^5
2 x 10^5
1 x 10^5
0
5500
6000
6500
7000
7500
Wavelength (angstroms)
5769.598 HgI
5790.663 HgI
5852.488 NeI
5881.895 NeI
5944.834 NeI
5975.534 NeI
6029.997 NeI
6074.338 NeI
6096.163 NeI
6143.063 NeI
6163.594 NeI
6217.281 NeI
6266.495 NeI
6304.789 NeI
6334.428 NeI
6382.992 NeI
6402.248 NeI
6506.528 NeI
6532.882 NeI
6598.953 NeI
6678.276 NeI
6717.043 NeI
6929.467 NeI
7032.413 NeI
7173.938 NeI
7245.167 NeI
7438.899 NeI
7488.871 NeI
7635.106 ArI

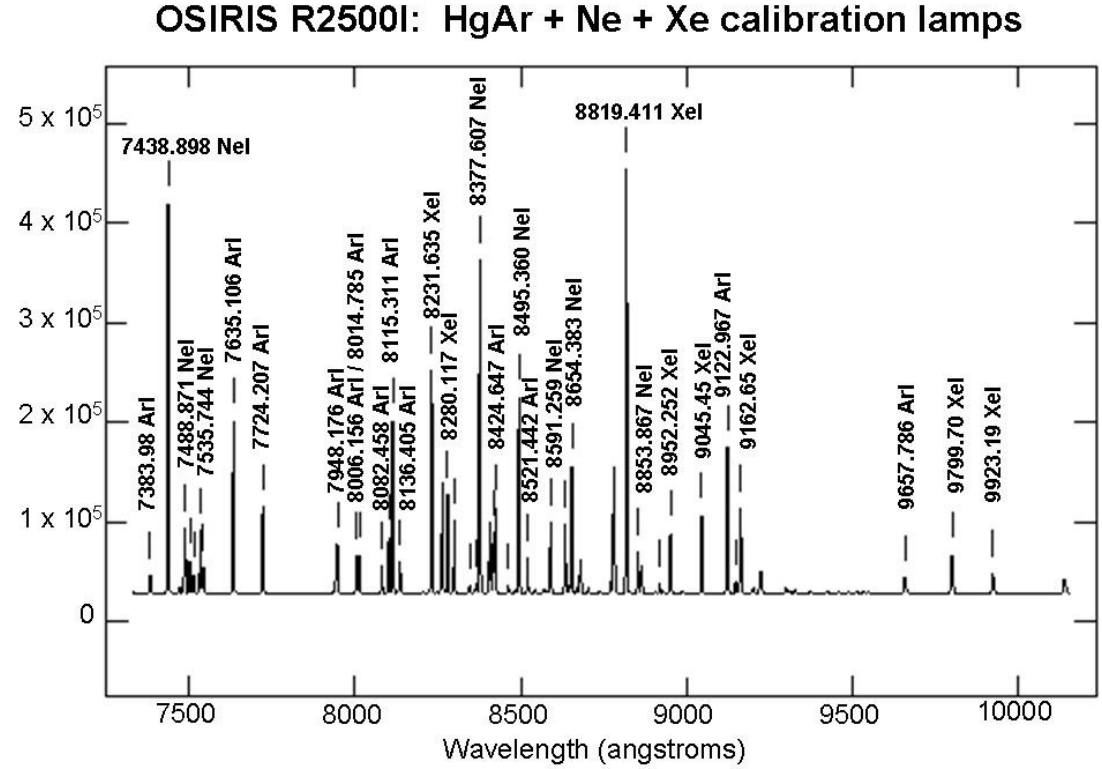
OSIRIS R2500I: HgAr + Ne + Xe calibration lamps
5 x 10^5
4 x 10^5
3 x 10^5
2 x 10^5
1 x 10^5
0
7500
8000
8500
9000
9500
10000
Wavelength (angstroms)
7383.98 ArI
7438.898 NeI
7488.871 NeI
7535.744 NeI
7635.106 ArI
7724.207 ArI
7948.176 ArI
8006.156 ArI / 8014.785 ArI
8082.458 ArI
8115.311 ArI
8136.405 ArI
8231.635 XeI
8280.117 XeI
8377.607 NeI
8424.647 ArI
8495.360 NeI
8521.442 ArI
8591.259 NeI
8654.383 NeI
8819.411 XeI
8853.867 NeI
8952.252 XeI
9045.45 XeI
9122.967 ArI
9162.65 XeI
9657.786 ArI
9799.70 XeI
9923.19 XeI

4.5.1 Arc-line ghosts

All the OSIRIS grisms show some minor ghost effects in the arc-line images. Those ghosts are due to internal reflections within the grisms, and can be identified as the curvature in these spectra differs from those of the main arc lines. The intensity of these ghosts is negligible and they do not affect the line identification or the science images.

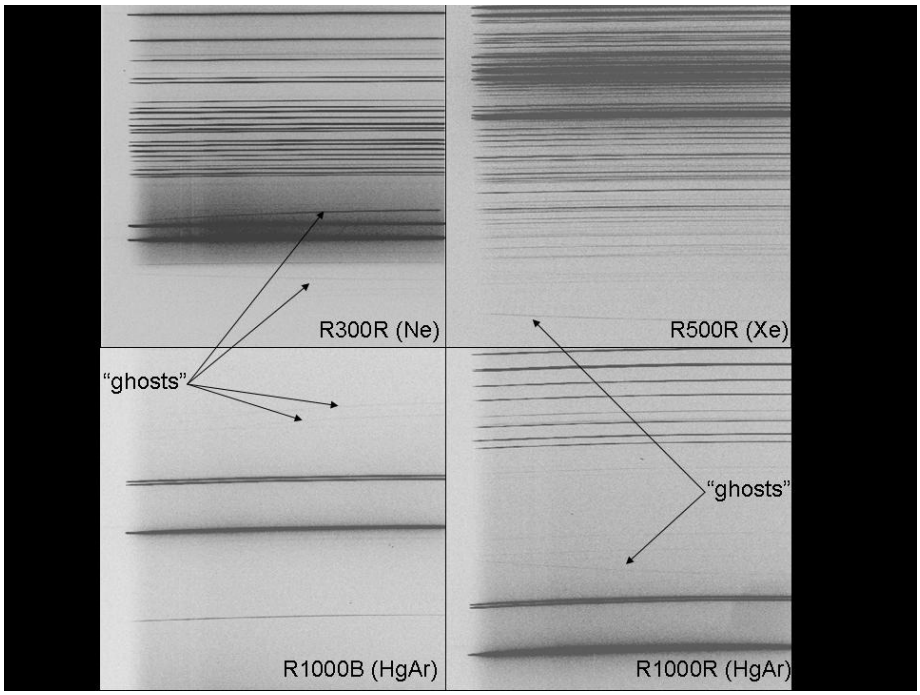

Figure 4.4.- OSIRIS grisms ghost effects shown in the arc images.

4.5.2 Spectral solutions

The following table shows the example solutions obtained with the IRAF routine IDENTIFY corresponding to the standard pointing in Long Slit Spectroscopy mode (X=250 in CCD2), as a guideline for the image reduction.

Grism/VPH	Lamps	# features	R.M.S	Function (order)
R300B	Ne + HgAr + Xe	31	0.1165	spline3 (5)
R300R	Ne + HgAr + Xe	30	0.2478	spline3 (5)
R500B	Ne + HgAr	42	0.0931	spline3 (5)
R500R	Ne + HgAr + Xe	43	0.1273	legendre (5)
R1000B	Ne + HgAr	34	0.0425	spline3 (3)
R1000R	Ne + HgAr + Xe	49	0.0651	spline3 (3)
R2000B	Ne + HgAr + Xe	20	0.0162	spline3 (3)
R2500U	HgAr + Xe	6	0.0178	spline3 (1)
R2500V	Ne + HgAr + Xe	20	0.0118	spline3 (3)
R2500R	Ne + HgAr	34	0.0151	spline3 (3)
R2500I	Ne + HgAr	41	0.0330	spline3 (3)

4.5.3 Spectral flat fields

Spectral flats can be obtained either by using dome lights or using the incandescent lamp of the instrument calibration module (ICM).

ICM spectral illumination is rather inhomogeneous and has a strong gradient from CCD1 to CCD2. For this reason, spectral flats obtained with the calibration unit are only recommended for targets placed in CCD2.

There are no significant dependences in the spectral flats with instrument rotator angle. Therefore, as with the arc lamps, the spectral flats for each observation can be taken at the beginning or at the end of the night regardless of the position of the rotator.

4.6 VPHs R2000/R2500 ghosting

The R2000 and R2500 VPHs suffer from a faint ghost image of the spectrograph slit that normally will have a negligible impact on the quality of the spectra. The ghost is negligible in the R2500I and R2500R VPHs, while in R2000B, R2500U, and R2500V the ghost is only noted in the spectral flat-field images and arc lamp frames, where a very faint slit image can be observed superimposed on the spectral flat / lamp arcs. The approximated position for those ghost images are: R2000B : from pixels Y = 988 to 996; R2500U : from pixels Y = 980 to 988; R2500V: from pixels Y = 992 to 1000.

There are no problems for the line identification as the intensity of the ghost is far below the average of the counts for the spectral lines. However, users must be aware when obtaining the flat-fielding correction in the pixels range described above, and only for R2000B, R2500U and R2500V. In the science images the effect is irrelevant for the complete set of VPHs (the average ratio between the ghost intensity and the integrated flux from the target that causes the ghost is on the order of 10^{-5}). The ghost in science images can be noted as a focused image from the target in the other CCD. (see Figure 4.5).

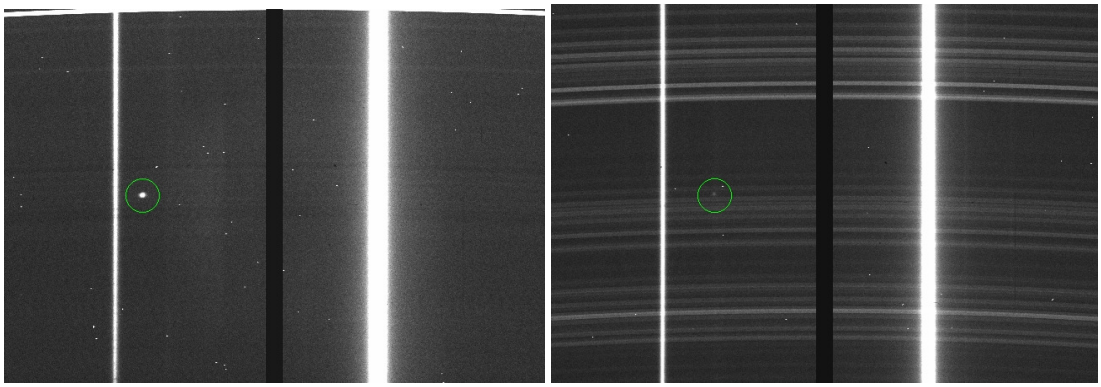

Figure 4.5.- Two examples of OSIRIS VPHs R2000/2500 ghosting, corresponding to R2500V (left) and R2500R (right). The focused image from the target (a bright standard star) can be observed in the opposite CCD respect to the spectra location, being much more fainter in the case of R2500R.

4.7 Second order contamination

All the OSIRIS red grisms/VPHs (R300R, R500R, R1000R, R2500R, and R2500I) are used in combination with an spectral order shorter filter (GR), which cuts out the light blueward from ~495 nm. However, there is a slight contamination in the spectrum due to the second order, as the spectral order shorter filter doesn't block completely the contribution for wavelengths lower that the defined cut level (see Figure 4.1). Hence, there is a distinguishable contribution for wavelengths at 480 – 490 nm, whose second order may contribute somewhat at 960 nm – 980 nm, depending of the source spectral distribution.

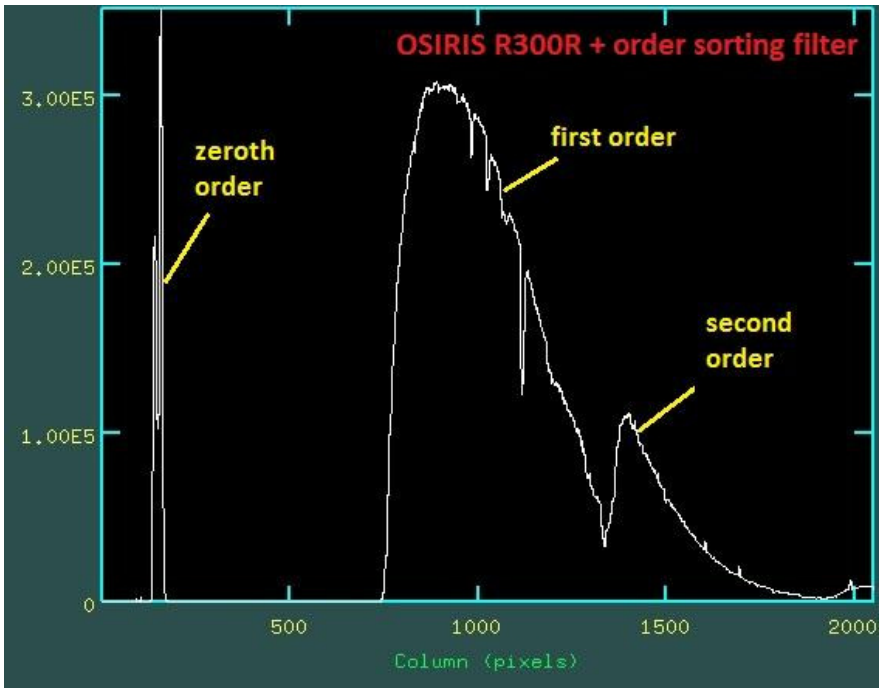

Figure 4.6.- Example spectrum of the flux standard star PG1545+035 taken with a 2.5 arcsec slit and 300 secs exposure time. The low-resolution spectrum with the R300R grism shows the first order of dispersion well centered on the CCD. Also visible is the zeroth order on the left, and the second order spectrum on the right-hand side of the graph. The effect is present in all the red grisms/VPHs but it's more noticeable at lower resolutions

4.8 Spectrophotometric standards

The complete list of spectrophotometric standard stars for flux calibration can be found in Section 10.

4.9 Spectroscopic photon detection efficiency

The overall photon detection efficiency in spectroscopic mode was measured during OSIRIS commissioning using a spectrophotometric standard star through a wide slit, as a function of wavelength and for different grisms. The results are displayed in the following two graphs. This first plot shows the AB magnitude that corresponds to the detection of one photon per second per Angstrom. The second plot gives the end-to-end overall percentage detection efficiency.

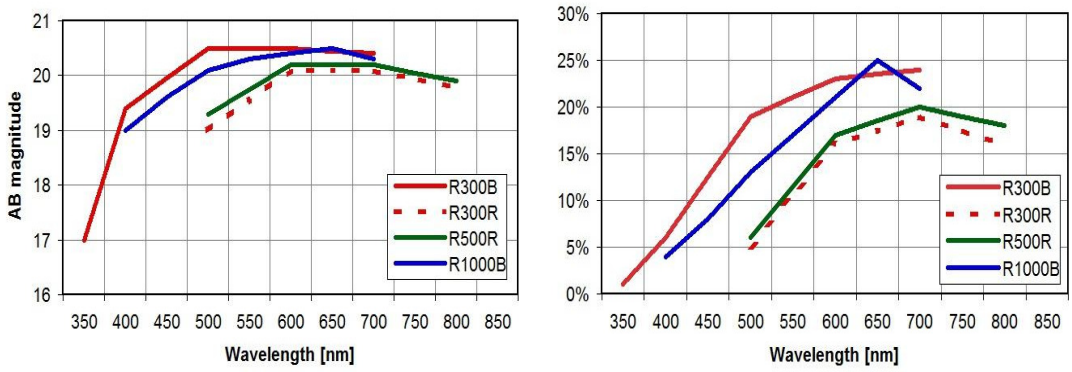

Figure 4.9.- Overall photon detection efficiency of GTC and OSIRIS in spectroscopic mode.

5 OBSERVING WITH OSIRIS

5.1 Exposure time calculator (ETC)

For preparing observations estimating exposure times for the different modes, the updated (as of February 2010 with available TF and Grisms efficiencies) ETC can be found in http://www.gtc.iac.es/en/pages/instrumentation/osiris.php

Also, for tunable-filter observations, it is highly recommended to use the TF Setup Tool (also available at http://www.gtc.iac.es/en/pages/instrumentation/osiris.php), before using the ETC. The TF Setup Tool allows to perform very useful estimates for the TF operation, as:

- obtaining the available widths for our wavelength of interest, as well as to define the corresponding Order Sorter Filter that has to be used for the observation.
- calculating the change in wavelength along the OSIRIS FOV.
- estimating the effect of the sky lines in our tuned filter.

Estimates from the ETC are obtained by using the most recent data coming from the instrument and are well in agreement with the obtained results in the scientific operation of the telescope. In any case, there are also some useful information to take into account when using the OSIRIS ETC:

- If you were awarded with 'Spectroscopic' night conditions, it's advisable to add +0.5 mag to the target magnitude when obtaining S/N estimates (as it was observed by daily monitorizing of OSIRIS zeropoints, see Section 2.1.1.1).

5.2 GTC Phase 2 tool

Observations with OSIRIS / GTC can be done both in queue or visitor mode, but in any case, observers must use the GTC Phase 2 tool in advance to prepare the observations. In queue mode, this is mandatory in order to provide to GTC SA staff with the instructions for completing the observing programmes; in visiting mode, this is highly recommended as the Phase 2 tool allows to the GTC SA staff to generate automatized observing sequences at the telescope, hence notably increasing the nightly operating efficiency.

For a complete help in how to use and complete this GTC Phase 2 tool, users are referred to the on-line help document available at:

http://gtc-phase2.gtc.iac.es/science/media/docs/phase2help.pdf

For other overall details in GTC queue observing mode please read carefully the section 'Observing with GTC' at GTC web pages:

http://www.gtc.iac.es/en/pages/observing-with-gtc.php

6 OSIRIS DATA PROCESSING

6.1 OSIRIS / GTC Keywords

Data files produced by OSIRIS on GTC have a standard FITS structure. In the standard operative mode of the instrument, both CCDs are read using a single amplifier. Data corresponding to each CCD are stored as independent subdimensions of the image.

The filenames have a structure which contains a unique run number, the date, instrument, and observing mode as follows: <number>-<date>-<instrument>-<mode>.fits

For example: 0000007448-20090703-OSIRIS-OsirisBroadBandImage.fits

Here is a complete list of available OSIRIS observing modes (the observing modes marked in red are not available yet):

Calibration Modes	Science Modes
OsirisBias	OsirisBroadBandImage
OsirisDark	OsirisTunableFilterImage
OsirisDomeFlat	OsirisLongSlitSpectroscopy
OsirisSkyFlat	OsirisMOS
OsirisSpectralFlat	OsirisFastBroadBandImage
OsirisCalibrationLamp	OsirisTunableFilterImage
	OsirisMOSNodAndShuflle
	OsirisMOSMicroShuffle
	OsirisFrameTransferBroadBandImage
	OsirisFrameTransferTunableFilterImage
	OsirisFrameTransferLongSlitSpectroscopy

The following table provides a listing and description of the OSIRIS FITS headers (please note that the complete list will be upgraded):

Keyword	Example entry	Description
SIMPLE	T	file does conform to FITS standard
BITPIX	16	number of bits per data pixel
EXTEND	T	FITS dataset may contain extensions
NAXIS	2	number of data axes
NAXIS1	2098	number of columns in the image
NAXIS2	4102	number of rows in the image
BSCALE	1	default scaling factor
BZERO	32768	offset data range to that of unsigned short
FILENAME	Oct10_200120.fits	Filename
DATE	2009-07-04T01:12:45	file creation data (YYYY-MM-DDThh:mm:ss UT)
INSTRUME	OSIRIS	Instrument Name
DETECTOR	E2V CCD44-82-BI	Detectors Model
DETSIZE	[1:4096,1:4102]	Maximum Imaging Pixel Area
OBSTYPE	OBSTYPE	Not used yet
OBSERVER	OBSERVER	Not used yet
SEQUENCE	SIMPLE	Readout sequence (simple, charge-shuffling, or frame-transfer)
OUTMODE	TWOCCDS_A	Indicates the readout mode of the two CCDs
NAMPS	2	Number of channels used for the CCD readout
RSPEED	SPEED_200	Readout Speed
EXPTIME	500.	Exposure Time in seconds
NUM_IMAG	1	Total number of images into the sequence (relevant for charge-shuffled series of images)
NUM_INDX	0	Image Index into sequence (relevant for charge-shuffled series of images)
NUM_SHIF	0	Number of rows per shift (relevant for charge-shuffled series of images)
NUM_LOOP	1	Number of loops into the sequence (relevant for charge-shuffled series of images)
general description The controller defines different types of windows indicated as follows. RDS is used for charge shuffling, shutterless operation, and for the last read in frame transfer modes. In this case only one window can be defined. RDI indicates (multiple) windows in case of simple, standard readout of the CCD. RDW is used in case of frame transfer mode and may refer to multiple windows.		
ROI_0X	0	X-Origin of ROI-0 in RDS
ROI_0Y	0	Y-Origin of ROI-0 in RDS
ROI_X	2098	X-Size of windows in RDS
ROI_Y	4102	Y-Size of windows in RDS
NUM_ROIS	1	Number of windows RDI-RDW
ROI_1X	0	X-Origin of ROI-1 in RDI-RDW
ROI_1Y	0	Y-Origin of ROI-1 in RDI-RDW
ROI_2X	0	X-Origin of ROI-2 in RDI-RDW
ROI_2Y	0	Y-Origin of ROI-2 in RDI-RDW
ROI_3X	0	X-Origin of ROI-3 in RDI-RDW
ROI_3Y	0	Y-Origin of ROI-3 in RDI-RDW

ROI_4X	0	X-Origin of ROI-4 in RDI-RDW
ROI_4Y	0	Y-Origin of ROI-4 in RDI-RDW
ROI_5X	0	X-Origin of ROI-5 in RDI-RDW
ROI_5Y	0	Y-Origin of ROI-5 in RDI-RDW
GAIN	GAIN_x9_5	Identification of gain scaling factor
VBIN	true	Vertical binning indicator
HBIN	true	Horizontal binning indicator
RNTIMES	1	Engineering Keyword
NSHIFTS	0	Number of exposures in the case is charge-shuffling, shutterless operation and frame-transfer mode
MOVTYPE	0	Parameter indicating the mode of charge transfer
FRAMETY	1	Frame Type (0: RDS or 1: RDI/RDW)
DEEP	2	Bytes per pixel
FRAMESI	8606008	Raw Data Size in bytes
TITLE	Not assigned value	Title given to the image
MOSAIC	true	Mosaic active or not
PRESCAN	true	Prescan (overscan) active or not
SIMULATE	false	Indicated whether an image is synthesised by the controller
HIERARCH simulateVal	0	Engineering Keyword
HIERARCH simulateType	0	Engineering Keyword
HIERARCH applyPreprocess	true	Reordering of data applies or not
OPENTIME	19:52:45.049	Open Shutter Time
CLOSTIME	20:01:05.502	Close Shutter Time
ELAPSED	500.453	Total elapsed time
GTCPROGI	GTC34-09B	Proposal code
GTCOBID	GTC34-09B_0010	Proposal observing block identifier
PI	Pablo Sanchez	Observer (for the time being Support Astronomer)
OBSMODE	OsirisBroadBandImage	Observation mode (each instrument has its own modes)
TELESCOP	GTC	Telescope
HIERARCH ASGDCENTRXY	[-77.6051 -443.499]	Focal plane X,Y coordinate where guiding was centred
ASGDEC	-12:43:39.131	d:m:s Dec of ASG centre
HIERARCH ASGDTARGDETXY	[33.1834 41.5767]	ASG detector X,Y coordinate where guiding target was located
HIERARCH ASGDTARGXY	[-73.6715 -434.314]	Focal plane X,Y coordinate where guiding target was located
ASGRA	+20:46:58.199	h:m:s RA of centre of ASG (guiding camera)
DEC	-12:52:15.752	d:m:s Dec of telescope (in the centre)
RA	+20:47:10.556	h:m:s RA of telescope (in the centre)
AG1ARM	38.1413125	degrees Actual position of AG arm 1
AG1DARM	38.1451446254256	degrees Demanded position of AG arm 1
AG1DROT	120.216466004046	degrees ASG field rotation wrt focal plane
AG1DTURN	168.797493861741	degrees Demanded position of AG turntable 1

AG1FOCUS	45.0005	Focus position of AG 1
AG1TURNT	168.797536337209	Actual position of AG turntable 1
AG2ARM	-50.000375	Actual position of AG arm 2
AG2TURNT	170.315830759448	Actual position of AG turntable 2
AIRMASS	1.35883552020977	Airmass
AZIMUTH	166.983854397316	degrees Azimuth in final moment of observation
DECDEG	-12.8710423171209	degrees Dec in degrees
ELEVAT	47.3367634069994	degrees Elevation in final moment of observation
IPA	150.54	degrees Instrument position angle (150.54 for N up and E to the left in the OSIRIS image. Any sky-PA translates into IPA = 150.54 - PA)
M2RX	0.000331365969032049	Actual positions of M2: M2 has 5 degrees of freedom given by M2RX (tip) and M2RY (tilt) in radians, alignment in X, Y (M2UX, M2UY in mm) and piston (M2UZ in mm), the latter is used to focus. These values are determined by a model of active optics which corrects for effects of elevation and temperature
M2RY	0.000108922118670307	See previous description
M2UX	-1.63107764720917	See previous description
M2UY	3.61354541778564	See previous description
M2UZ	-2.13678193092346	See previous description
RADEG	311.793981603427	degrees RA in degrees
ROTANG	30.7088195736652	degrees Rotator in final moment of observation
SFSDER	0.0203125	Posicion of SFS (wave front sensor) derotator
EKW1	1	OSIRIS engineering keyword: OSIRIS filter wheel 1 position
EKW12	0	OSIRIS engineering keyword: X position of red TF (parallelism value in X of TF)
EKW13	0	OSIRIS engineering keyword: Y position of red TF (parallelism value in Y of TF)
EKW16	0	OSIRIS engineering keyword: "positionAutoAdjustmentX" of red TF
EKW17	0	OSIRIS engineering keyword: "positionAutoAdjustmentY" of red TF
EKW18	0	OSIRIS engineering keyword: "positionAutoAdjustmentZ" of red TF
EKW2	2	OSIRIS engineering keyword: OSIRIS filter wheel 2 position
EKW3	5	OSIRIS engineering keyword: OSIRIS filter wheel 3 position
EKW4	3	OSIRIS engineering keyword: OSIRIS grism wheel position
EKW5	0	OSIRIS engineering keyword: OSIRIS mask charger position
EKW6	0	OSIRIS engineering keyword: "DisplacementZ" of red TF (actual value)
EKW7	0	OSIRIS engineering keyword: "offsetZ" of red TF (value obtained before TF observation). With EKW6-EKW7 the tabulated value of each lambda /

		FWHM combination can be recovered. Shortly, two additional keywords based on those will be generated automatically, containing information of TF central wavelenth and tuned band width.
OSIVERS	1.	OSIRIS software and hardware version
OSISTAT	1	OSIRIS status: 1=ok
OPTCENTX	1000.	OSIRIS Optical Center X
OPTCENTY	1001.	OSIRIS Optical Center Y
GRISM	OPEN	GRISM identifier
FILTER4	OPEN	Filter 4 device identifier
FILTER1	OPEN	Filter identifier in wheel 1
OSFILT		Order Sort Filter identifier
OSWAV	0.	Order Sort Filter central wavelength
FILTER2	Sloan_g	Filter identifier in wheel 2
FILTER3	OPEN	Filter identifier in wheel 3
MASKNAME	NOMASK	Focal plane mask identifier
SLITW	0.	Slit width
SLITPA	0.	Slit position angle
PCOUNT	0	required keyword; must = 0
GCOUNT	1	required keyword; must = 1
INHERIT	T	inherit keyword
EXTNAME	CCD_1_L1	Extension Name
CCDNAME	CCD_1: 01394_17_01	CCD Name (1,2): Serial Number
AMPNAME	CCD_1: Left	Output amplifier name
CCDSIZE	[1:2048,1:4102]	CCD Size in pixels
CCDSUM	1 1	Indicates whether binning is activated ("1") or not ("0"). This first digit refers to X and the second to Y
CCDSEC	[1:2048,1:4102]	Pixel section used for binning
AMPSEC	[1:2048,1:4102]	Pixel section read by each amplifier
DATASEC	[51:2098,1:4102]	Pixel section with real data (excluding overscan region) where binning is relevant
DETSEC	[1:2048,1:4102]	Pixel section for the CCD considered within the mosaic of two detectors
ATM1_1	1.	CCD to amp transformation
ATM2_2	1.	CCD to amp transformation
ATV1	0.	CCD to amp transformation
ATV2	0.	CCD to amp transformation
LTM1_1	1.	CCD to image transformation
LTM2_2	1.	CCD to image transformation
LTV1	50.	CCD to image transformation
LTV2	0.	CCD to image transformation
DTM1_1	1.	CCD to detector transformation
DTM2_2	1.	CCD to detector transformation
DTV1	0.	CCD to detector transformation
DTV2	0.	CCD to detector transformation
BIASSEC	[1:50,1:4102]	BIAS section
TRIMSEC	[1:2048,1:4102]	TRIM section

6.2 Astrometry with OSIRIS

This section of the User Manual is devoted to explain how to perform a sub-pixel precision astrometry of OSIRIS images from minimum header information. The instructions are given in an example-oriented fashion.

As mentioned in Section 1.1, the instrument contains a camera composed by a mosaic of two CCDs arranged along the largest dimension, with 4192 x 2098 physical pixels each (throughout this section of the Manual, any reference to pixel coordinates is given in the physical system). A `fits` image (extensions 1 and 2) with 2 headers plus a zero extension header is generated for each detector reading. Both non-zero extensions include information about the telescope pointing, expressed through the keywords `RA` and `DEC` (provisionally with identical values in all headers). The projection of the telescope optical axis on detector 1 roughly coincides with the pixel (917,1982). If the position angle of rotator (header keyword `IPA`) is 150.54036 degrees, the images are oriented with North up, East left. At first order, the mean plate scale is 0.12718 arcsec/pixel and the physical gap between CCDs is 26 pixel wide. Additionally, the CCD2 is shifted in 4 pixels with respect to the CCD1 in the positive Y-direction.

6.2.1 Input Data

As initial condition, individual extension frames to be astrometrically calibrated must be corrected for zero level (including overscan) and flat field.

- Construct an input source catalog with logical positions of astrometric sources (preferably point-like objects) by using the task `daofind` in `IRAF noao.digiphot.apphot` package, specifying input image, mean FWHM of image features to be detected, as well as the detection threshold and standard deviation of the background. Alternatively, the `SExtractor` software (Bertin & Arnouts, 1996) can be used for this purpose. The `Starlink GAIA` software has the `SExtractor` embedded: after loading any image, it is possible to obtain a catalog of sources invoking the task `Object Detection`, in the `Image-Analysis` menu. `GAIA` provides the facility to see the extracted sources on the image, pick on a specific source and edit the output list. You can also play with background parameters and re-do detection/extraction. In both cases, the required output is a list with x,y logical positions (here named `xy.cat`).

- Construct a catalog with the reference positions of astrometric stars in equatorial coordinates for a defined equinox (usually J2000.0) and epoch of observation (i.e. proper motion corrected coordinates). This catalog is simply an ASCII file with an ID (optional), right ascension and declination in degrees (here called `radec.cat`). It doesn't matter if the angular coverage of the catalog exceeds the OSIRIS field for a given detector.

- Match both files using `IRAF imcoords.ccxymatch`. The output file is `radecxy.cat`, an ASCII list with the matched coordinates in a suitable format to be used as input in the following task. An example of the line command is:

```
ccxymatch xy.cat radec.cat radecxy.cat toleranc=5 ptoleranc=40
xin=xxxx.x yin=yyyy.y xmag=0.127 ymag=0.127 xrotation=180.
yrotation=0. projection="tan" lngref=aaa.aaaaaa latref=+/-dd.dddddd
lngcolumn=2 latcolumn=3 xcolumn=2 ycolumn=3 lngunits="degrees"
latunits="degrees" matchin="triangles" nmatch=40
```

Some cautions should be taken before running `ccxymatch`: (i) it is necessary that a position on the detector (given by parameters `xin, yin`) corresponds to a previously known sky position (given by parameters `lnref, latref`); ideally, this position should be close to the image centre, (ii) `xrotation` and `yrotation` correspond to a image orientation with north up and east left, (iii) depending on the method used for generating input files, the parameters `lngcolumn, latcolumn, xcolumn` and `ycolumn` could change, and (iv) `nmatch` must be smaller than the number of lines in `xy.cat`. Possible redundancies in the output file will be naturally discarded in the following step. Use the command `help ccxymatch` at the `IRAF` prompt to obtain more information.

6.2.2 Astrometric Solution

To find the astrometric solution for each frame, the `IRAF imcoords.ccmap` task should be used. Figure 17.1 below (from Cepa et al. 2010, in preparation) represents the mean distortion vectors (in the sense of deviation of positions from linear solution respect to the general -full precision- astrometric solution) in pixels (5 times magnified), for each OSIRIS detector and without filter. For any broad-band filter, measured distortions are similar.

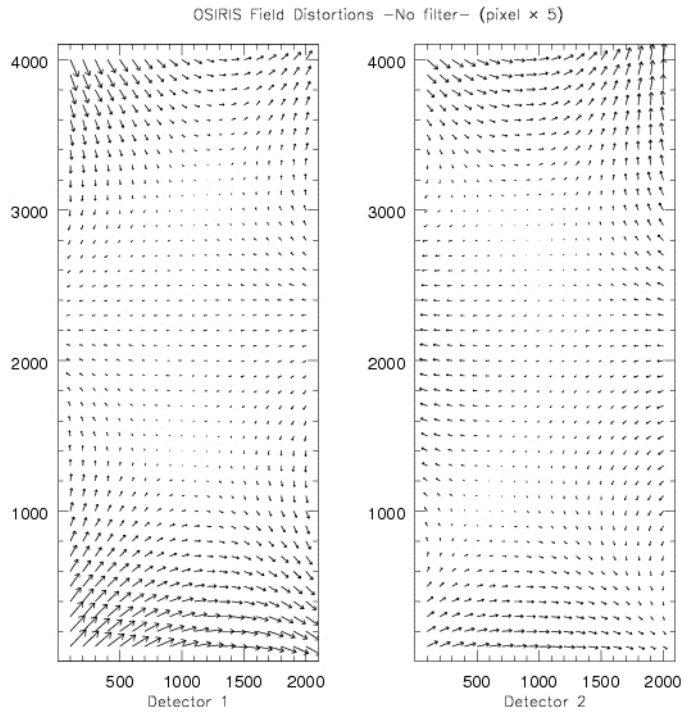

Figure 6.1.- OSIRIS Field distortion without filters.

Obviously, the non-linear components of an astrometric solution for both detectors are not negligible. For this reason, a "`general`" scheme (linear terms plus distortion) must be chosen to find a solution with sub-pixel precision. An example of a `ccmap` task command could be the following:

```
ccmap radecxy.cat image.db images="image" results=image.res xcol=3
ycol=4 lngcol=1 latcol=2 lngunits="degrees" latunits="degrees"
insystem="j2000" refsystem="j2000" projection="tnx"
fitgeometry="general" function="polynomial" xxorder=5 yyorder=5
yxorder=5 xyorder=5 xxterms="full" yxterms="full" maxiter=100
reject=3.0 update=yes pixsyst="logical"
```

It is desirable to execute the task in interactive mode. With this feature activated you can pick the outliers of the initial fit (e.g. encircled plus marks in figure below) and find a satisfying solution clicking on 'f' key:

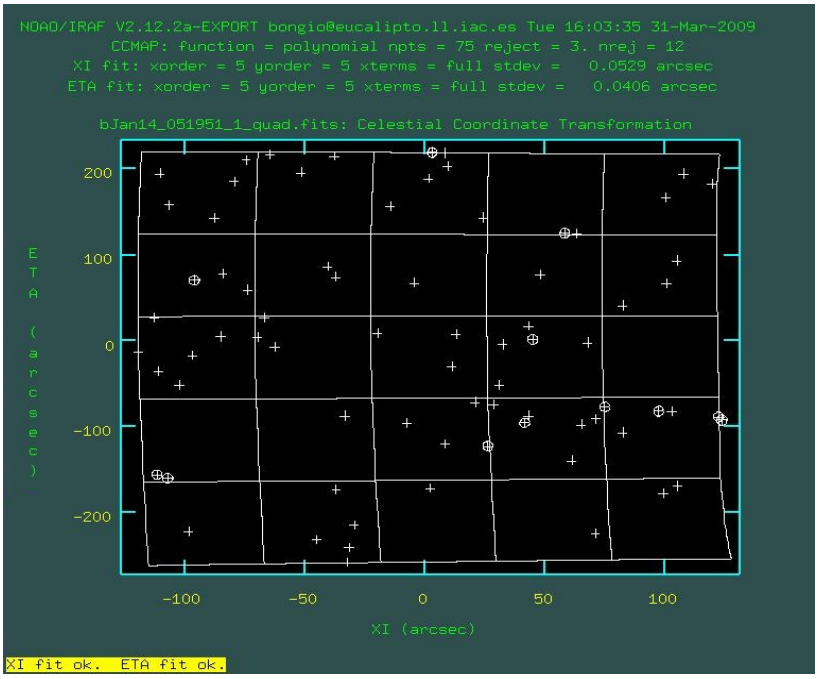

Figure 6.2.- Example of the IRAF task ccmap solution.

The commands associated to the interactive option and further details are given in the task's help. If `update` parameter is turned to "`yes`", the task appends the parameters of the astrometric solution (here named `image.db`) to the image header. A `tnx` projection is highly recommended. As additional output, the file `image.res` contains a line for each astrometric object with the following structure:

```
Column 1: X (pixels)

Column 2: Y (pixels)

Column 3: Ra / Longitude (degrees)
```

```
Column 4: Dec / Latitude (degrees)

Column 5: Fitted Ra / Longitude (degrees)

Column 6: Fitted Dec / Latitude (degrees)

Column 7: Residual Ra / Longitude (arcseconds)

Column 8: Residual Dec / Latitude (arcseconds)
```

6.2.3 Mosaic Composition

To optionally create a mosaic in WCS from individually corrected frames, use first the `mscimage` task of the `mscred` package. This task puts in a common system both WCS referenced frames of any scientific image. Input images are the exposures to be resampled into a single image and the output must match the number of input images. Use a minimum of 30 grid points (`nx`, `ny`) over the input image to determine the mapping function. Also, the parameters `fitgeometry`, `function`, `x/y orders` and `x/y terms`, should match those previously selected in the `ccmap` task. Once both frames are in a common reference system, you can combine both frames to obtain a single image using the task `imcombine`, setting before the parameter `offsets` to "`wcs`". An example of a resulting mosaic is shown below (an astrometrically calibrated image of the Galactic cluster M67 with 2MASS point sources overlaid; standard deviation of the fit: 0.04 arcsec):

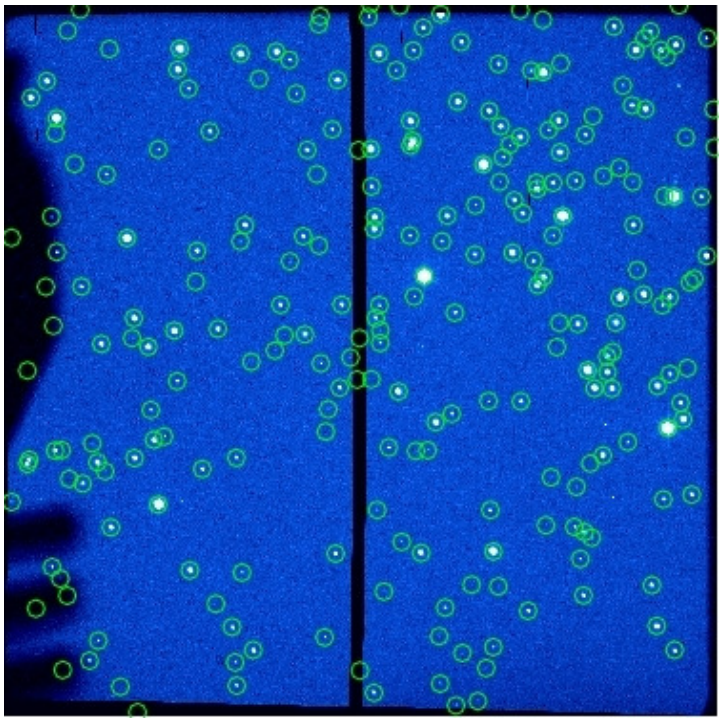

Figure 6.3.- Example of OSIRIS mosaic.

6.2.4 Composing a first-order Mosaic from raw data

To create directly a mosaic from the raw frames of a scientific image (valid up to first order), proceed as follows:

- Create an empty fits image with 4224 × 4108 pixel.
- Rotate the CCD2 frame in -0.045605 degrees around the pixel (893.4, 1989.8).
- Copy the CCD1 frame in the region [1:2098, 1:4102] and the rotated CCD-2 frame in the region [2125:4222, 5:4106] of the empty image recently created.
- Apply the instructions above to obtain a WCS solution for the whole mosaic.

7 OSIRIS OS FILTER CHARACTERISTICS

The following table lists the complete OS filter set corresponding to OSIRIS red-optimized TF (the OS marked in red are outside of the current range of operation for the RTF).

OS	λ_C (nm)	$\Delta\lambda$ (nm)	TF range (nm)
643 / 27	**643.1**	**27.7**	**646.2 - 651.6**
648 / 28	648.4	27.9	651.6 - 657.0
657 / 35	657.2	35.0	657.0 - 667.6
666 / 36	666.8	35.5	667.6 - 677.4
680 / 43	680.2	43.2	677.4 - 692.7
694 / 44	694.4	44.0	692.7 - 707.1
709 / 45	708.8	44.9	707.1 - 721.8
723 / 45	723.3	45.2	721.8 - 736.4
738 / 46	738.0	46.1	736.4 - 751.3
754 / 50	754.2	49.6	751.3 - 768.5
770 / 50	770.6	49.7	768.5 - 784.9
785 / 48	785.6	47.6	784.9 - 799.4
802 / 51	802.0	51.3	799.4 - 816.8
819 / 52	819.0	52.4	816.8 - 834.1
838 / 58	838.6	57.8	834.1 - 854.9
858 / 58	858.2	57.9	854.9 - 874.7
878 / 59	878.2	59.3	874.7 - 895.1
893 / 50	893.2	49.6	895.1 - 907.9
902 / 40	902.4	40.1	907.9 - 914.7
910 / 40	910.6	40.5	914.7 - 923.0
919 / 41	918.9	40.8	923.0 - 931.5
923 / 34	923.8	34.2	931.5 - 934.6
927 / 34	**927.9**	**34.4**	**934.6 - 938.7**

932 / 34	**932.0**	**34.5**	**938.7 - 942.9**
936 / 35	**936.2**	**34.7**	**942.9 - 947.1**
940 / 35	**940.3**	**34.8**	**947.1 - 951.2**

The figures below show the measured central spectral response of OS so far available according to increasing wavelength, for normal incidence. Central wavelength and bandpass as indicated on top of each plot.

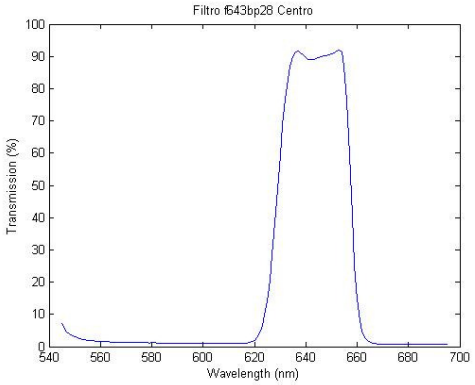

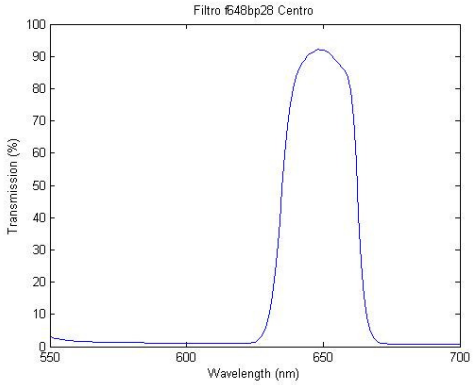

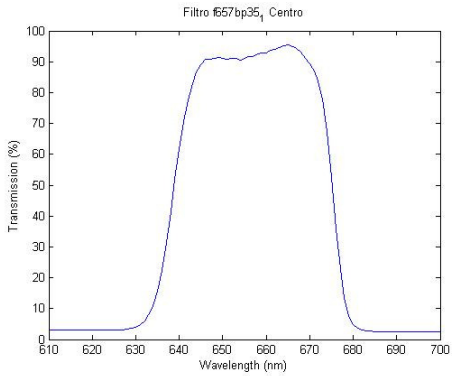

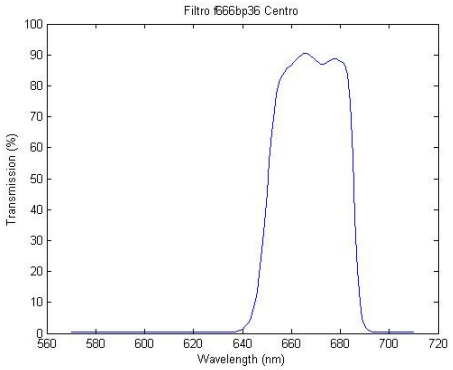

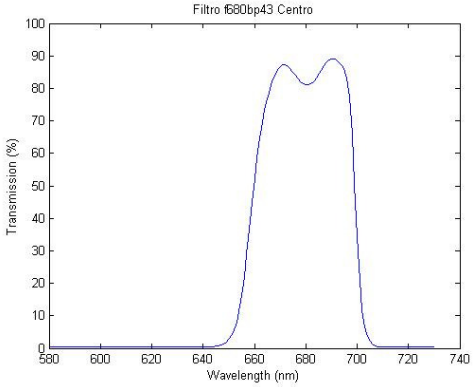

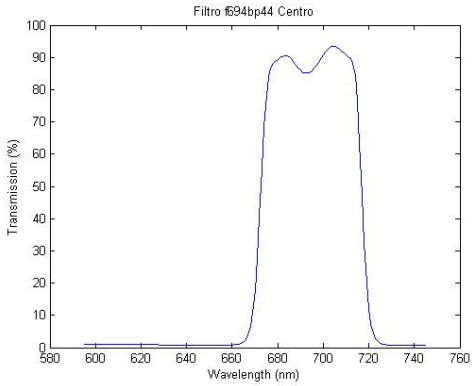

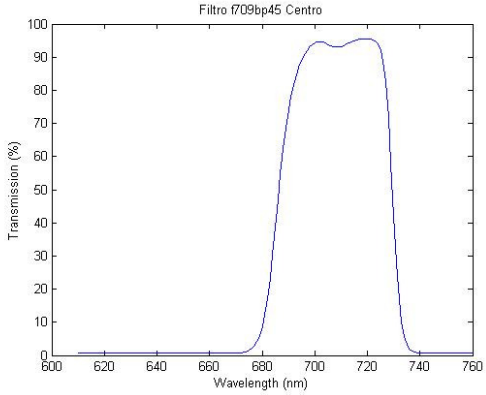
Filtro f709bp45 Centro
Transmission (%)
Wavelength (nm)

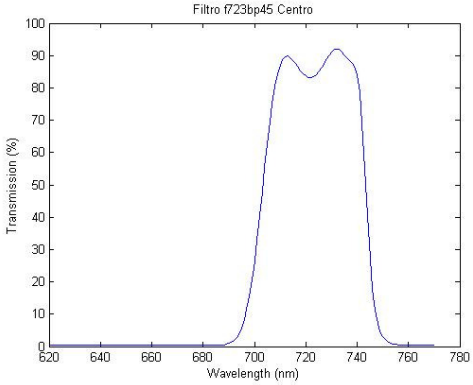
Filtro f723bp45 Centro
Transmission (%)
Wavelength (nm)

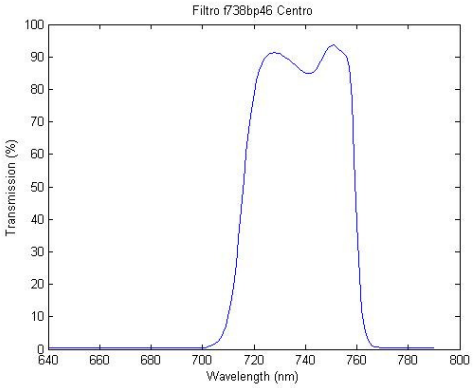
Filtro f738bp46 Centro
Transmission (%)
Wavelength (nm)

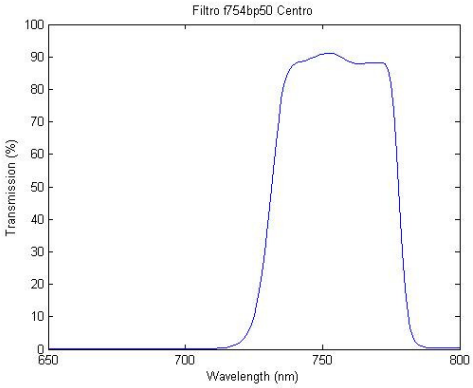
Filtro f754bp50 Centro
Transmission (%)
Wavelength (nm)

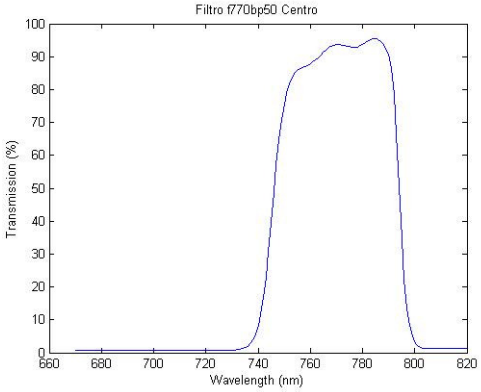
Filtro f770bp50 Centro
Transmission (%)
Wavelength (nm)

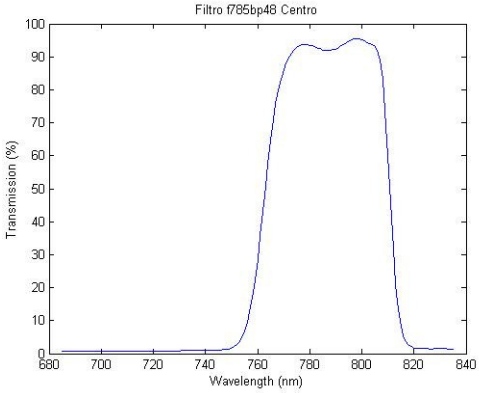
Filtro f785bp48 Centro
Transmission (%)
Wavelength (nm)

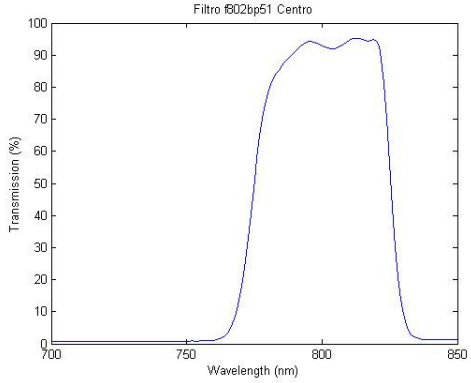
Filtro f802bp51 Centro
Transmission (%)
Wavelength (nm)

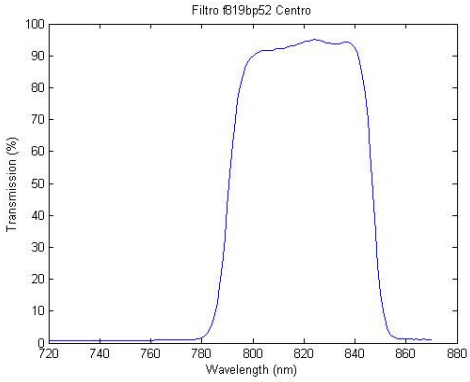
Filtro f819bp52 Centro
Transmission (%)
Wavelength (nm)

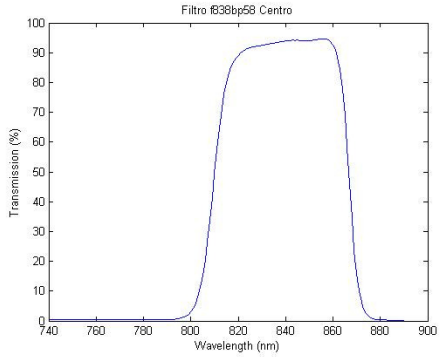
Filtro f838bp58 Centro
Transmission (%)
Wavelength (nm)

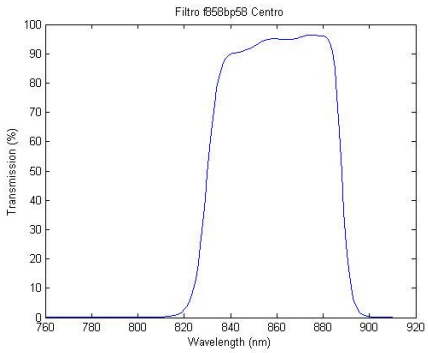
Filtro f858bp58 Centro
Transmission (%)
Wavelength (nm)

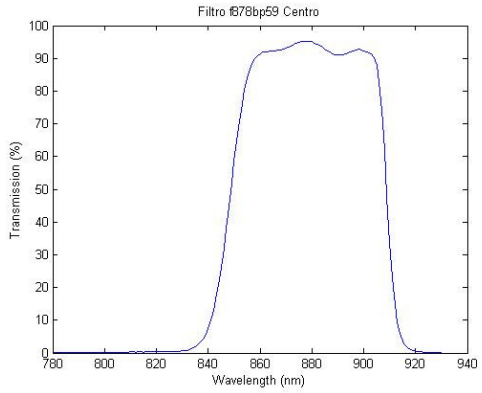
Filtro f878bp59 Centro
Transmission (%)
Wavelength (nm)

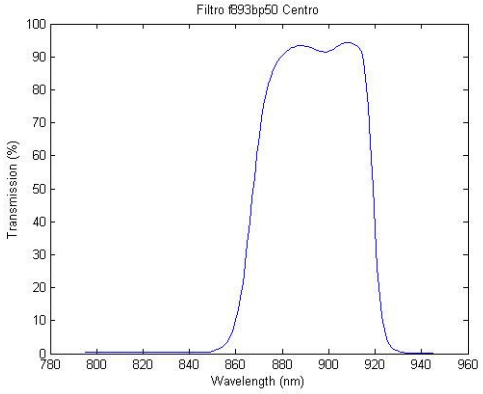
Filtro f893bp50 Centro
Transmission (%)
Wavelength (nm)

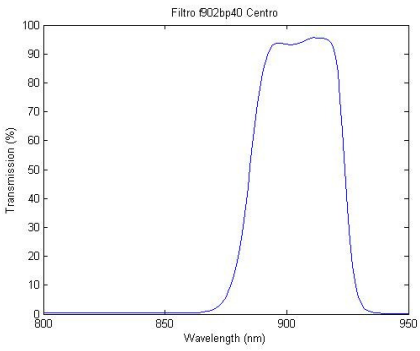
Filtro f902bp40 Centro
Transmission (%)
Wavelength (nm)

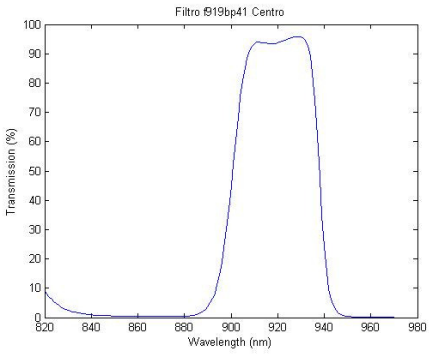
Filtro f919bp41 Centro
Transmission (%)
Wavelength (nm)

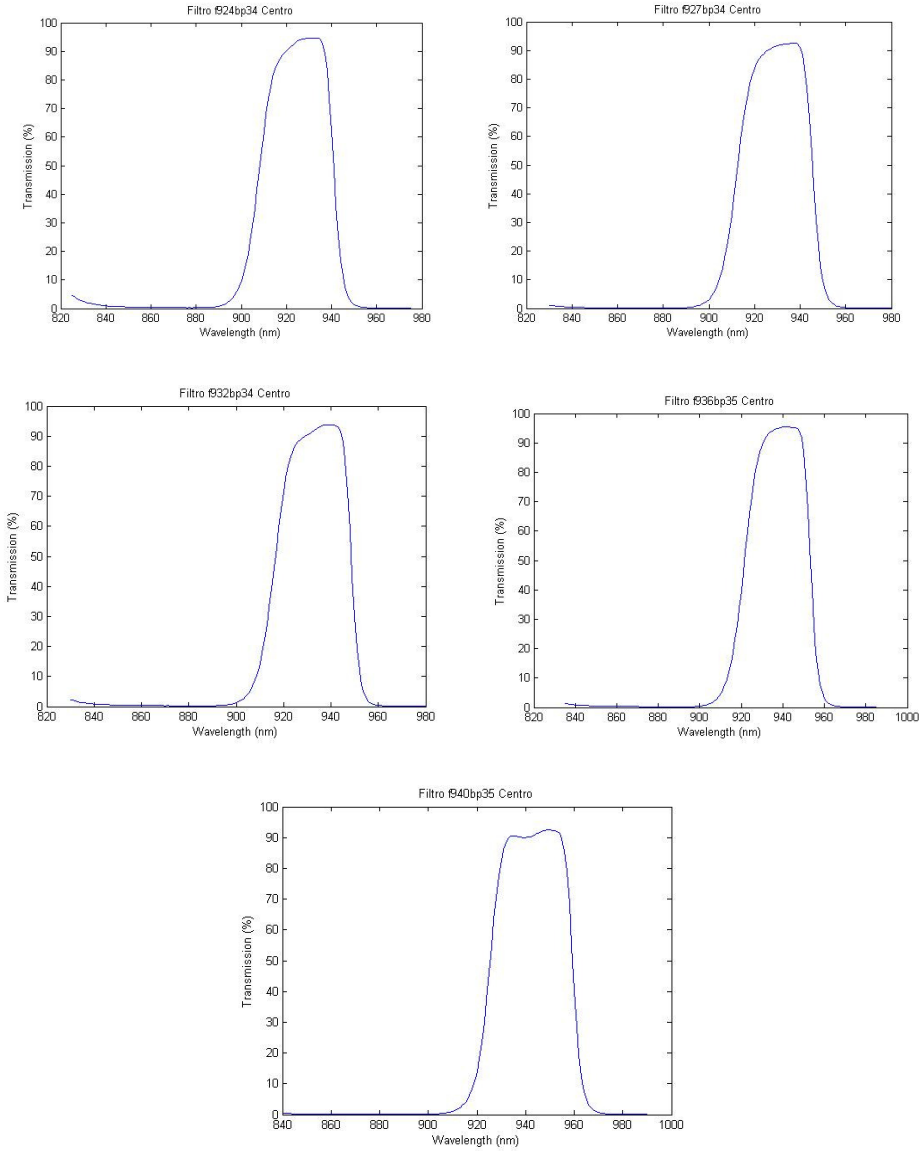

Figure 7.1.- From left to right and top to bottom: measured central spectral response of OS according to increasing wavelength, for normal incidence. Central wavelength and bandpass as indicated on top of each plot.

8 OSIRIS GRISMS/VPH EFFICIENCIES

Efficiency curves of the OSIRIS grisms/VPHs have been measured during commissioning, and are shown below (These transmission curves include all the system (telescope + OSIRIS optics + detectors)::

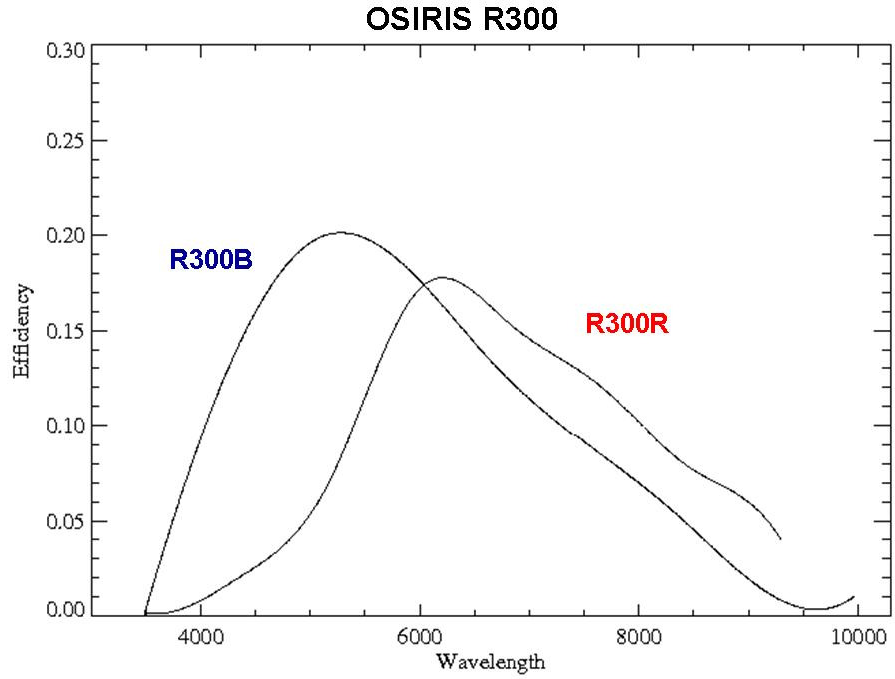

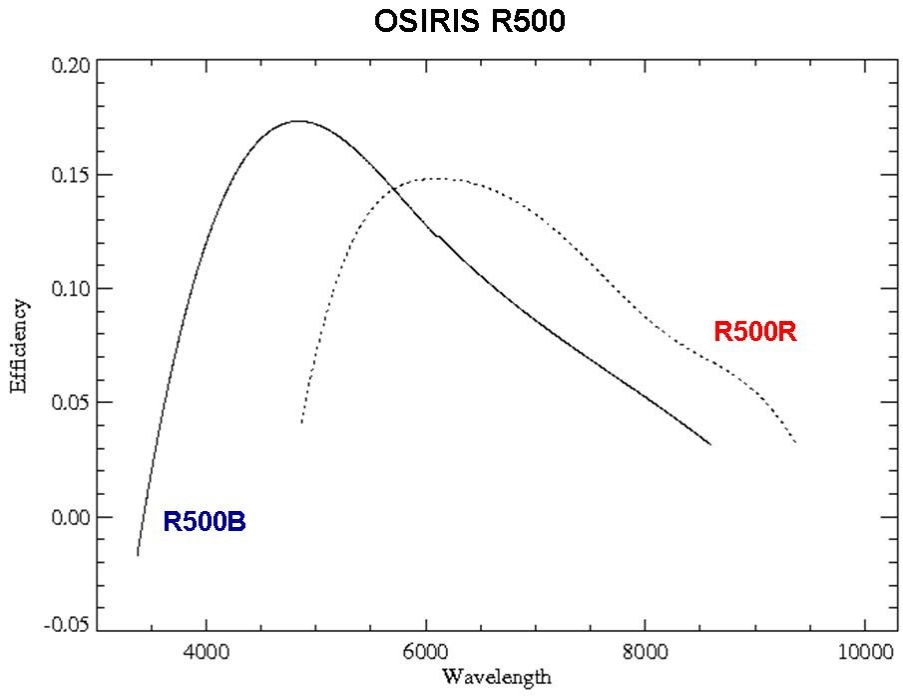

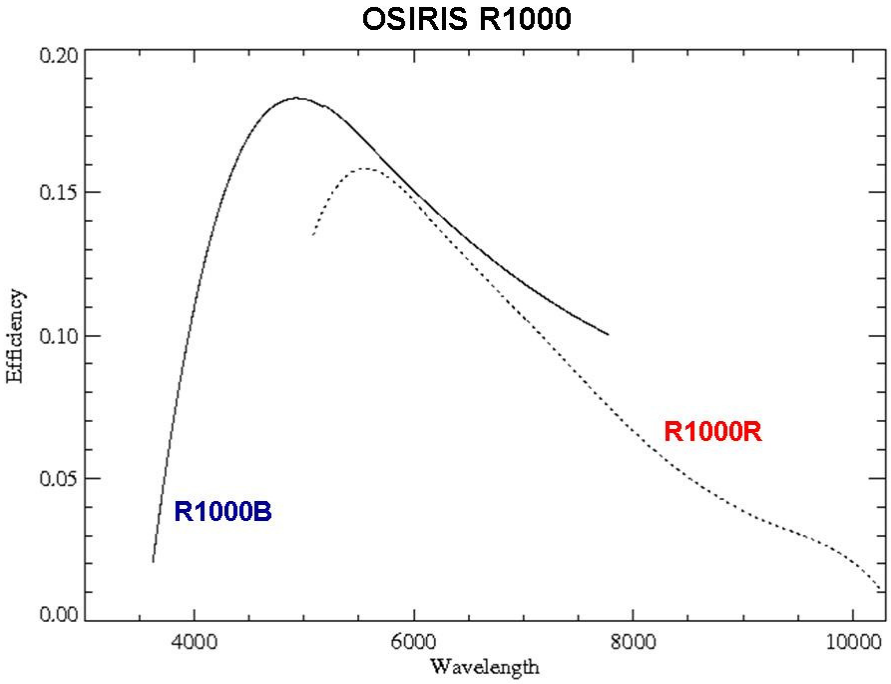
OSIRIS R1000
Efficiency
0.20
0.15
0.10
0.05
0.00
4000
6000
8000
10000
Wavelength
R1000B
R1000R

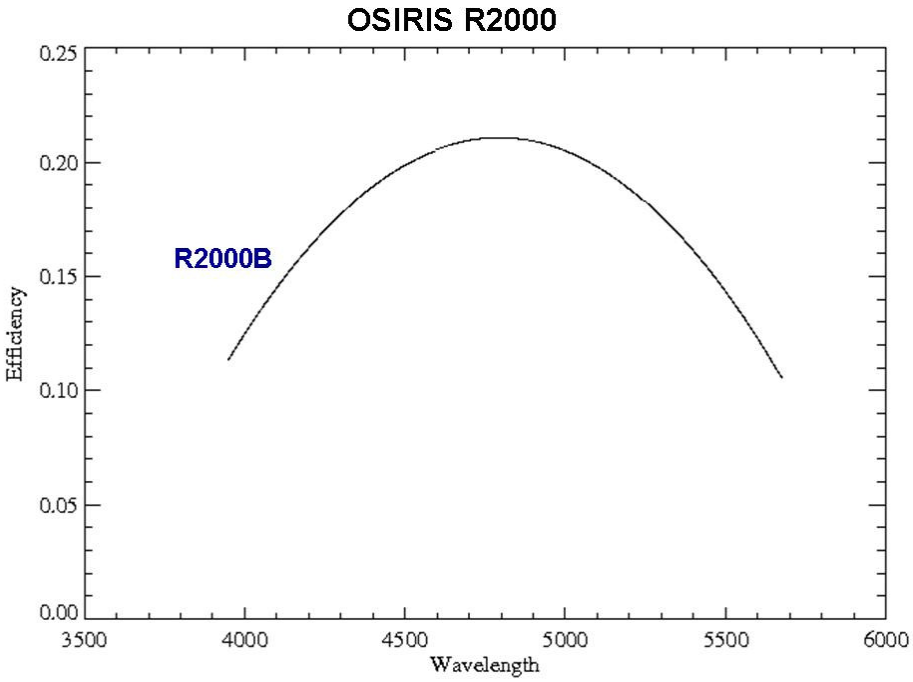
OSIRIS R2000
Efficiency
0.25
0.20
0.15
0.10
0.05
0.00
3500
4000
4500
5000
5500
6000
Wavelength
R2000B

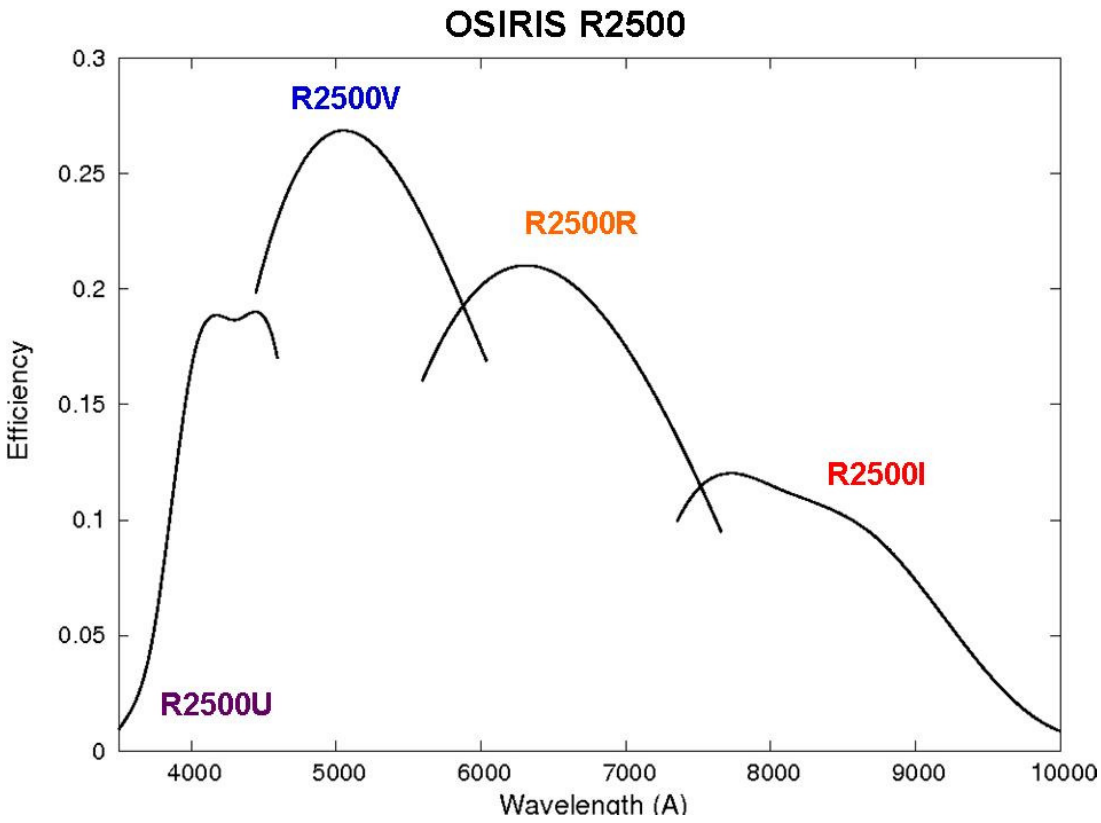

Figure 8.1.- From top to bottom, overall efficiencies for OSIRIS grisms/VPHs.

9 SLOAN PHOTOMETRIC STANDARDS

Photometric calibration for OSIRIS Broad Band imaging is done via a Sloan standard set taken from Smith el al. (2002, AJ, 123, 2121):

Name	RA (J2000)	DEC (J2000)	r'	u'-g'	g'-r'	r'-i'	i'-z'
G 158-100	00:33:54.60	-12:07:58.9	14.691	1.101	0.510	0.222	0.092
SA 92 282	00:56:46.86	+00:38:30.9	12.936	1.000	0.136	0.021	-0.009
Feige 22	02:30:16.62	+05:15:50.6	13.024	0.050	-0.333	-0.303	-0.273
SA 95 193	03:53:20.59	+00:16:34.7	13.844	2.489	1.097	0.407	0.214
Ross 49	05:44:56.81	+09:14:32.2	11.163	1.130	0.467	0.162	0.049
Hilt 566	06:32:09.67	+03:34:44.4	10.787	1.125	0.673	0.341	0.211
Ru 149F	07:24:14.02	-00:31:38.2	13.119	2.469	0.867	0.317	0.166
SA 100 280	08:53:35.47	-00:36:41.0	11.689	1.143	0.308	0.084	0.003
PG0918+029D	09:21:21.94	+02:47:28.7	11.937	2.227	0.817	0.324	0.166
SA 101 316	09:54:52.03	-00:18:34.4	11.438	1.152	0.309	0.073	0.007
G 162-66	10:33:42.81	-11:41:38.7	13.227	-0.183	-0.387	-0.354	-0.303
Feige 34	10:39:36.73	+43:06:09.2	11.423	-0.509	-0.508	-0.347	-0.265
PG1047+003A	10:50:05.65	-00:01:11.3	13.303	1.385	0.519	0.212	0.087
G 163 50	11:07:59.97	-05:09:26.0	13.266	0.215	-0.277	-0.272	-0.271
Feige 66	12:37:23.52	+25:03:59.9	10.747	-0.345	-0.476	-0.367	-0.316
SA 104 428	12:41:41.31	-00:26:26.5	12.330	2.153	0.763	0.279	0.147
PG1323-086D	13:26:05.26	-08:50:35.7	11.928	1.210	0.397	0.132	0.032
Ross 838	14:01:44.47	+08:55:17.4	11.327	1.277	0.573	0.239	0.111
PG1528+062B	15:30:39.55	+06:01:13.1	11.828	1.235	0.419	0.143	0.036
G 15-24	15:30:41.76	+08:23:40.4	11.277	1.035	0.412	0.151	0.052

BD+33 2642	15:51:59.88	+32:56:54.3	10.979	-0.018	-0.332	-0.284	-0.212
Ross 530	16:19:51.66	+22:38:20.2	11.319	1.273	0.558	0.229	0.103
Wolf 629	16:55:25.66	-08:19:13.1	11.129	3.013	1.413	1.466	0.648
SA 109 381	17:44:12.26	-00:20:32.7	11.514	1.477	0.547	0.223	0.094
Ross 711	18:35:19.17	+28:41:55.3	11.295	0.837	0.282	0.104	0.015
SA 110 232	18:40:52.33	+00:01:54.8	12.287	1.390	0.552	0.237	0.094
SA 111 1925	19:37:28.62	+00:25:03.1	12.345	1.397	0.200	0.061	0.051
Wolf 1346	20:34:21.89	+25:03:49.7	11.753	-0.016	-0.351	-0.309	-0.291
SA 112 805	20:42:46.74	+00:16:08.4	12.174	1.183	-0.087	-0.135	-0.090
SA 113 260	21:41:48.03	+00:23:53.3	12.284	1.217	0.331	0.080	0.015
BD+28 4211	21:51:11.02	+28:51:50.4	10.750	-0.517	-0.511	-0.379	-0.313
G 93-48	21:52:25.37	+02:23:19.6	12.961	0.107	-0.308	-0.307	-0.261
SA 114 656	22:41:35.06	+01:11:09.8	12.326	1.961	0.756	0.293	0.156
GD 246	23:12:23.07	+10:47:04.2	13.346	-0.491	-0.504	-0.378	-0.367
PG2336+004B	23:38:38.26	+00:42:46.4	12.312	1.101	0.336	0.100	0.014

10 OSIRIS SPECTROPHOTOMETRIC STANDARDS

Flux calibration for OSIRIS Long Slit Spectroscopy and TF imaging is done via the following subset of standards taken from the ING spectrophotometric standards list:

Name	RA/DEC (J2000)	mag (5556)	Wavelength coverage	Reference
G158-100 (SP0031-124)	00:33:54.5 -12:07:58	14.8	320-1000 nm	Oke 1990, AJ 99, 1621 Filippenko & Greenstein 1984, PASP 96, 530
PG0205+134 (SP0205+134)	02:08:03.4 +13:36:25	14.9	320-800 nm	Massey 1988, ApJ 328, 315
PG0310+149 (SP0310+149)	03:13:37.2 +15:06:22	15.6	320-800 nm	Massey 1988, ApJ 328, 315
HZ15 (SP0437+085)	04:40:39.32 +08:40:45.3	12.6	320-840 nm	Stone 1977, ApJ 218, 767
G191-B2B (SP0501+527)	05:05:30.6 +52:49:56	11.9	320-1000 nm	Oke 1974, ApJ Supp. 27, 21 Massey 1988, ApJ 328, 315 Oke 1990, AJ 99, 1621
GD 99-47 (SP0548-001)	05:51:19.48 -00:10:21.3	14.5	320-1000 nm	Oke 1974, ApJ Supp. 27, 21
He 3 (SP0644+375)	06:47:37.99 +37:30:57.0	12.1	320-940 nm	Oke 1974, ApJ Supp. 27, 21
PG0823+546 (SP0823+546)	08:26:49.4 +54:28:01	14.4	320-800 nm	Massey 1988, ApJ 328, 315
PG0939+262 (SP0939+262)	09:42:50.8 +26:01:01	14.9	320-800 nm	Massey 1988, ApJ, 328, 315
Feige 34 (SP1036+433)	10:39:36.7 +43:06:10	11.3	320-900 nm	Stone 1977, ApJ 218, 767 Massey 1988, ApJ 328, 315 Oke 1990, AJ, 99, 1621
GD 140 SP1134+300)	11:37:05.1 +29:47:58	12.4	320-1000 nm	Massey 1988, ApJ 328, 315 Oke 1974, ApJ. Supp. 27, 21
HZ 21 (SP1211+332)	12:13:56.6 +32:56:30	14.7	320-900 nm	Oke 1990, AJ 99, 1621

Feige 92 (SP1409+503)	14:11:31.87 +50:07:04.1	11.6	320-840 nm	Stone 1977, ApJ 218, 767
PG1545+035 (SP1545+035)	15:48:24.2 +03:22:51	14.3	320-800 nm	Massey 1988, ApJ 328, 315
Ross 640 (SP1626+368)	16:28:25.03 +36:46:15.4	13.8	320-1000 nm	Oke 1974, ApJ. Supp. 27, 21
PG1708+602 (SP1708+602)	17:09:15.9 +60:10:10	13.9	320-800 nm	Massey 1988, ApJ 328, 315
Grw+70 8247 (SP1900+705)	19:00:10.25 +70:39:51.2	13.1	340-920 nm	Oke 1974, ApJ Supp. 27, 21
BD+25 3941 (SP1942+261)	19:44:26.13 +26:13:16.6	10.4	320-840 nm	Stone 1977, ApJ 218, 767
G24-9 (SP2011+065)	20:13:55.7 +06:42:45	15.8	320-1000 nm	Oke 1990, AJ, 99, 1621 Filippenko & Greenstein 1990, PASP 96, 530
L1363-3 (SP2140+207)	21:42:41.00 +20:59:58.2	13.3	320-1000 nm	Oke 1974, ApJ. Supp. 27, 21
G157-34 (SP2311-068)	23:14:25.19 -06:32:47.8	15.4	320-1000 nm	Filippenko & Greenstein 1984, PASP 96, 530

A. LIST OF REFERENCE DOCUMENTS

1	Lauer T. & Valdés F. 1997, NOAO Newsletter 52 (http://www.noao.edu/noao/noaonews/dec97/node23.html)
2	Valdés F. 2000, Mosaic Data Structures (http://iraf.noao.edu/projects/ccdmosaic)
3	*The Zen of IRAF*. A Spiritual User's Guide to the "Image Reduction and. Analysis Facility" for the LINUX Novice. A. Charles Pullen. A User's Guide to CCD Reductions with IRAF, Philip Massey, February 1997

B. REFERENCES

- Castro F.J. et al. 2007, *Optical Data of GTC*, GTC Internal Report
- Cuillandre et al. 1994, A&A 281, 503
- Francis P.J. & Bland-Hawthorn J. 2004, MNRAS 353, 301
- Jester S. et al. 2005, AJ 130, 873
- Jones, Shopbell & Bland-Hawthorn 2002, MNRAS 329, 759
- Landolt A.U. 1992, AJ 104, 340
- Sánchez-Portal et al. 2010, arXiv:1012.1750
- SESO 2006, Collimator Unit Measurement Report
- Smith et al. 2002, AJ, 123, 2121